Optical Pulse Distortion and Manipulation Through Polarization Effects and Chromatic Dispersion

by

Patrick Chien-pang Chou

Submitted to the Department of Electrical Engineering and Computer Science
in partial fulfillment of the requirements for the degree of
Doctor of Philosophy in Electrical Engineering
at the
MASSACHUSETTS INSTITUTE OF TECHNOLOGY
February 2001

Author .....
Department of Electrical Engineering and Computer Science
January 15, 2001

Certified by .....
Hermann A. Haus
Institute Professor
Thesis Supervisor

Certified by .....
William Kelleher
Group Leader
The Charles Stark Draper Laboratory, Inc.
Thesis Supervisor

Accepted by .....
Arthur C. Smith
Chairman, Department Committee on Graduate Students

Optical Pulse Distortion and Manipulation Through Polarization Effects and Chromatic Dispersion

by

Patrick Chien-pang Chou

Submitted to the Department of Electrical Engineering and Computer Science
on January 15, 2001, in partial fulfillment of the
requirements for the degree of
Doctor of Philosophy in Electrical Engineering

Abstract

Pulse distortion and shaping mechanisms play a significant role in optical fiber communication and sensing. In this thesis we shall investigate techniques which alleviate pulse deterioration due to polarization effects, and utilize large chromatic dispersion for system performance enhancement.

We first demonstrate a method of mitigating polarization mode dispersion (PMD) in fiber optic communication systems. PMD has been a known effect for over a decade. However, it was not an impediment to system performance until recent advances in communication system bit rates. Today, with 10 Gb/s and 40 Gb/s channel rates appearing in new system equipment, PMD prohibits the use of many fiber cables already installed. Current PMD compensation techniques that require feedback control have difficulty meeting the speed and reliability requirements of telecom standards. In the first part of this thesis we investigate alternative compensation schemes which reduce the complexity of the feedback schemes.

We next exploit the recent availability of ultra-long length chirped fiber Bragg gratings (FBG). Their enormous chromatic dispersion enables methods of improving current techniques in sensing and high speed optical sampling. In one experiment, we modulate the frequency of a standard distributed Bragg reflector (DBR) laser, and then apply the dispersion of the ultra-long FBG. Picosecond pulses are formed, whose repetition rate is independent of the laser cavity length. Since the gain of the laser is not modulated, the timing jitter is fundamentally limited only by the frequency noise of the laser.

Finally, we again utilize the large delay of an ultra-long chirped FBG to implement arbitrary dynamic optical filtering of pulse spectra. In sensing applications such as fiber gyroscopes and optical coherence tomography (OCT), a wide Gaussian spectrum is ideal for low error in the gyro, and high image resolution in OCT. A modelocked fiber laser provides very wide spectra, but the shape can be irregular. We stretch the modelocked pulse temporally with an FBG, and access the frequency components in the time domain. We can then selectively suppress frequencies with an amplitude modulator to synthesize a Gaussian spectrum.

Polarization effects and chromatic dispersion will inevitably appear in many optical systems. It is the goal of this thesis to show that their effects can be minimized or utilized for system performance enhancement.

Thesis Supervisor: Hermann A. Haus
Title: Institute Professor

Thesis Supervisor: William Kelleher
Title: Group Leader
The Charles Stark Draper Laboratory, Inc.

Acknowledgment of Fellowship Support

This thesis was prepared at the Charles Stark Draper Laboratory, Inc., under IR&D account 13031, contract number 01-0-1024-1 (Sensor Development Program).

Publication of this thesis does not constitute approval by Draper of the findings or conclusions contained herein. It is published for the exchange and stimulation of ideas.

Personal Acknowledgements

More than a few people were astonished when I told them I would return to MIT for graduate school. "Didn't you swear you'd never go back to such a godawful depressing hellhole?" some would ask. I don't hide the fact that my undergraduate career here was an emotional low point. Although the technical education at MIT cannot be beaten, I blamed the Institute for not providing an environment conducive to personal growth, the type that is desperately needed by youths clawing their way out of teenagerhood. I know that others share these feelings. Why else would it be fashionable to yell profanities at Lobby 7 on graduation day? Why else would it be that when volunteer fundraisers phone wealthy alumni, the only donation they receive is an earful of "I paid all that tuition and now you want more?!?" And why else would the letters "IHTFP" appear around and about campus so often?

But after having spent four years away from MIT, to the surprise of many, I thought I would give it a second try. During those years away, I saw a phenomenal turn of good fortune. While working on my Master's degree at USC I encountered a new world. People there were different. Many were not even engineers – what a novel concept! Most importantly, through a chain of unlikely random events, I met my future wife there. It's amazing how one's attitude can change so profoundly and so rapidly. Later, I was dumbfounded to find in my lap the rare opportunity to work at Bell Labs, where I shared hallways with Nobel laureates and worked for and alongside the most revered and decorated researchers in the field.

This is why, armed with a new outlook, a beautiful new wife, and some work experience under my belt, I felt ready for round two at MIT. Upon arrival, I was pleased to discover that there are plenty of opportunities to live a full life here. And contrary to natural instincts, not only do they fail to hinder your technical work, they can enhance your creativity and add important skills which you simply cannot develop while sitting in a lab tweaking mirrors and lenses. I studied performance skills while rehearsing African music and dance concerts; I learned about the challenges and joys of organizing a group of people, whether the cause is managing a musical ensemble or developing a business plan; just across the Charles River I learned about songwriting techniques at the Berklee College of Music. So where was all this hiding when I was an undergraduate? Of course, these types of opportunities were always there, but I didn't have the initiative to venture out and find them. Thus, I too am at fault for my misery in college. I still do believe the MIT environment could use a lot of improvement, but it's not hopeless. You just have to look harder.

As expected, the technical education I received as a graduate student was the best anyone could ever dream of. I am forever in debt to Professor Haus. He may be tired of hearing praise from students because he receives it as often as I reboot my Windows computer, but I'll add to the collection anyway. Professor Haus is not only a big reason for me wanting to return to MIT, but I feel blessed to have been allowed by him to return. The strength of his leadership can be seen in his example of integrity, dedication, compassion, and intelligence. Words cannot express how grateful I am to him for giving me this second opportunity to be a member of his group.

I am also constantly in awe of Professor Ippen. I regret not having initiated more

interaction with him. Perhaps it was the fear of hearing constructive criticism of my ideas. While it is generally difficult to hear the words "it won't work" it is especially painful coming from him because he is ALWAYS right.

Everyday I thank the stars that John Fini was able to pull himself away from solving deep quantum problems to work on PMD compensation. Beating our PMD problems with his math hammer really did the trick. Plus, it was fun taking the first ever MIT Italian class with him. Working in the semiconductor laser lab was also a joy. I'm especially grateful for the opportunity to work with Harry Lee and his advisor Professor Rajeev Ram, who is not only the brightest young professor around, but also happens to be an old buddy of mine. We go way back, back to when I was unhindered by the thought that he would one day tell my wife embarrassing stories about me. Thanks Rajeev! It was also a blast hanging out with others in his group, like Erwin Lau, Farhan Rana, Steve Patterson, Holger Schmidt, Mathew Abraham, Peter Mayer, Margaret Wang, and Ravi Dalal.

I appreciate the alternate perspectives offered by Charles Yu, who is still not convinced that despite my spending a total of 8.5 years at MIT, my break in the middle excludes me from "lifer" status. It really does make a difference! I am truly lucky to have had other great officemates like Shu Namiki, Mike Watts, Farzana Khatri, Stephen Boppart, Moti Margalit, Boris Golubovic, and Hanfei Shen. I have enjoyed many lunchroom conversations with labmates Dan Ripin, J.P. Laine, Juliet Gopinath, Pei-Lin Hsiung, William Wong, Po-Hsiu Cheng, Leaf "Wing-Wing-Wing-Wing-Wing" Jiang, Matt Grein, Peter Rakich, Erik Thoen, Lynn Nelson, David Jones, and Jerry Chen. Of course I enjoyed other conversations, both technical and nontechnical, with other group members such as Brent Little, Kazi Abedin, Masayuki Matsumoto, Franz Kärtner, Wolfgang Drexler, Günter Steinmeyer, Stefano Longhi, Miloš Popović, Jalal Khan, Jay Damask, Christina Manolatou, Seong-Ho Cho, Sam Wong, Chris Lin, Tony Ko, Bryan Robinson, Jessica Tan, Palma Catravas, Luc Boivin, Kaoru Minoshima, and Yijiang Chen. I'll always appreciate the generosity of Dr. Masataka Shirasaki, who always finds the time to evaluate my hare-brained ideas and schemes, and Kohichi Tamura, who despite graduating before I started grad school, continued to offer advice and wisdom. I enjoyed running into Prof. Shaoul "Ziggy" Ezekiel in the halls on several occasions where we would discuss everything from fiber gyros to recurring structures found in various languages. I was fortunate to be in a group that employs talented administrative assistants Cindy Kopf, Mary Aldridge, and Donna Gale, and to be part of RLE which has a tireless staff, including Dave Foss, Gerry Power, Mary Young, and Maxine Samuels. Thanks to Jonathan O'Brien of Fish & Richardson P.C., for bravely assuming the difficult task of writing our PMD patents.

Nearly all the experiments in this thesis are possible only because of the wonderful collaboration between our group and Jim Brennan of 3M. His ultra-long fiber gratings enabled many experiments, and I am personally grateful that he generously took it upon himself to look out for my well being. He is also the reason that the PMD work was made possible, as he is the one who jumpstarted our PMD program funded by 3M. Thanks to Terry Smith for supervising the program, and to Barb DeBaun, Mike Matthews, and Jack Biersdorf for providing extra technical help. Special thanks to Nestor Ho, who on short notice filed a patent for me and Jim in a matter of days.

My cherished memories in the MIT African music and dance performance group, MITCAN, would not exist if not for its founder and original director Prof. James Makubuya, as well as members of the executive committee Eric Traub, Roz Takata, Neela Rafizadeh, Oludotun Fashoyin, and Candice McElroy. I learned a great deal from $50K entrepreneurship competition teammates Sophia Chong, childhood friend Stacy Ho, Pankaj Lad, Gert-Hartwig Lescow, Dr. Paul Sandhu, Ryan T'Kindt, and our mentor Ralph Grabowski. Speaking of entrepreneurship, it is the opportunity to work at a startup company that has provided so much extra motivation. I look forward to joining fellow USC grads and working for USC Professor Alan Willner, who has founded a company with Bogdan Hoanca, who I sensed right away is of exceptional capability and knows what it takes to build a great company.

I still reminisce about experiences at Bell Labs, where I worked for renowned researchers such as Ivan Kaminow and Corrado Dragone of the "Dragone router" fame (truly an *ottima idea*!). I benefited a great deal from other members of the lab like Martin Zirngibl, Chuck Joyner, and Chris Doerr, whose kindness and work ethic are truly inspiring. My earlier technical education began during high school when, in a ham radio store, I met my future mentor Don Gillespie. It must have been cosmic intervention that caused that chance meeting. If not for his teachings, which continue to this day, I never would have enjoyed the science fair projects that whetted my apetite for exerimental work.

I am grateful to Neil Barbour and Bill Kelleher of Draper Labs, who generously provided my fellowship over the years and provided other support in the form of lab space, equipment, and components. Thanks to Charlie Tapalian who served as a thesis reader, and Steve Smith who was always willing to hear my ideas and provide constructive criticism. I enjoyed sharing the lab with Jacques Govignon, who works harder than most grad students, Rick Stoner, Jack Haavisto, Fran Rogomentich, Melody Lynch, Oldrich Laznicka, and the wonderful people who maintained the lab: Bruno Nardelli, Ralph Todino, Betty Skinner, Paul Jones, Ralph Garry, and Bill Worley. I also appreciate the help from George Schmidt, Mike Villani, and Loretta Mitrano at the education office, Rick Flanagan, Will Elias, and administrative assistants Linda Habib, Lisa Davis, and Diana Bonaventura.

Finally I'd like to dedicate this thesis to my wife Suky. I thank her for her support over the years and for aiding my ongoing effort to become a complete person. I am forever in great debt to my parents for sacrificing so much, just so that I could receive the best education possible even when outrageously overpriced. My brother and sister have always been there for me, no questions asked. And through my wife, I am very lucky to have acquired a lively new family who showers me with care and attention that many only dream of.

There have been so many pivotal moments during the last several years, and miraculously they all seemed to lead upward. I can't imagine how things would have turned out if not for this sequence of coincidences, and without the contributions of the wonderful people mentioned above. I couldn't have planned it any better.

Patrick Chou
Cambridge, MA

Contents

List of Figures

Chapter 1

Introduction

The dynamics of optical pulse propagation in fiber have long been an area of interest for both scientific and technological research. Early studies of nonlinear effects and linear pulse broadening mechanisms paved the way for high speed optical communications as well as other applications requiring large optical bandwidth. While many of the recent technological developments in fiber optics have been driven by the astronomical growth of Internet traffic, applications such as optical sensing for medical and military applications continue to advance as well.

In both communications and sensors, pulse broadening and manipulation via group velocity dispersion (GVD) and random polarization effects in fiber are topics of recent study. This thesis will describe three ways of utilizing or removing these dispersive effects in optical systems.

1.1 First Order Polarization Mode Dispersion Compensation

Chapter 2 provides background on the phenomenon of polarization mode dispersion (PMD), which results from random sections of residual birefringence in optical fiber. In general, the birefringent disturbances result in a complicated polarization dependent distortion of optical pulses [1, 2, 3]. However, to first order, it simply splits

a pulse into two orthogonally polarized components with different time delays [4]. The two polarization states are called Principal States of Polarization (PSPs). As with any other pulse broadening mechanism, PMD limits transmission length and bit rate in communication systems unless compensated. While there is much variation between different fibers, approximately 30% of 10 Gb/s fiber links already installed are limited by PMD, and PMD will likely prohibit the feasibility of most 40 Gb/s systems.

In Chapter 3 we propose a technique for characterizing first order PMD parameters for the purpose of compensation in real time. Most PMD compensators are feedback systems with at least three feedback parameters [12, 36, 37, 38, 39] and are designed to respond only to slow thermal fluctuations [13]. Data obtained from installed systems [14] indicate that PMD parameters can vary at a millisecond time scale due to fiber handling and acoustic vibrations.

The number of feedback parameters is inherently large because there are several unknowns in a PMD system: two for the PSP orientation, one for the relative delay, and one for the relative power in each PSP. This complexity adds to the difficulty in building fast compensators. The compensation scheme presented here requires only one feedback parameter, and in principle can be expanded into a feedback-free system. In this scheme the PSPs are characterized in real-time with a fast polarimeter [12]. One can then use standard polarization transforming optics to align them to a polarization dependent delay which can put the two pulses back together.

Because of the large number of unknowns, a single polarimeter measurement is not sufficient to characterize the PSP orientations [1]. The scheme thus requires the polarization state to be modulated before entering the PMD fiber (In many long haul systems, polarization modulation is already favored for its mitigating effect on polarization hole burning in EDFAs [149, 150, 151, 152]). For every modulation cycle, the PSP detection device samples several output states of polarization (SOPs) and their corresponding degrees of polarization (DOPs) for different input SOPs. Because the output DOP is a function of the input SOP and its relation to the PSPs, the PSP orientation can be determined with a sufficient number of samples. This process

requires no feedback and is limited in speed only by computing power, bandwidth of the polarimeter photodetectors, and input SOP modulation rate. Once the system aligns the PSPs to the axes of the polarization dependent delay, the latter can then compensate actual pulse splitting. The delay can be feedback controlled more easily because there is only one parameter remaining.

1.2 Pulse Generation With Constant Intensity Laser

In Chapter 4, we demonstrate a short pulse generation technique using an ordinary DBR (Distributed Bragg Reflector) laser, but frequency modulated at a high frequency and large modulation depth. The method utilizes an ultra-long chirped fiber Bragg grating (FBG) for generating short optical pulses without mode-locking [61], Q-switching [62], nor gain modulation. The optical source is a frequency modulated DBR laser [63] with a DC driven gain section. Because gain switching is not present, this technique could potentially provide pulse trains with low timing jitter for use in optical sampling.

1.2.1 Previous Work on FM Mode-Locking

Historically, most efforts on frequency modulation (FM) of lasers were directed toward FM mode-locking. It began in the mid-1960s when Harris et al investigated FM oscillations in a He-Ne laser [64]. As described in [62], using an electrooptic crystal, the lasing frequency was modulated at a rate synchronous with a harmonic of the inverse cavity roundtrip time. In this manner, frequency modulated electromagnetic waves were generated such that they were identical to FM radio waves, but at an optical carrier frequency. Optical spectra were measured with a scanning Fabry-Perot interferometer and confirmed to resemble FM radio spectra.

Years later, successful demonstrations of pulse generation using frequency modulated semiconductor lasers were reported [65, 66, 67] both with and without the aid of external dispersion. In [67] the DBR laser was tuned at a rate of 1.5 GHz to generate 24 ps pulses with a spectrum 0.25 nm wide. In [65] a Fabry-Perot laser was passively

FM mode-locked via four-wave mixing; pulses were formed when external dispersion was present.

In any mode-locked laser, the repetition rate is tied to the roundtrip time within the cavity and is sensitive to environmentally induced fluctuations in the cavity length. A more versatile source would be one that is frequency modulated, but not mode-locked. External electrooptic frequency modulation [68] and frequency modulated distributed feedback (DFB) lasers [69] have been demonstrated, but the modulation index is small because of the limited wavelength sweep range.

While pulse generation through FM mode-locking has been an area of interest for decades, FM without mode-locking has been difficult. In [68] the modulation is applied outside the laser cavity, where a strong phase modulator is necessary. The amount of dispersion required to compress the pulses is also large. Described in Chapter 4 is a method in which the frequency modulation is performed by tuning a filter inside a laser cavity and the dispersion is all external, provided by an ultra-long FBG [71].

1.2.2 Ultra-Long Length Fiber Bragg Grating

The first FBG is a classic example of a serendipitous discovery that eventually transformed an entire industry. Many developments have occurred since the first observation of a fiber grating formed by a standing wave [72, 73]. They are now written into a photosensitive germanium doped fiber from the side [74] using a high power ultraviolet (UV) laser and a phase mask to generate a periodic pattern of grating teeth. Today, FBGs are used for dense WDM multiplexing and demultiplexing in commercial telecom systems.

Other applications and more complex structures continue to be investigated. One such variation is the chirped FBG, which has clear potential for pulse shaping and dispersion compensation in telecommunications. The magnitude of dispersion is determined by the desired bandwidth and by the length of the grating, which is limited by phase mask or UV beam size. While mask lengths can be up to 15 cm [75], longer FBGs have been fabricated by stitching mask patterns together [76, 77, 78]. But the

process is difficult because the stitching must be done with sub-wavelength precision.

Recently, alternate methods of writing long FBGs have been proposed and demonstrated, the most successful of which is the method developed by Brennan et al at 3M Corporation [71, 75]. They have written FBGs greater than 10 meters in length. The process still involves UV illumination through a phase mask, but the fiber is translated longitudinally as it is illuminated so that the total illumination length is not limited by the mask length.

1.3 Mode-locked Fiber Laser As Pseudo-Low Coherence Source

In Chapter 5 we propose a novel method of exploiting large amounts of GVD in sensing applications for which an incoherent light source is desired. Specifically, we focus on externally conditioning the spectrum of a stretched pulse laser to be both broad and Gaussian. Experimental demonstrations are again enabled by an ultra-long chirped fiber Bragg grating (FBG) that provides the large GVD necessary for the technique to be practical.

Low coherence sources have found a place in many optical sensing applications, most notably fiber gyros [87, 88] and coherence based techniques in medical imaging [109, 110]. The sources generally consist of fluorescence or amplified spontaneous emission (ASE) sources such as LEDs or superluminescent diodes (SLDs). Here, we propose the use of a stretched pulse additive pulse mode-locked laser (SP-APM) laser [125] in conjunction with recently developed long FBGs as an alternative.

1.3.1 Stretched Pulse Erbium Doped Fiber Laser

Fiber lasers have been a subject of great interest since the early 1960's when glass hosts were first doped with rare-earth ions [126, 127]. Erbium has since blossomed as a dopant due to its applicability to the 1.55 μm wavelength range for long distance telecom use [128]. In 1992 a stable passively mode-locked erbium doped fiber

ring laser was demonstrated as a means of generating 452 fs pulses [129]. Its sech-like spectrum was approximately 9 nm wide and contained sidebands from nonlinear pulse shedding resonant with the laser cavity [130]. The mode-locking mechanism, polarization additive pulse mode-locking (P-APM) was based on nonlinear polarization rotation in the fiber. Since the nonlinearity results from the Kerr effect in the fiber, the artificial saturable absorber created by the P-APM responded at a femtosecond time scale. This helped generate clean and quiet pulses [131, 132].

Soon afterward, the "stretched pulse" version of the P-APM laser was introduced [133, 125]. It utilized the same passive mode-locking mechanism, but with added benefits. Although the net dispersion in the cavity was nearly absent, the local dispersion could be relatively high. As a result, the width of the pulse could breathe as it propagated through alternating sign dispersion inside the ring cavity. The accumulated nonlinear phase was reduced, thus increasing the soliton length and alleviating pulse instabilities for a given pulse energy. Consequently, perturbations such as cavity gain and loss could be increased, resulting in shorter output pulses with higher energies. Eventually, a width of 63 fs [134] and an energy of 2.7 nJ [135] were achieved in separate experiments.

To support the shorter pulses, a wider optical bandwidth was generated. Generated by SPM in the fiber, it could be as wide as 60 nm, exceeding the bandwidth of the erbium gain spectrum. As described by a revised master equation [136, 137, 138, 139], the spectrum of the solution was Gaussian shaped to first order [140]. Even though it is not truly an incoherent source, its wide Gaussian spectrum made the SP-APM EDFL an attractive candidate as a substitute for low coherence sources.

1.3.2 Applications in Fiber Gyroscopes

The combination of the broad spectrum SP-APM laser and a high GVD long FBG presents great opportunity for applications requiring low coherence sources. Here we introduce one such application, the fiber gyro, also known as an interferometric fiber optic gyroscope (IFOG) [89, 90]. Rotation rate sensors are essential components for inertial navigation systems in a wide array of vehicles including cars, ships,

submarines, and airplanes. The IFOG is a rotation rate sensor of particular interest for high performance applications such as inertial grade gyros because it contains no moving parts. Stability and reliability are therefore greater for IFOGs than for mechanical gyros.

Although Sagnac himself first demonstrated optical rotation sensing in 1913 [91], optical gyros based on Sagnac loops did not advance significantly until the 1970s when low loss optical fiber became available. The scale factor is proportional to the length of fiber in the loop, and for the first time light could propagate through hundreds of meters of fiber without appreciable power loss. Research efforts resulted in the advent of the IFOG minimum configuration [92] which increased performance by orders of magnitude.

An incoherent source is best for an IFOG because it minimizes the amount of noise from coherent Rayleigh scattering in the fiber [87, 88]. Additionally, it has been shown that an incoherent source generates less Kerr effect error [93, 94, 95, 96, 97]. The traditional choice is the superluminescent diode (SLD), although recently amplified spontaneous emission (ASE) from erbium doped fiber (EDF) has been demonstrated to be both incoherent and stable [98, 99]. A key advantage is that unlike SLDs, EDF is inherently compatible with the IFOG fiber via fusion splicing. Additionally, EDF development has already been driven by telecom research.

A broad spectrum source that had not been considered is the passively modelocked SP-APM laser [140, 137, 138, 125, 136, 131, 132, 134, 128, 141, 142], even though its spectrum is routinely a few times as wide as that of an SLD [135, 112]. An immediate drawback is the short pulse output; the high peak intensities induce considerable nonlinear effects in the fiber of the Sagnac loop. However, simply stretching the pulses with large GVD reduces the peak intensity without affecting the spectrum. Evidence has shown that such a conditioned pulse source could indeed perform as a broadband incoherent source [100].

1.3.3 Spectral Shaping For Gyro And Medical Applications

We shall demonstrate a technique to further condition the output of a SP-APM laser so that it is suitable as a pseudo-low coherence source. The ideal IFOG source spectrum is broad and Gaussian shaped so that its coherence function is narrow and free of side lobes. The same requirement applies to optical coherence tomography (OCT) sources [109, 110, 111]. The spectrum of the stretched pulse laser, while broad, has an irregular shape that is not easily controlled and can vary with environmental conditions. In principle, standard thin film optical filters could be designed to reshape the spectrum and yield a smooth Gaussian profile. However, the complexity of the shape and environmental instability of the spectrum make this impractical. A dynamically and arbitrarily programmable filter is much more appropriate. Such filtering has been demonstrated in [113]. But because it relies on angular dispersion of prisms and a spatial light modulator (SLM), optical alignment is generally difficult and prohibits its viability outside the laboratory.

The technique presented here performs the filtering in the time domain instead of the spatial domain. All components are fiber pigtailed and therefore require no physical alignment. The prisms and SLM are replaced with their time domain analogs, a highly dispersive FBG and a lithium niobate amplitude modulator driven by a programmable arbitrary waveform generator. Similar techniques have been demonstrated for communications purposes, in which the dispersive element consists of tens of kilometers of fiber [114].

1.4 Summary

The experiments presented in this thesis demonstrate optical pulse manipulation and generation through linear effects and devices. As communications systems and devices advance, new phenomena will surface and give rise to new applications in all optical technologies.

Chapter 2

Polarization Mode Dispersion Background and Experimental Methods

A major challenge of designing high speed fiber optic communication systems is dealing with pulse broadening effects. This chapter describes the modeling and latest methods of alleviating a distortion mechanism that arises from random polarization disturbances in optical fiber. Known as "polarization mode dispersion" (PMD), it has recently been recognized as a dominant performance limiting factor in 10 Gb/s and 40 Gb/s systems.

2.1 Introduction to Polarization Mode Dispersion

PMD is the result of birefringence in optical fiber. Physical origins are illustrated in Figure 2-1. The total birefringence is due to the combination of two major categories of effects: intrinsic manufacturing defects such as core ellipticity and internal strain, and external stresses caused by cabling and laying.

A simple form of PMD is uniform birefringence in a short section of fiber. This can be considered a multiple order retardation plate, the birefringence of which defines two eigenstates. Each axis is associated with a distinct group delay (see Figure 2-

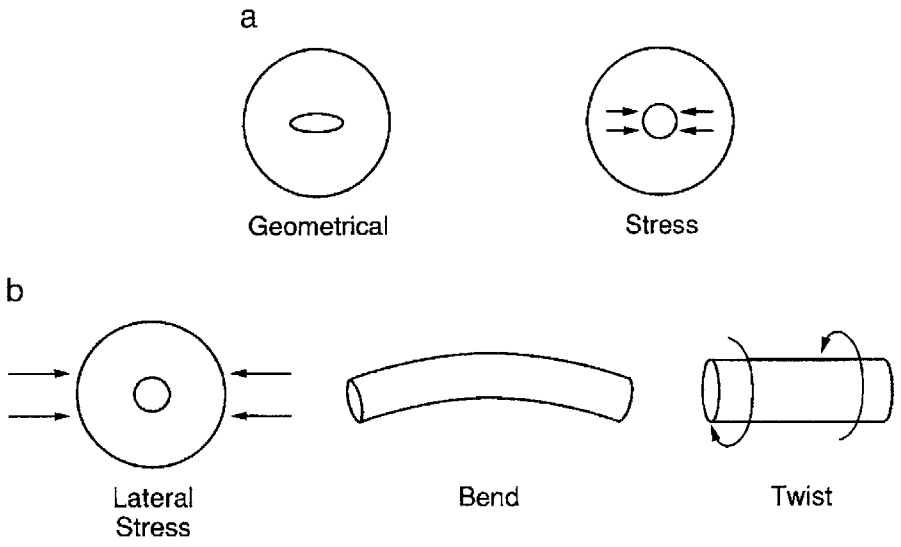

Figure 2-1: (a) Intrinsic and (b) extrinsic mechanisms of fiber birefringence (reproduced with permission from [10] copyright ©1997 by AT&T).

2). When both eigenstates are excited, the total pulse envelope undergoes temporal broadening.

PMD generally refers to the concatenation of a large number of randomly sized and oriented birefringent elements. The result of the concatenation is a more complicated polarization transformation than that of a single retarder (see Figure 2-3). The state of polarization (SOP) at the output of the fiber need not have a deterministic relation to the input. Additionally, it is highly sensitive to phase disturbances along the fiber and the degrees of freedom will drift with temperature and stress.

A phenomenological model for PMD was first described by Poole and Wagner in 1986 [4]. They showed that PMD does bear some resemblance to a single birefrigent section. To first order, there exist two orthogonal principal states of polarization (PSPs) which behave similarly to the eigenstates of a birefringent fiber. If one launches a pulse whose polarization is aligned with a PSP, it undergoes no distortion (to first order). But if both principal states are excited, the pulse is split into two orthogonally polarized components, each separated by a differential group delay (DGD). This is illustrated in Figure 2-4. PSPs differ from the eigenstates of

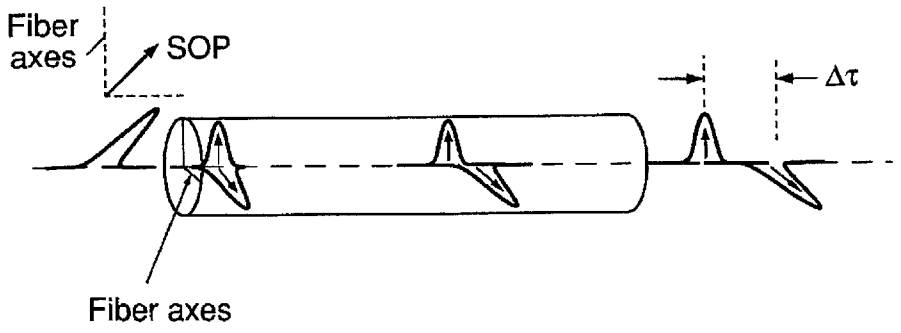

Figure 2-2: Time-domain effect of simple polarization mode dispersion in a birefringent section of fiber (reproduced with permission from [10] copyright ©1997 by AT&T).

a short birefringent section, however, in that eigenstates remain constant throughout the propagation length. PSPs are instead transformed randomly and are not correlated at the input and output ends of the fiber.

2.2 Polarization Representations

Polarization analyses are most conveniently expressed in either Jones or Stokes space. Before presenting a PMD model, we first review these polarization representations.

2.2.1 Jones Calculus

A common representation of state of polarization (SOP) is the Jones vector, introduced by R. C. Jones in 1941 [15, 16, 17, 18]:

$$\vec{E} = \begin{bmatrix} E_x e^{i\xi_x} \\ E_y e^{i\xi_y} \end{bmatrix} \tag{2.1}$$

E_x and E_y are the $\hat{x}$ and $\hat{y}$ components of the electric field vector and $\Delta\xi = \xi_y - \xi_x$ is their relative phase. Absolute phase is not necessarily preserved in this description.

Polarization state transformations are expressed by 2×2 complex Jones matrices.

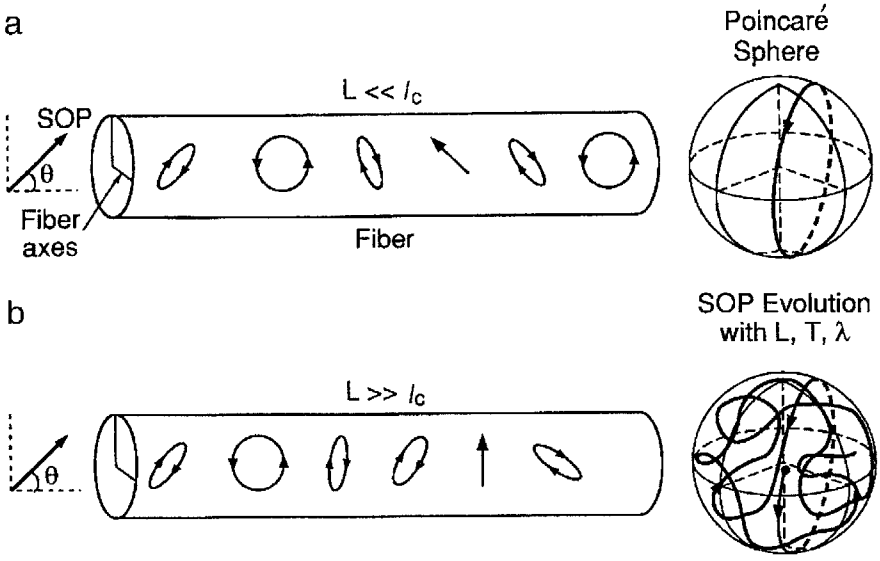

Figure 2-3: Output polarization evolution for (a) a simple birefringent section and (b) a concatenation of random birefringent sections under varying length, temperature, or wavelength (reproduced with permission from [10] copyright ©1997 by AT&T).

The transformation matrix of a lossless birefringent wave plate is unitary and has only one degree of freedom, again because we ignore absolute phase:

$$\begin{bmatrix} e^{-i\phi/2} & 0 \\ 0 & e^{i\phi/2} \end{bmatrix} \tag{2.2}$$

ϕ represents the retardation. For example, $\phi = \pi/2$ corresponds to a quarter-wave plate.

The matrix for a rotatable wave plate takes the form:

$$R(-\theta) \begin{bmatrix} e^{-i\phi/2} & 0 \\ 0 & e^{i\phi/2} \end{bmatrix} R(\theta) \tag{2.3}$$

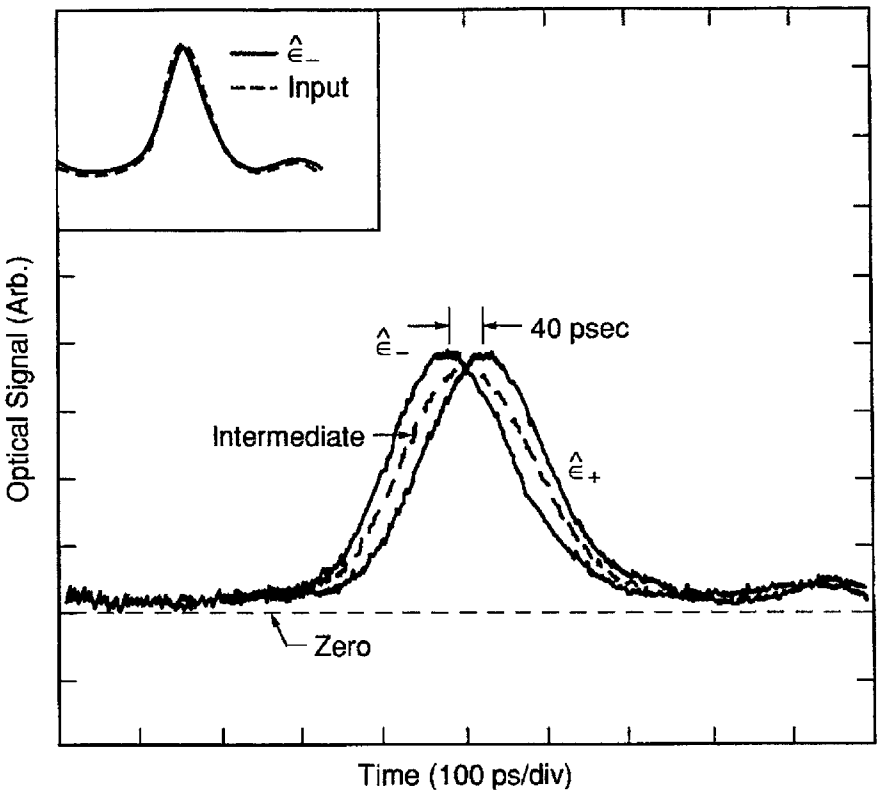

Figure 2-4: Measured differential delay time due to PMD in 10 km of dispersion-shifted fiber (reproduced with permission from [6] copyright ©1988 Optical Society of America).

where $R(\theta)$ is the rotation matrix

$$R(\theta) = \begin{bmatrix} cos(\theta) & -sin(\theta) \\ sin(\theta) & cos(\theta) \end{bmatrix} \tag{2.4}$$

A half-wave plate therefore rotates a linear SOP by 2θ. For instance, an $\hat{x}$ SOP rotated by a half-wave plate oriented $\theta = \pi/4$ is transformed into a $\hat{y}$ SOP. In Jones space, this is stated as the following:

$$i\begin{bmatrix} 0 \\ 1 \end{bmatrix} = \begin{bmatrix} \frac{1}{\sqrt{2}} & \frac{1}{\sqrt{2}} \\ -\frac{1}{\sqrt{2}} & \frac{1}{\sqrt{2}} \end{bmatrix}\begin{bmatrix} -i & 0 \\ 0 & i \end{bmatrix}\begin{bmatrix} \frac{1}{\sqrt{2}} & -\frac{1}{\sqrt{2}} \\ \frac{1}{\sqrt{2}} & \frac{1}{\sqrt{2}} \end{bmatrix}\begin{bmatrix} 1 \\ 0 \end{bmatrix} \tag{2.5}$$

The $\frac{\pi}{2}$ absolute phase of the vector does not affect the SOP.

2.2.2 Stokes Parameters and the Poincaré Sphere

Jones vectors and matrices are compact and relatively easy to calculate. But to gain insight it is often beneficial to use a basis which lends itself better to visual interpretations. Such a basis is formed by the normalized Stokes parameters s_1, s_2, and s_3.

To convert normalized Jones complex 2-vectors into Stokes real 3-vectors, we utilize the Pauli spin vector:

$$\hat{s} = \hat{E}^{\dagger}\vec{\sigma}\hat{E} \tag{2.6}$$

where the elements of the Pauli spin vector $\vec{\sigma}$ are the Pauli spin matrices σ_1,σ_2, and σ_3:

$$\sigma_1 = \begin{pmatrix} 1 & 0 \\ 0 & -1 \end{pmatrix} \tag{2.7}$$

$$\sigma_2 = \begin{pmatrix} 0 & 1 \\ 1 & 0 \end{pmatrix} \tag{2.8}$$

$$\sigma_3 = \begin{pmatrix} 0 & -i \\ i & 0 \end{pmatrix} \tag{2.9}$$

The elements of $\hat{s}$ can also be expressed directly by in terms of the complex electric field vectors:

$$s_1 = E_x E_x^* - E_y E_y^* \tag{2.10}$$

$$s_2 = E_x E_y^* + E_x^* E_y \tag{2.11}$$

$$s_3 = i(E_x E_y^* - E_x^* E_y) \tag{2.12}$$

The real elements s_1, s_2, and s_3 are known as the normalized Stokes parameters and define a unique SOP. Plotted as x, y, and z coordinates, a pure SOP lies on the

unit Poincaré sphere [19] and has two degrees of freedom. A sketch of the Poincaré sphere is shown in Figure 2-5. As seen in the figure, orthogonal polarizations lie on opposite ends of the sphere. Linear SOPs lie on the equator. $\hat{x}$ and $\hat{y}$ are on the right and left, while $+45$ and -45 are on the front and back. The two circular SOPs occupy the north and south poles. All other states are elliptical and fill the space in between, with right-handed states on the upper hemisphere and left-handed states in the lower.

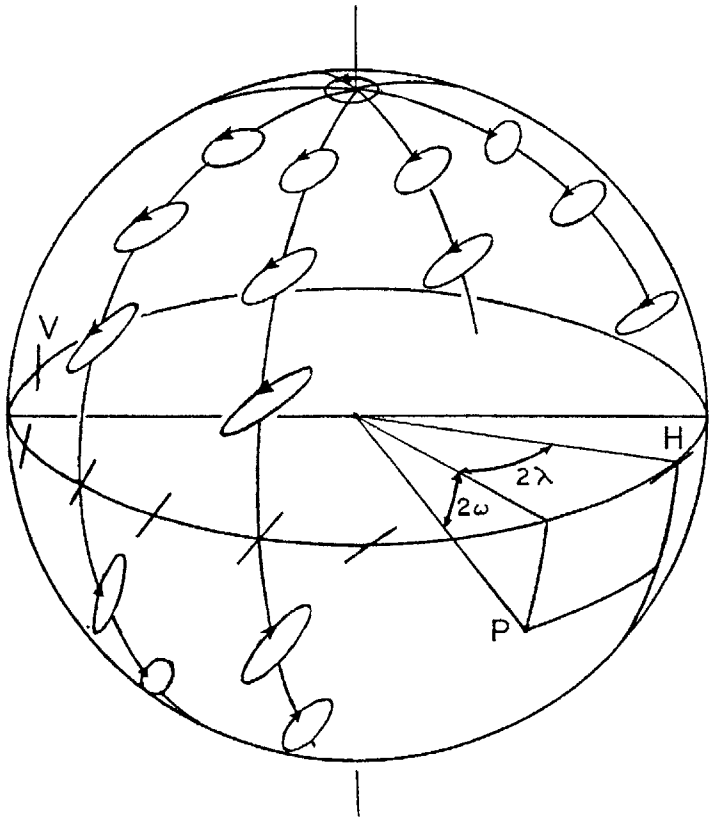

Figure 2-5: The Poincaré sphere. All points on the sphere correspond to a unique state of polarization (reproduced with permission from [17] copyright ©1962 by the President and Fellows of Harvard College).

In Stokes space, the effect of a wave plate is a simple rotation about an axis. Figure 2-6 illustrates the example of a quarter-wave plate, which corresponds to a $\frac{\pi}{2}$ rotation about an axis R within the equatorial plane. The angular orientation of the

axis is 2λ, or twice the angular orientation in real space. The two linear eigenstates R and $-R$ lie on the axis itself; therefore rotation would have no effect on them.

A wave plate combination capable of complete arbitrary transformations, that is, a device which can transform any arbitrary SOP into any other arbitrary SOP, requires at least two wave plates with appropriate retardations. An example is a $\frac{\pi}{2}$ - π - $\frac{\pi}{2}$ combination: The first quarter-wave plate rotates any SOP onto the equator if oriented properly. The half-wave plate then converts that linear SOP to any other SOP. Finally, the last quarter-wave plate rotates the SOP back to any desired state if the half-wave plate is adjusted correctly.

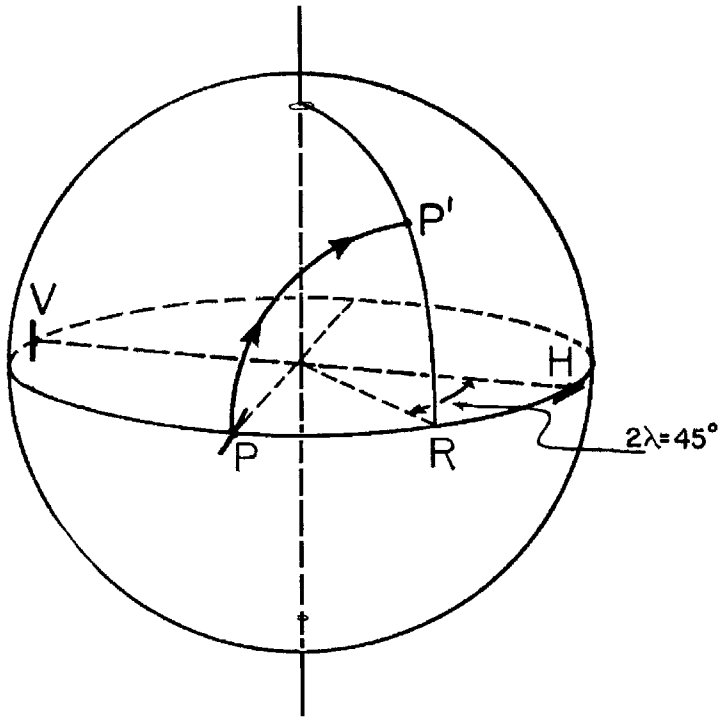

Figure 2-6: Effect of a quarter-wave plate in Stokes space. The polarization state P is rotated $\pi/2$ about the axis R, which is defined by the wave plate orientation 2λ (reproduced with permission from [17] copyright ©1962 by the President and Fellows of Harvard College).

2.3 Principal States Model

In 1986 [4] Poole and Wagner introduced the principal states model of frequency dependent PMD for a random concatenation of birefringent fiber sections. In contrast with the mode coupling model [20, 10], which predicts average DGDs, the principal states model can describe in detail the distortion of a coherent pulse.

2.3.1 Derivation of Principal States Using Group Velocity

An eigenvalue equation can be derived from a physical perspective using the concept of group velocity, as outlined in [1]. If we construct a wavepacket at the input with two polarized waves with slightly different frequencies $\vec{E}_a(\omega)$ and $\vec{E}_a(\omega+\Delta\omega)$ we can write the output as the sum of $\vec{E}_b(\omega) = T\vec{E}_a(\omega)$ and

$$\vec{E}_b(\omega+\Delta\omega) = \vec{E}_b(\omega) + \Delta\omega\frac{d}{d\omega}\vec{E}_b(\omega) \tag{2.13}$$

$$= \vec{E}_b(\omega) + \Delta\omega\left[\frac{d}{d\omega}T\right]\vec{E}_a(\omega) \tag{2.14}$$

where T is a 2 by 2 complex lossless matrix with four degrees of freedom.

In order to define a group velocity, one must track the series of electric field nulls between which the energy is trapped. Nulls will occur only if the term $\Delta\omega\frac{d}{d\omega}\vec{E}_b(\omega)$ is aligned with $\vec{E}_b(\omega)$. This gives the relation

$$\frac{d}{d\omega}\vec{E}_b = \frac{dT}{d\omega}\vec{E}_a(\omega) = \lambda\vec{E}_b(\omega) = \lambda T\vec{E}_a(\omega) \tag{2.15}$$

which leads to the eigenvalue equation

$$T^\dagger\frac{dT}{d\omega}\vec{E}_a(\omega) = \lambda\vec{E}_a(\omega) \tag{2.16}$$

2.3.2 Phenomenological Derivation of Eigenvalue Equation

This section presents the original phenomenological derivation of principal states by Poole and Wagner [4]. We rewrite the frequency dependent complex Jones matrix T

representing the transmission of light through a fiber with PMD:

$$T(\omega) = e^{\alpha(\omega)} U(\omega) \tag{2.17}$$

where

$$U(\omega) = \begin{pmatrix} u_1(\omega) & u_2(\omega) \\ -u_2^*(\omega) & u_1^*(\omega) \end{pmatrix} \tag{2.18}$$

and $\alpha(\omega)$ is a complex quantity. $u_1(\omega)$, $u_2(\omega)$ are normalized such that

$$|u_1|^2 + |u_2|^2 = 1 \tag{2.19}$$

In general the matrix T contains eight degrees of freedom. However, we impose losslessness and a reference phase onto the matrix U, leaving it with three adjustable parameters. The imaginary part of α adjusts the phase of T. Although polarization dependent loss (PDL) is not included, frequency dependent loss appears as a fifth degree of freedom, the real part of α. For a lossless T, α would be a pure imaginary number, and T would contain only four degrees of freedom.

The T matrix relates the input and output electric field vectors of a fiber:

$$\vec{E}_b(\omega) = T(\omega)\vec{E}_a(\omega) \tag{2.20}$$

where $\vec{E}_a$ and $\vec{E}_b$ are the Jones vectors at the input and output, respectively. Each can be expressed in terms of a normalized Jones vector $\hat{E}$, phase ϕ, and scalar magnitude E:

$$\vec{E}_a = \begin{bmatrix} E_a^x \\ E_a^y \end{bmatrix} = E_a e^{i\phi_a} \hat{E}_a \tag{2.21}$$

$$\vec{E}_b = \begin{bmatrix} E_b^x \\ E_b^y \end{bmatrix} = E_b e^{i\phi_b} \hat{E}_b \tag{2.22}$$

The normalized Jones vectors $\hat{E}_a$ and $\hat{E}_b$ are of the form:

$$\hat{E}_a = \begin{bmatrix} a_x \\ a_y e^{i\phi_a^{xy}} \end{bmatrix} \tag{2.23}$$

$$\hat{E}_b = \begin{bmatrix} b_x \\ b_y e^{i\phi_b^{xy}} \end{bmatrix} \tag{2.24}$$

$$\tag{2.25}$$

where $\phi_{a,b}^{xy}$ are relative phases between the x and y components, and the amplitudes are normalized such that $(a_x^2 + a_y^2) = (b_x^2 + b_y^2) = 1$.

In [4], an eigenvalue equation is derived in the following manner. The derivative of Equation 2.20 with respect to frequency yields:

$$\frac{d\vec{E}_b}{d\omega} = \frac{dT}{d\omega}\vec{E}_a = e^{\alpha(\omega)}(\alpha'(\omega)U + U')\vec{E}_a \tag{2.26}$$

where the prime indicates differentiation with respect to frequency. We assume the input polarization $\vec{E}_a$ is fixed. Differentiating Equation 2.22 also gives us

$$\frac{d\vec{E}_b}{d\omega} = \left(\frac{E_b'}{E_b} + i\phi_b'\right)\vec{E}_b + E_b e^{i\phi_b}\frac{d\hat{E}_b}{d\omega} \tag{2.27}$$

Then, combining Equations 2.26 and 2.27 with the help of 2.17 and 2.20 allows us to write

$$E_b e^{i\phi_b}\frac{d\hat{E}_b}{d\omega} = e^{\alpha}(U' - ikU)\vec{E}_a \tag{2.28}$$

where

$$k = \phi_b' + i\left(\alpha' - \frac{E_b'}{E_b}\right) \tag{2.29}$$

A condition of zero dispersion sets the left-hand side of Equation 2.28 to zero, and we are left with the eigenvalue equation

$$(U' - ikU)\hat{E}_a = 0 \tag{2.30}$$

as written by Poole, or equivalently

$$(U^{\dagger}U' - ikI)\hat{E}_a = 0 \tag{2.31}$$

This is the same as equation 2.16.

By setting the determinant of the matrix $(U_{\omega}U^{\dagger} - ikI)$ to zero, we can determine the eigenvalues to be

$$k_{\pm} = \pm\sqrt{|u_1'|^2 + |u_2'|^2} \tag{2.32}$$

The eigenvectors are the principal states, with a group delay difference $\Delta\tau$ of $2\sqrt{|u_1'|^2 + |u_2'|^2}$. They are found by inserting the eigenvalues back into equation 2.30, yielding

$$\hat{E}_{a\pm} = e^{i\rho}\begin{bmatrix} \frac{[u_2' - ik_{\pm}u_2]}{D_{\pm}} \\ -\frac{[u_1' - ik_{\pm}u_1]}{D_{\pm}} \end{bmatrix} \tag{2.33}$$

ρ is an arbitrary phase and $D_{\pm}$ is given by

$$D_{\pm} = \sqrt{2k_{\pm}(k_{\pm} - Im[u_1^*u_1' + u_2^*u_2'])} \tag{2.34}$$

The value of $\Delta\tau$ is derived from $\phi_{b\pm}$ by recognizing the conditions to satisfy equations 2.29 and 2.32:

$$\frac{E_{b+}'}{E_{b+}} = \frac{E_{b-}'}{E_{b-}} = Re[\alpha'] \tag{2.35}$$

$$\phi_{b\pm}' = \tau_{\pm} = Im[\alpha'] \pm \sqrt{|u_1'|^2 + |u_2'|^2} \tag{2.36}$$

where $\phi_{b\pm}'$ are the group delay times for the two principal states. Note that in the case of lossless T, $Re[\alpha] = 0$ and the magnitudes $E_{b\pm}$ do not change, as indicated in 2.35.

Since we assume that there is no PDL in the system, we can write

$$\Delta\tau = \tau_+ - \tau_- = 2\sqrt{|u_1'|^2 + |u_2'|^2} \tag{2.37}$$

The principal states form an orthonormal polarization basis, suitable for decom-

position of an input polarization:

$$\begin{aligned}\vec{E}_a(t) &= E_a e^{i\omega t}\hat{E}_a \\ &= E_a e^{i\omega t}[c_+(\omega)\hat{E}_{a+}(\omega) + c_-(\omega)\hat{E}_{a-}(\omega)]\end{aligned} \tag{2.38}$$

The weighting constants are simply the projections onto the principal states:

$$c_\pm(\omega) = \hat{E}_a \cdot \hat{E}^*_{a\pm}(\omega) \tag{2.39}$$

At the output, the decomposition is similarly

$$\vec{E}_b(t) = E_a e^{(i\phi+i\omega t)}[e^{i\Delta\phi}c_+(\omega)\hat{E}_{b+}(\omega) + c_-(\omega)\hat{E}_{b-}(\omega)] \tag{2.40}$$

2.3.3 The $\vec{\Omega}$ Vector

In Stokes space, the principal states are represented by a general $\vec{\Omega}$ vector which points in the direction of the slow PSP, and whose magnitude is equal to the differential group delay $\Delta\tau$. The distances d_+ and d_- of an SOP from the PSPs on the Poincaré sphere is dictated by its weighting constants c_+ and c_-

$$\frac{|c_-(\omega)|^2}{|c_+(\omega)|^2} = \frac{d_-}{d_+} \tag{2.41}$$

The evolution of an output SOP is described by the differential equation:

$$\frac{d\vec{s}}{d\omega} = \vec{\Omega} \times \hat{s} \tag{2.42}$$

where $\vec{\Omega}$ defines the direction and speed of rotation, and $\hat{s}$ is the output SOP that precesses around $\vec{\Omega}$. It is determined by $\Delta\tau$ and the principal states P_+ and P_-:

$$\vec{\Omega} = \frac{d\Delta\phi}{d\omega}\hat{P}_{b-} = \frac{d}{d\omega}(\phi_+ - \phi_-)\hat{P}_{b-} \tag{2.43}$$

where

$$\Delta\tau = \tau_+ - \tau_- = \frac{d\Delta\phi}{d\omega} \tag{2.44}$$

From 2.43 and 2.44 we can see that

$$|\vec{\Omega}| = \Delta\tau \tag{2.45}$$

2.3.4 Dynamical Equation

In [5], Poole et al derive a dynamical equation which relates the frequency dependence of $\vec{\Omega}$ with its evolution along the fiber length z. The derivation starts by stating the individual dependences of the polarization state $\hat{s}$:

$$\frac{\partial\hat{s}}{\partial z} = \vec{W}(\omega, z) \times \hat{s} \tag{2.46}$$

$$\frac{\partial\hat{s}}{\partial\omega} = \vec{\Omega}(\omega, z) \times \hat{s} \tag{2.47}$$

$\vec{W}$ is the local birefringence in the fiber due to any number of effects such as manufacturing defects and strain (see Figure 2-1). By taking the derivative of 2.46 with respect to ω and of 2.47 with respect to z, and with the help of the vector identity

$$(a \times b) \times c = a \times (b \times c) - b \times (a \times c) \tag{2.48}$$

we arrive at the dynamical equation

$$\frac{\partial\vec{\Omega}(z,\omega)}{\partial z} = \frac{\partial\vec{W}(z,\omega)}{\partial\omega} + \vec{W}(z,\omega) \times \vec{\Omega}(z,\omega) \tag{2.49}$$

2.3.5 Concatenation Rules in Stokes Space

A proof of the simple rules for concatenation of $\vec{\Omega}$ vectors is outlined by Gordon and Kogelnik in [11]. We begin by defining R as the relation between the input SOP $\hat{s}$

and output SOP $\hat{t}$ of a PMD medium in Stokes space:

$$\hat{t} = R\hat{s} \tag{2.50}$$

R is related to the Jones space U matrix by the spin vector $\vec{\sigma}$:

$$R\vec{\sigma} = U^{\dagger}\vec{\sigma}U \tag{2.51}$$

The PMD vectors at the input, $\vec{\Omega}$, and at the output, $\vec{\Omega}_s$ are also related by R:

$$\vec{\Omega} = R\vec{\Omega}_s \tag{2.52}$$

$\vec{\Omega}$ is expressed as a function of R in [11] as

$$\vec{\Omega}\times = R_{\omega}R^{\dagger} \tag{2.53}$$

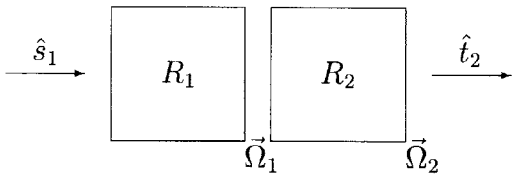

Figure 2-7: Concatenation of two PMD sections R_1 and R_2, each with their own $\vec{\Omega}$ vectors.

Now we let R be a combination of two PMD sections R_1 and R_2, each with their own respective $\vec{\Omega}_1$ and $\vec{\Omega}_2$.

$$R = R_2R_1 \tag{2.54}$$

According to 2.53, the $\vec{\Omega}$ vector of the combination is

$$\vec{\Omega}\times = R_{\omega}R^{\dagger} = R_{2\omega}R_1R_1^{\dagger}R_2^{\dagger} + R_2R_{1\omega}R_1^{\dagger}R_2^{\dagger} \tag{2.55}$$

Since $R_1 R_1^\dagger = 1$, and by applying 2.53 and the relation

$$(R_2\vec{\Omega}_1)\times = R_2(\vec{\Omega}_1\times)R_2^\dagger \tag{2.56}$$

we can simplify 2.55 to yield

$$\vec{\Omega} = \vec{\Omega}_2 + R_2\vec{\Omega}_1 \tag{2.57}$$

This concatenation rule is conveniently simple and intuitive, and can be generalized to the sum rule for concatenation of many sections:

$$\vec{\Omega} = \sum_{n=1}^{m} R(m, n+1)\vec{\Omega}_n \tag{2.58}$$

2.4 Characterization Techniques

Initial ideas for characterizing first order PMD came about quickly [21, 22], and by 1997 PMD compensating (PMDC) methods surfaced as well [37, 36]. A turning point occured in the late 1990's when a massive push toward OC192 (10 Gb/s) and OC768 (40 Gb/s) channel rates materialized due to demand from the explosive growth of Internet traffic. A clear indication of the demand was seen at OFC (Optical Fiber Communications conference) 1999, where much work was presented by labs at Lucent, Alcatel [49, 40], Siemens [38], and others. By then PMD characterization techniques had become more sophisticated and included higher order PMD [2] and the use of Rayleigh scattering [23, 24, 25] to enable field diagnostics. Today the work continues and new compensation devices and schemes have also surfaced since then [41, 42, 44].

The compensation scheme to be discussed in Chapter 3 relies on a simple real-time characterization technique. Older and more comprehensive techniques already exist, but they are mainly for laboratory use and field tests. They range from interferometric and fringe counting methods to electrical analysis of the detected signal. The most common ones are the Poincaré sphere method [26, 27], the Jones Matrix eigenanalysis (JME) method [21, 22], and the Müller matrix method (MMM) [2].

2.4.1 Poincaré Sphere Method

The Poincaré sphere method measures the precession of an output SOP about $\vec{\Omega}(\omega)$ as a function of frequency. Using two different input SOPs, the corresponding output SOPs $\hat{s}_i$ and $\hat{s}_j$ are measured at each frequency. By evaluating the cross product of the two derivatives, one can determine the axis of rotation for a given ω. Equation 2.42 provides the calculation of $\vec{\Omega}(\omega)$:

$$\vec{\Omega} = \frac{\frac{d\vec{S}_i}{d\omega} \times \frac{d\vec{S}_j}{d\omega}}{\left[\frac{d\vec{S}_i}{d\omega} \cdot \hat{s}_j\right]} \tag{2.59}$$

which is derived from Equation 2.42 and the vector identity $a \times b \times c = (a \cdot c)b - (b \cdot a)c$.

The normalized principal states are parallel and anti-parallel to $\vec{\Omega}$:

$$\hat{P}_{b-} = -\hat{P}_{b+} = \frac{\vec{\Omega}}{|\vec{\Omega}|} \tag{2.60}$$

2.4.2 Jones Matrix Eigenanalysis and Müller Matrix Method

The Jones Matrix Eigenanalysis (JME) [21, 22] and the Müller Matrix Method (MMM) [2] are both very comprehensive techniques which provide full characterization of the PMD in a fiber. They measure the polarization rotation for individual wavelengths within a desired range, and by examining derivatives with respect to frequency, the PSPs and DGD can be found, as well as high order PMD parameters.

The JME method is outlined by Heffner in [21]. Three distinct SOPs are injected into the fiber under test: horizontal, vertical, and 45 degrees. A Jones matrix is calculated from the constants k_i which are derived from polarimeter measurements at the output for each of the three inputs. They are defined in terms of the $\hat{x}$ and $\hat{y}$ components of three output SOPs h, v, and q corresponding to the three input SOPs:

$$k_1 = \frac{h_x}{h_y} \tag{2.61}$$

$$k_2 = \frac{v_x}{v_y} \tag{2.62}$$

$$k_3 = \frac{q_x}{q_y} \tag{2.63}$$

$$k_4 = \frac{k_3 - k_2}{k_1 - k_3} \tag{2.64}$$

The Jones matrix T is then

$$T = \beta \begin{bmatrix} k_1 k_4 & k_2 \\ k_4 & 1 \end{bmatrix} \tag{2.65}$$

where β is an arbitrary complex number.

To calculate the DGD, an approximate form of the eigenvalue equation (Equation 2.30) is used:

$$[T(\omega + \Delta\omega)T^{-1}(\omega) - (1 + i\tau_g \Delta\omega)I]E_b = 0 \tag{2.66}$$

If the $\tau_g \Delta\omega$ corresponding to each of the eigenvalues is small, then $1 + i\tau_g \Delta\omega \approx exp(i\tau_g \Delta\omega)$ and the DGD $\Delta\tau$ can be written as

$$\Delta\tau = |\tau_{g,1} - \tau_{g,2}| = \left| \frac{Arg(\rho_1/\rho_2)}{\Delta\omega} \right| \tag{2.67}$$

where ρ_1 and ρ_2 are the eigenvalues of Equation 2.66.

The MMM method is similar, except that it requires only two input SOPs. All calculations are done in Stokes space, making the algorithms more simple. The concept is similar to the Poincaré sphere technique, but large $\Delta\omega$ steps are allowed, reducing sensitivity to measurement noise. It accomplishes this by calculating the full rotation matrices for each wavelength, and can exhibit high precision using interleaving techniques.

All of these methods are useful for laboratory measurements, but their speed is limited. Because they require wavelength scanning, a single measurement requires several minutes and drifting of the fiber properties could occur during that time, distorting the measurement.

2.5 PMD Compensation

The current feedback-based PMD compensators come in a variety of shapes and flavors. All fit into one of four categories outlined by Karlsson et al in [42]:

1. Alignment of input signal and PSP
2. First-order PMD compensation with a tunable DGD
3. First-order PMD compensation with a fixed DGD
4. The use of a polarizer

In recent research, the most commonly demonstrated method, because of its relative ease of implementation, is of the fixed DGD type (number 3). It was first demonstrated by Takahashi et al [45] and further pursued by researchers at Alcatel [49, 50], AT&T [46, 47], and Nortel [48]. The basic setup is shown in Figure 2-8.

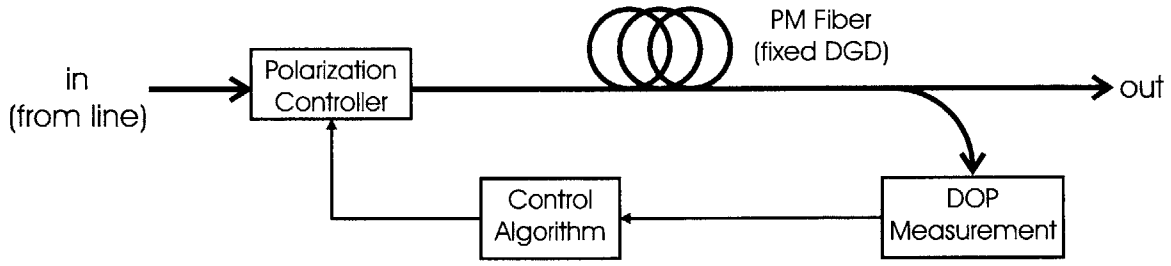

Figure 2-8: Fixed DGD compensator.Although initially nonintuitive, this design is capable of compensating PMD with a range of DGD values.

The corrupted signal is sent through a polarization controller and then a fixed DGD component such as a length of polarization maintaining fiber. The signal distortion is then monitored via a coupler and a polarimeter which monitors degree of polarization (DOP), defined by the polarized and unpolarized optical power as:

$$DOP \equiv \frac{P_{polarized}}{P_{polarized} + P_{unpolarized}} \tag{2.68}$$

A computer optimizes the polarization controller to maximize the DOP, or equivalently minimize the PMD.

The diagram is deceiving at first glance. One is inclined to assume that the optimal operating point is always when the polarization controller has aligned the fiber PSPs anti-parallel to the polarization-maintaining (PM) fiber axes. This is only true when the transmission line DGD equals the compensator DGD, however, and is illustrated in Figure 2-9a where the DGD corresponds to the lengths of the PMD vectors Ω_{comp} and Ω_{line}. But the line PMD varies with time and is not necessarily the same magnitude as the fixed compensator PMD. As shown in Figure 2-9b, the general effect of the polarization controller is to rotate Ω_{comp} so that at the transmitter frame of reference the input signal and the resultant $\Omega_{comp} + \Omega_{line}$ are aligned. This results in the excitation of only one PSP. Because the PMF DGD is not adjustable, the resultant $\vec{\Omega}$ may be large, leaving high order PMD present. The consequence is that if the PMD is small to begin with, the performance can actually be worse than if the compensator were not there (see Figure 2-10).

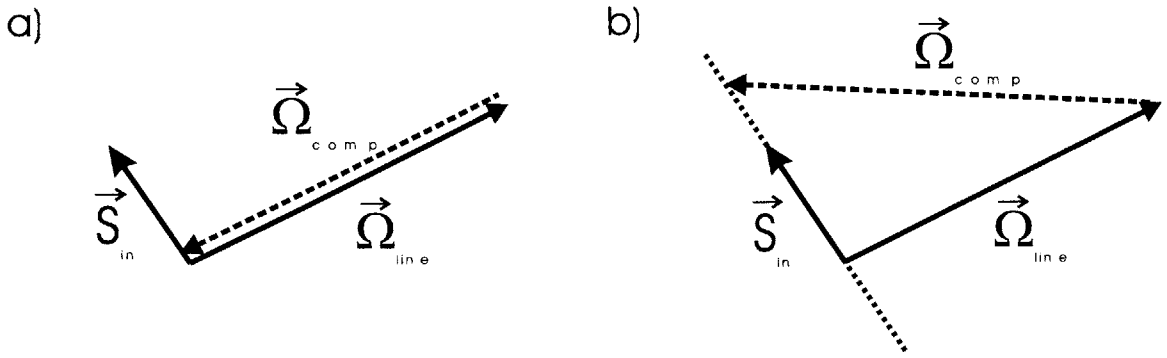

Figure 2-9: PMD vectors of the transmission line $\vec{\Omega}_{line}$ and the compensator $\vec{\Omega}_{comp}$. In a), $|\vec{\Omega}_{line}| = |\vec{\Omega}_{comp}|$ and the resultant can be zero. In b), $|\vec{\Omega}_{comp}|$ is fixed, while $|\vec{\Omega}_{line}|$ wanders. DOP optimization aligns the resultant with the input polarization state $\vec{S}_{in}$.

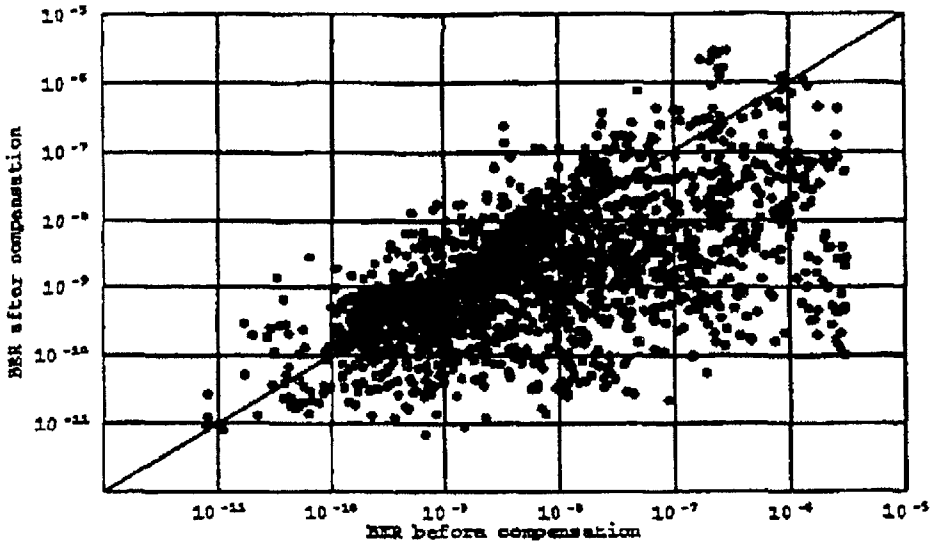

Figure 2-10: Results of measurements using the fixed DGD compensator in an installed system (reproduced with permission from [40] copyright ©1999 Optical Society of America). Data points above the line of unit slope indicate that the compensator sometimes degrades performance.

2.5.1 RF Spectrum

An alternative to the DOP measurement is to monitor the RF spectrum. In the time domain, PMD convolves the pulse envelope with a pair of delta functions separated by the DGD. The associated action in the RF domain is a sinusoidal modulation envelope on top of the NRZ data spectrum. The period of the envelope depends on the DGD. Figure 2-11 shows examples of these envelopes for various DGDs and relative excitation of PSPs.

By measuring RF power in selected subharmonic bands, one can extract a measure of pulse quality. This technique has been used in research demonstrations [51].

2.5.2 Reset-Free Polarization Control Algorithms

For the feedback-based compensators to work, they must employ a class of polarization control algorithms known as reset-free algorithms. Ideally, an inherently endless polarization controller can be constructed from wave plates. In practice, however,

electrically driven devices such as liquid crystal, electro-optic, and piezoelectric devices are preferred for their speed and robustness. Unlike wave plates, electrical devices have a limited range of tolerable input voltages. A hiccup due to the wrap-around of a voltage signal is not acceptable. Heismann et al [52] and Weber et al [53] have demonstrated reset-free algorithms which alleviate this problem. The challenges of these algorithms are discussed further in Section 3.1.2.

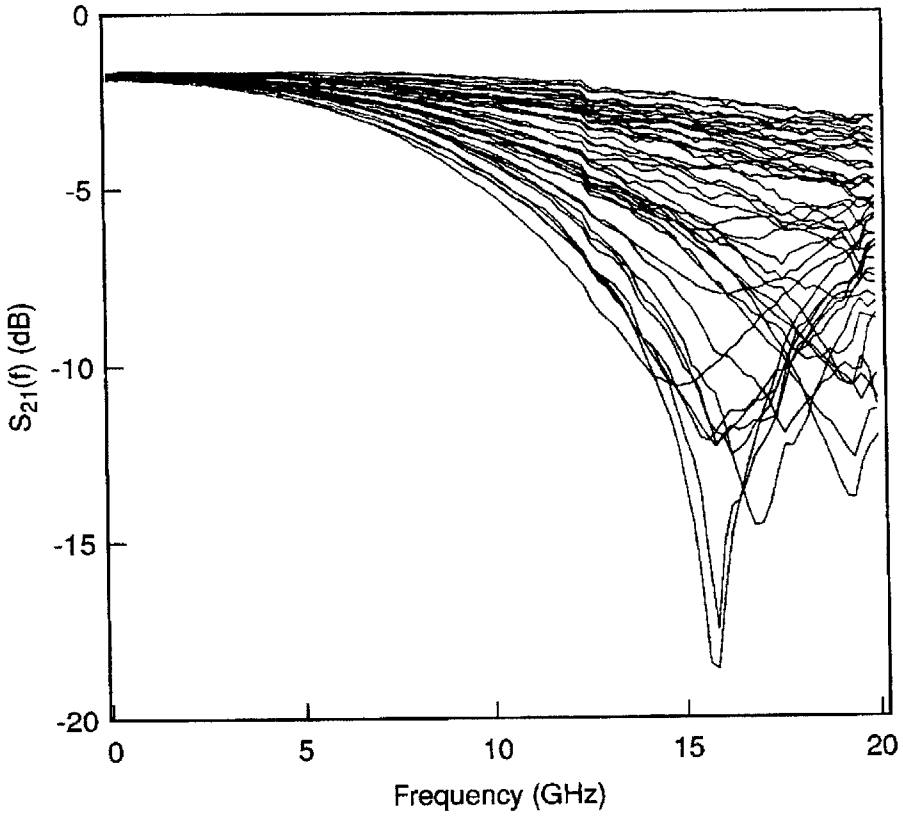

Figure 2-11: PMD causes an echo in the time domain. The result in the pulse envelope RF spectrum is sinusoidal filtering. These measurements (from [10]) were taken by an externally modulated laser, a fiber with 23 ps of average DGD, and a photodiode. The RF response is measured with a network analyzer. Various levels of DGD and PSP excitation are shown.

Chapter 3

Real-Time PMD Characterization and Feedback-Free Compensation

As we have seen in Chapter 2, PMD is a complicated phenomenon modeled by a theory rich enough to support countless analyses and experimental techniques. While the research community sees opportunities for interesting problems to solve, it is the bane of communication system designers, who would be much happier if PMD never existed.

For the past few years, there has been considerable effort to develop PMD compensators, but at the time of this writing there still does not exist a clearly successful product on the market. That this is true, despite the immense funding and manpower thrust into this problem by large corporations and venture capitalists alike, is an indication that the problem is more difficult than it may first appear. Much frustration is derived from the multi-parameter feedback system that comprises a standard compensator. And when higher order PMD is considered, more parameters must be added and will exacerbate the problem. This chapter presents methods for circumventing the use of feedback in an effort to simplify the compensator design.

3.1 Limitations in Current Compensators

The central idea of this chapter is to eliminate or reduce the feedback in a PMD compensator. This section describes the problems with current feedback techniques and develops the reasons for investigating feedback-free techniques.

3.1.1 Speed Requirements

PMD varies with time and thus requires dynamic compensators. Measurements show [14, 46] that there are two basic components. The first is a slow drift due to daily temperature cycles, which causes changes occuring over several minutes (see Figure 3-1). The second is due to vibrations in the fiber, which can appear when someone handles the fiber cable itself. This can happen wherever the fiber is exposed, for instance at the central office. These variations contain fluctuations at a millisecond time scale and have been measured in installed cables, as seen in Figure 3-2.

While the use of faster optical devices can improve overall speed, many systems are still limited by the speed of its feedback circuitry. Therefore, the elimination or reduction of feedback would be beneficial to operation speed.

3.1.2 Reset-Free Algorithms

A major drawback of current compensation techniques is the difficulty of smooth search algorithms. Stable reset-free algorithms are inherently difficult, as described in [53] and [52]. The problem is the following: To track a moving target polarization state, one can envision following a corresponding point on the Poincaré sphere by dithering control voltages one at a time. Dithering in this case could refer to applying slight offsets, both positive and negative. The distance from the target on the Poincaré sphere would be measured and the offset yielding the closer point would be adopted.

This can work well even though the feedback parameters are usually coupled to each other. But problems arise if the target travels a cyclical path. For instance, it may walk along the Poincaré equator infinitely. Rotating waveplates can handle this and are adequate for laboratory polarization controllers, but commercial controllers

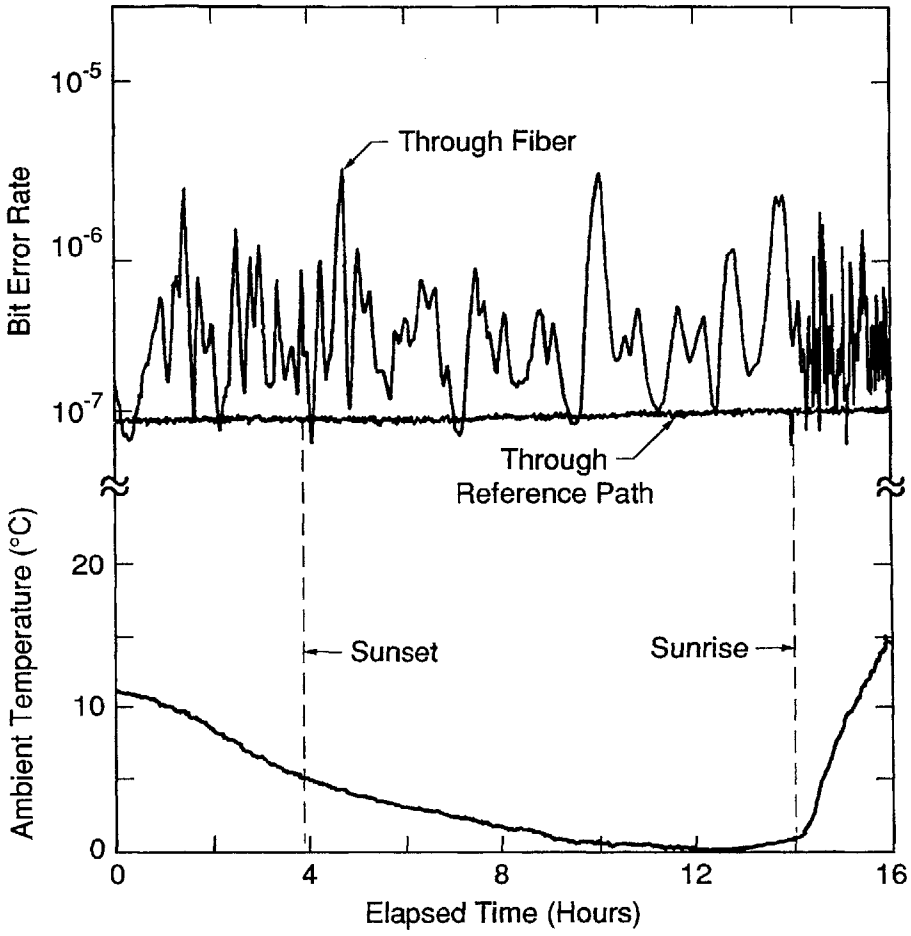

Figure 3-1: Slow variations of PMD parameters in an installed fiber cable due to thermal fluctuations between night and day (reproduced with permission from [8] copyright ©1991 IEEE).

consist of faster elements which function as variable retardation plates in which the applied voltage controls the retardation ϕ (see Equation 2.2). Each element, then, is not inherently cyclical and has voltage limits. Therefore, when a control voltage reaches a maximum or minimum, it must be reset without inducing errors in the output polarization.

First order PMD compensators employing this type of polarization tracking have been pursued for years [50, 38, 41, 37, 54]. With the exception of the technique described in [44], all schemes [42, 43] rely on similar feedback loops containing several

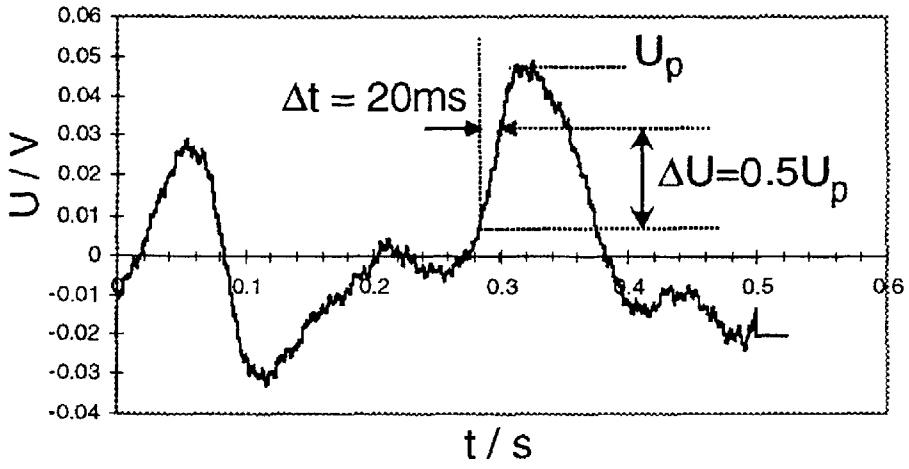

Figure 3-2: Millisecond level variations in PMD parameters (reproduced with permission from [14] copyright ©1999 Optical Society of America). Fluctuations at this scale are presumably due to cable handling inside central offices.

control parameters. In the polarization controllers, redundant control elements are added so that one element can gradually be pulled back to the middle of its range, while the others compensate for this and continue to track the target. Accuracy is affected, however. And if more than one voltage reaches a limit simultaneously, the device could lose its ability to track. One could argue that such occurences are rare, but outage probability requirements for communications systems are extremely stringent. In short, resets are unacceptable and a pseudo-endless algorithm employing redundancy does not necessarily guarantee an acceptable outage rate.

In addition to first order PMD, high order PMD has also been recognized as a limitation in future 40 Gb/s systems. Even with first order compensators distributed along a transmission line, the high order PMD will still accumulate and ultimately limit the line length and capacity [28]. The problems with feedback-based compensation become even more severe when high order PMD compensation is addressed, and further highlight the importance of simplifying the operation of a compensator by avoiding the use of feedback.

3.1.3 Feedback-Free Compensation Schemes

A simple diagram for a feedback-free compensation scheme is shown in Figure 3-3. The polarization state of an optical source is rapidly modulated or scrambled before encountering PMD on a fiber. The received signal is analyzed by a polarimeter and a compensation device is adjusted to remove the PMD. A compensator using this approach can quickly adjust for changes in PMD parameters such as principal states of polarization (PSP) and differential group delay (DGD).

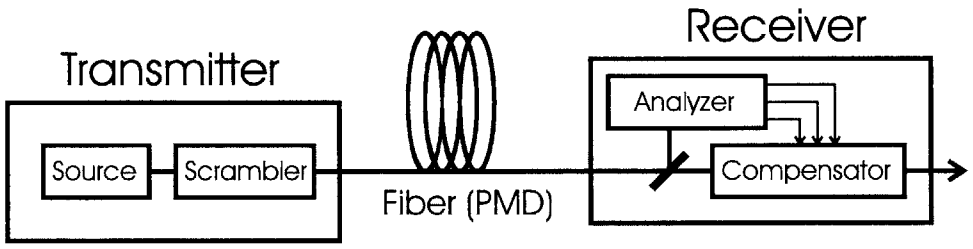

Figure 3-3: Basic concept of a feedback-free PMD compensator.

Figure 3-4 shows variations of Figure 3-3, in which different levels of feedback are employed. In a), the PSPs are characterized and compensated without feedback. The DGD, however, is left as an independent variable to be compensated with feedback, utilizing a second polarimeter for a monitor signal. b) and c) display systems which are almost entirely feedback-free, except the characterization technique is not able to determine the sign of the DGD on its own. b) also uses a second polarimeter, and c) compares the pulse envelope phases of the two PSPs, separated by a polarization beamsplitter (PBS) inside the variable DGD device. d) shows a fully feedback-free system which preprocesses the signal with a fixed known PMD. As long as this reference DGD is larger than the incoming PMD, it will shift the $\vec{\Omega}$ vector into a region where the net resultant PMD is of only one sign. This technique is discussed further in Section 3.2.4.

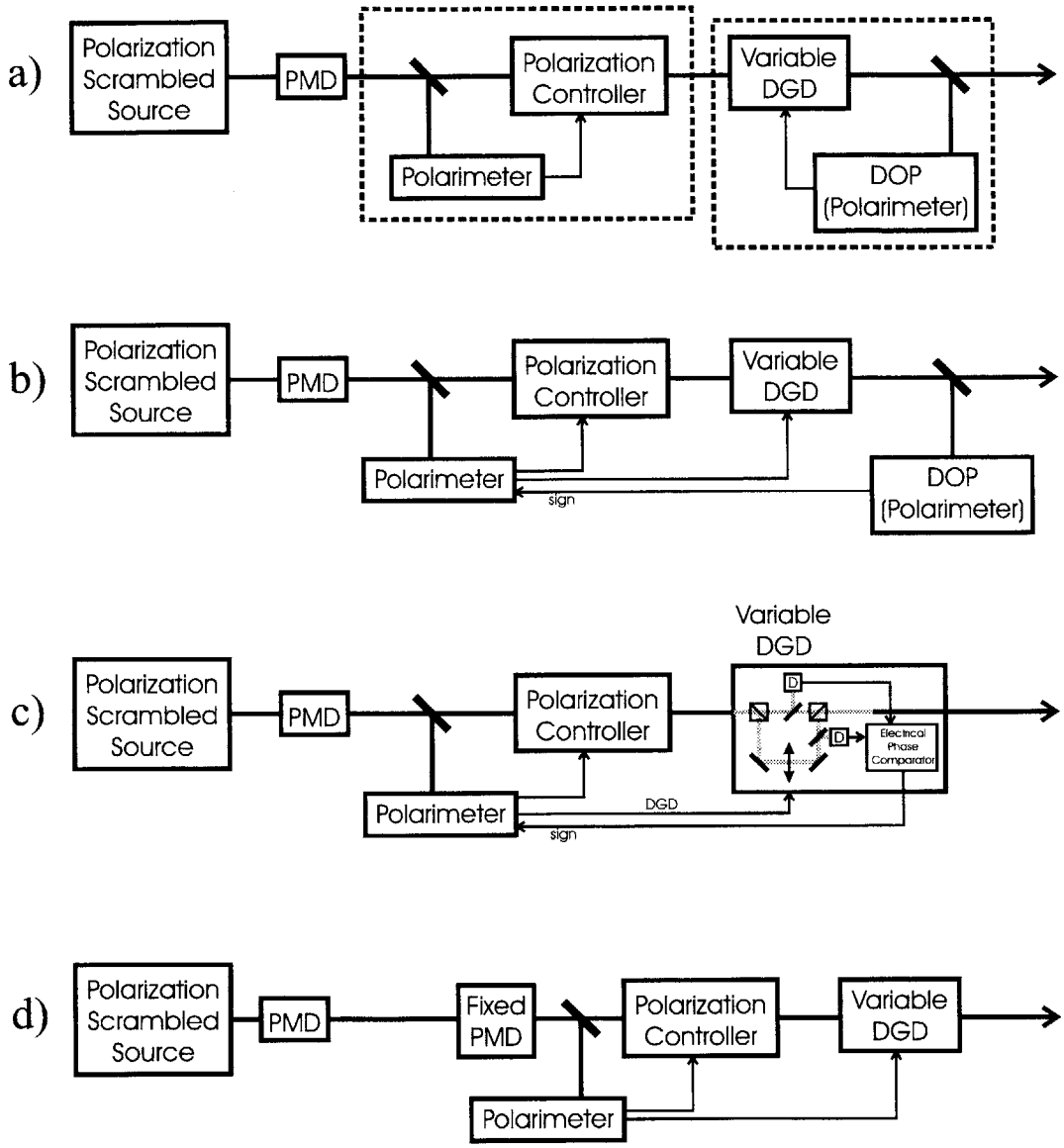

Figure 3-4: PMD compensators employing various levels of feedfoward information. a) Two stage system with feedforward PSP alignment and independent feedback controlled DGD. b) Feedforward control of PSP and DGD, but with a separate polarimeter providing DGD sense information. c) Similar to b), but using fast detectors for DGD sense detection. d) Use of known fixed PMD to shift the line PMD and remove sign ambiguity.

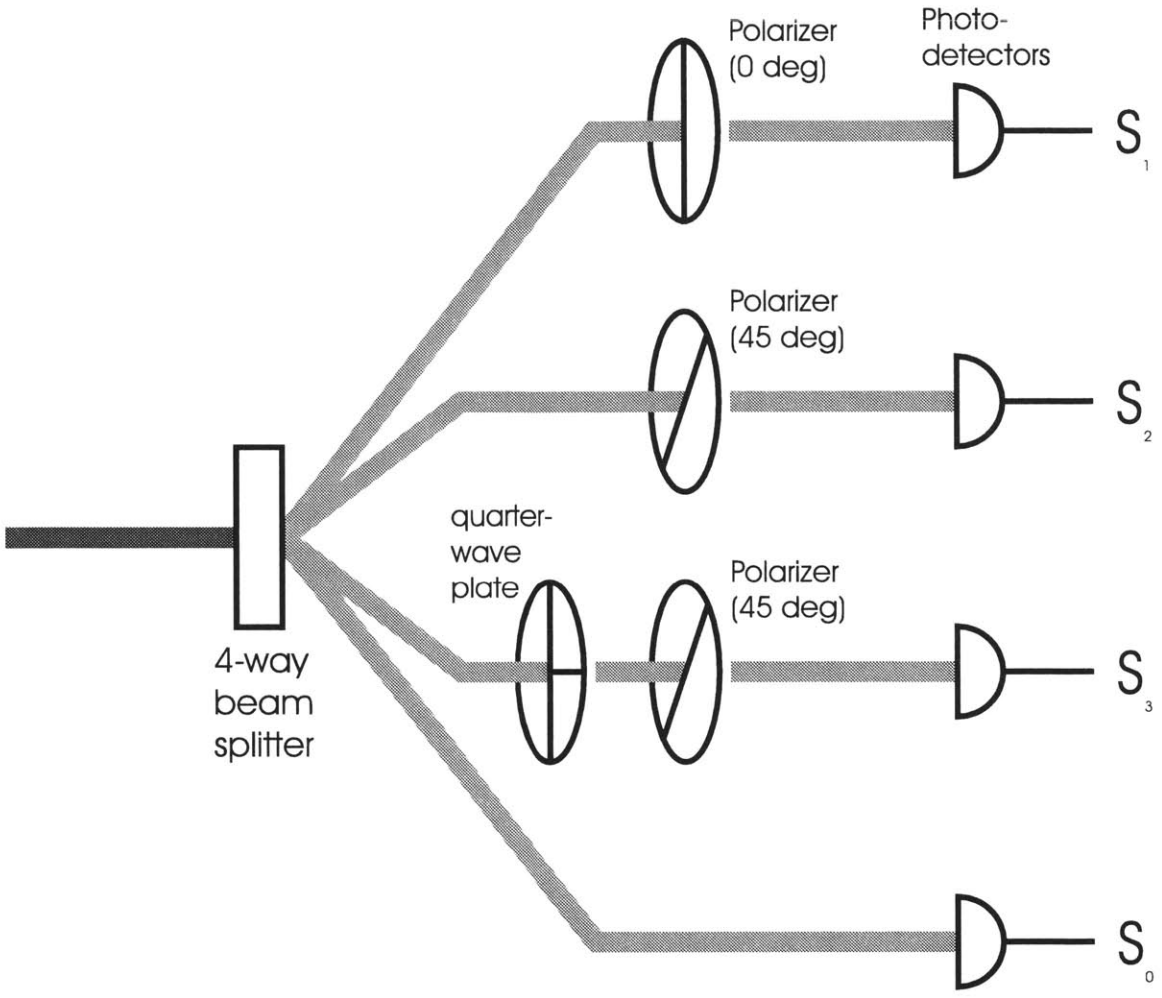

Figure 3-5: Schematic diagram of a polarimeter [29]. A 4-way beamsplitter distributes the signal to be measured by separate devices, each measuring one of the 4 non-normalized Stokes parameters: S_1 (linear x component), S_2 (linear +45 component), S_3 (left-circular component), and S_0 (total power).

3.2 PSP Characterization With Scrambling and Polarimetry

A single polarimeter measurement of a signal at the receiver does not provide enough information to characterize PMD. In the laboratory techniques described in Section 2.4, the transmitter frequency is swept in order to acquire enough information about the PMD. In this section a PSP characterization technique [59] is presented which is tailored to real-time *in situ* operation in an installed system. Because frequency sweeping is not an option in this scenario, the technique uses polarization scrambling at the transmitter.

The method estimates the PSPs by measuring a signal at the output of a fiber with PMD. A polarimeter (see Figure 3-5) measures the state of polarization (SOP) and corresponding degree of polarization (DOP) averaged over the bandwidth of the instrument. Because the DOP is a predictable function of the angle between the SOP and PSP Stokes vectors, each measurement can be used to estimate the orientation of the PSPs.

Sets of multiple polarimeter measurements at the output of the PMD medium are acquired for various input SOPs. It is thus necessary to insert a polarization scrambler or modulator at the transmitter. An additional benefit to scrambling is reduced polarization hole burning effects in erbium amplifiers. These effects are well known [56, 57] and in fact polarization scramblers are standard components in new undersea cable systems.

The experimental setup of a demonstration is shown in Figure 3-6. The output of a 1543.2 nm DFB laser is amplitude modulated by a lithium niobate Mach-Zehnder interferometer driven by a 10 GHz oscillator and biased to generate a background free 10 Gb/s stream of optical pulses. The SOP is modulated by a liquid crystal polarization controller which randomizes the SOP at a rate on the order of 10 Hz. A variable DGD emulator generates first order PMD. A fiber coupler taps 10% of the output signal, whose SOP and DOP are measured by a polarimeter. A computer then processes the data and determines the PSP orientations. All components are fiber

pigtailed. For subsequent compensation, a polarization transformer and a variable DGD compensator would be placed in the main signal path and controlled by the computer.

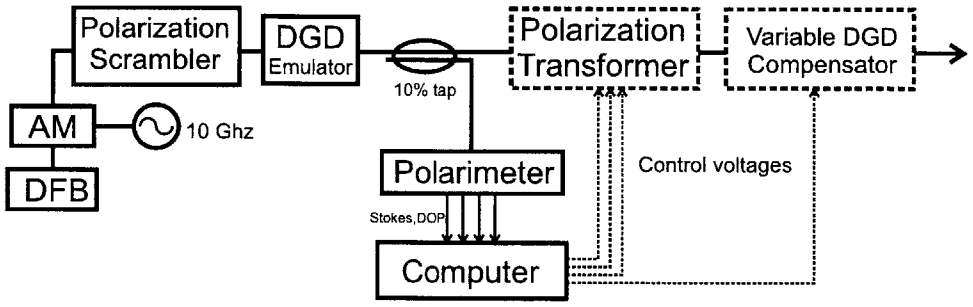

Figure 3-6: Experimental setup for real-time PSP alignment. AM: amplitude modulator, DFB: distributed feedback laser. For PMD compensation, the computer would align the PSPs to a DGD compensator via polarization transformers after PSP characterization.

3.2.1 DOP Function

The pulse-averaged output SOP and DOP are functions of the input SOP relative to the PSPs. DOP can be measured directly by the polarimeter of Figure 3-5 and can be written as a function of the non-normalized Stokes parameters:

$$DOP = \frac{\sqrt{S_1^2 + S_2^2 + S_3^2}}{S_0} \tag{3.1}$$

S_0 is a measure of total power; S_1, S_2, and S_3 are the linear x, linear +45, and left circular polarization components respectively.

In Stokes space, the PSPs are directly opposite each other on the Poincaré sphere. If the input SOP is parallel to the PSPs, there is no pulse envelope distortion and, in the absence of higher order PMD, the DOP is 100%. If an SOP is equidistant from both PSPs, power is divided evenly between the two PSPs. The average DOP then reaches a minimum value which is equal to the autocorrelation of the pulse shape as a function of the DGD.

Figure 3-7a illustrates a pulse split by first order PMD. Since the front (+) and back (-) tails are aligned with the PSPs and orthogonally polarized, they are interpreted as unpolarized light when averaged by the polarimeter, resulting in a reduction of DOP. Another effect of PMD is illustrated in Figure 3-7b. One PSP contains more energy than the other and its tail is not completely cancelled. The leftover shaded region then contributes to the total measured SOP. In short, the average output SOP is drawn toward the nearest PSP.

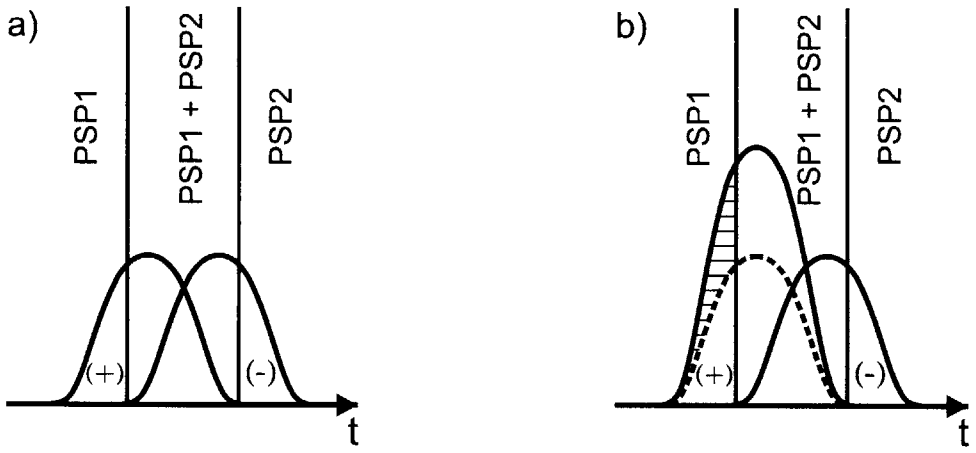

Figure 3-7: A pulse split by PMD. In a), the two PSPs are excited equally and the front and back tail are orthogonally polarized. In b) they are still orthogonal, but of different amplitude. The leftover shaded region draws the average SOP toward PSP1.

The dependence of DOP on the SOP direction can be expressed compactly in Stokes vector notation. If $\vec{s}$ represents the output Stokes vector [11], $\hat{s}$ is the unit vector in the same direction, and $|\vec{s}|$ is the DOP. First order PMD then gives:

$$DOP \equiv |\vec{s}| = \frac{1 - |\vec{P}|^2}{|\hat{s} - (\vec{P} \cdot \hat{s})\vec{P}|} \tag{3.2}$$

In Stokes space $|\vec{s}|$ forms the surface of an ellipsoid whose major axis is aligned with the PSP directions $\hat{P}$ and $-\hat{P}$.

Figure 3-8a shows an example of a set of 1000 SOPs, measured with 15 ps of DGD present. The polarimeter naturally scales the magnitudes of the SOPs $\vec{s}_i$ by the average DOP. The points therefore lie on the ellipsoidal surface described in

Equation 3.2, shown in Figure 3-8b. Note that the ellipsoid is in contact with the unit Poincaré sphere at the two points corresponding to the PSPs.

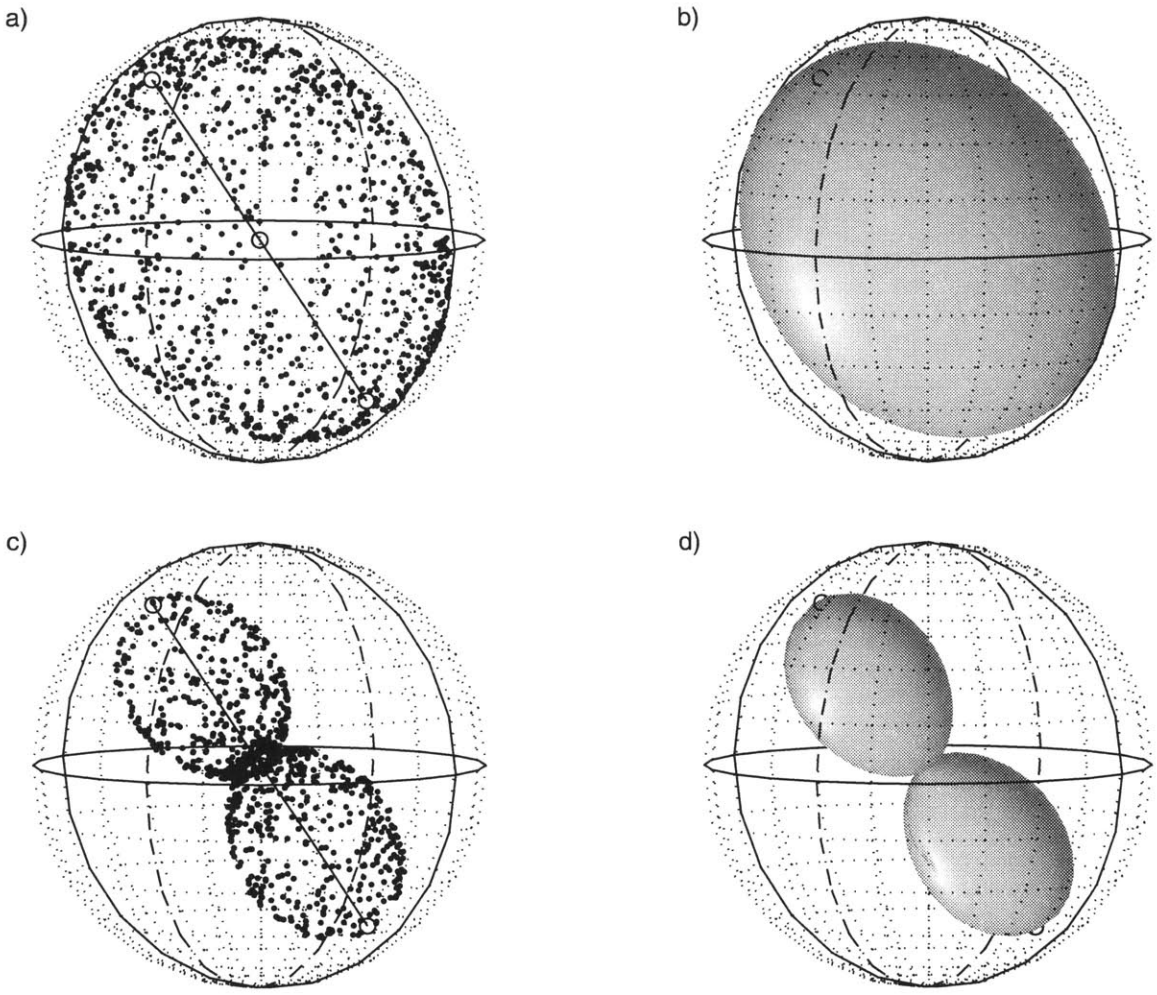

Figure 3-8: a) 1000 SOPs in 3-dimensional Stokes space. They lie on the ellipsoidal surface calculated in b). In c), the same data are rescaled by γ_i and displayed as $\vec{r}_i$. d) shows an analogous calculated surface. The axis of symmetry represents the mean estimated principal states.

3.2.2 Algorithm For Finding PSPs

Two different algorithms are demonstrated: an eigenvector calculation and a nonlinear least-squares fit. The former requires very little computation time and the latter exhibits extremely high precision.

The first algorithm senses the direction of the PSP axis by taking n measurements of SOP and corresponding DOP at the PMD output, and maximizing the following quantity on unit vector $\hat{x}$:

$$\sum_{i=1}^{n} (\hat{x} \cdot \vec{r}_i)^2 \tag{3.3}$$

The data $\vec{r}_i$ consist of measured SOPs $\hat{s}_i$ rescaled by a factor γ_i:

$$\vec{r}_i = \gamma_i \hat{s}_i \tag{3.4}$$

where

$$\gamma_i \equiv \frac{DOP_i - DOP_{min}}{1 - DOP_{min}} \tag{3.5}$$

The minimum DOP, DOP_{min}, corresponds to the DOP measured when both PSPs are equally excited. The value depends on the pulse spectrum and the DGD.

For a set of input SOPs uniformly scattered on the Poincaré sphere, the output measurements cluster on the PSP axis and create a maximum for Equation 3.3. The optimum $\hat{x}$ is calculated quickly by finding the eigenvector corresponding to the largest eigenvalue of a real 3 by 3 matrix generated from the data $\vec{r}_i$.

$\vec{s}_i$ could be used in place of $\vec{r}_i$, but when DOP_{min} is large, γ_i provides much greater contrast and thus higher precision estimations. Figure 3-8c shows the same measured SOPs converted to $\vec{r}_i$, with a corresponding calculated surface in Figure 3-8d.

The second algorithm applies a nonlinear least-squares curve fit to Equation 3.2. It is much more precise, but requires more computation time.

3.2.3 Experimental Precision of PSP Estimates

1000 estimates of a PSP axis were calculated from measurements taken with the setup of Figure 3-6. The eigenvector algorithm was applied to 40 polarimeter measurements

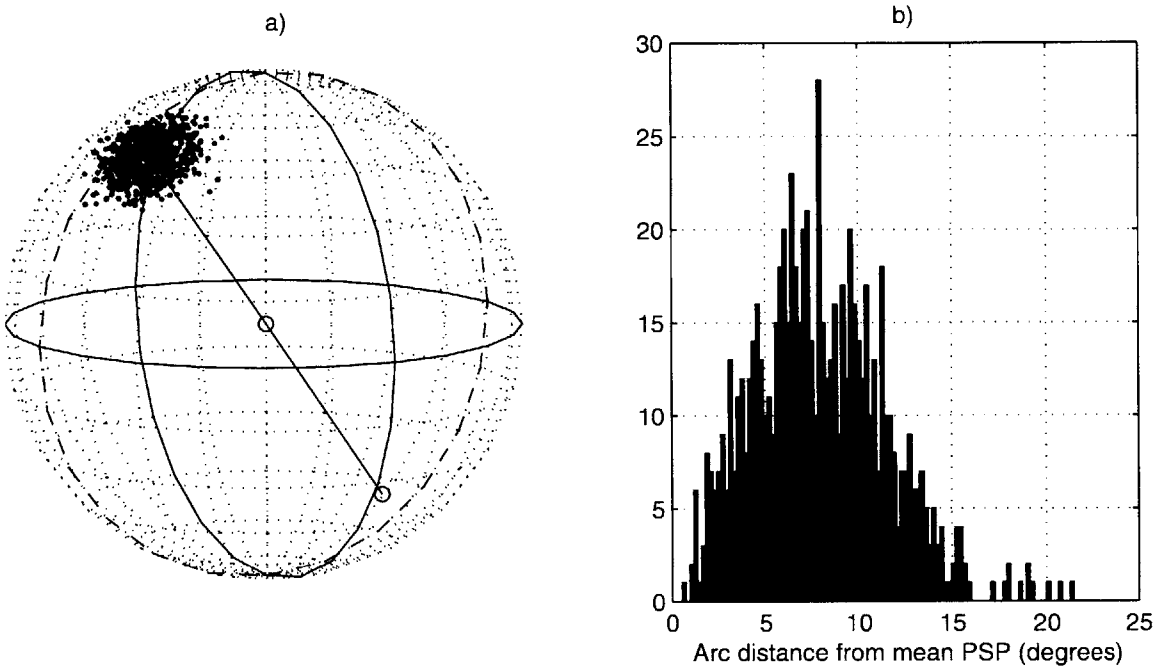

Figure 3-9: a) 1000 estimates of the same PSP viewed in Figure 3-8. 40 polarimeter measurements are used for each PSP estimate using the eigenvector method. A histogram of the distances from the mean estimated PSP are plotted in b).

for each of the estimates, which are displayed in Figure 3-9a. The mean of these estimates is indicated as the line through the origin. The histogram in Figure 3-9b shows a distribution of the distance, in degrees of arc length on the Poincaré sphere, of each estimate from this mean. The standard deviation of the distance is 8.7 degrees, corresponding to a polarization extinction ratio of -22.4 dB.

Figure 3-10 shows the standard deviations of estimated PSP distances from the mean for different measurement set sizes and DGDs. For 5 ps of DGD, 50 measurements are required to reach a precision below 10 degrees, or -21.2 dB of polarization extinction. 5 ps is well below the commonly accepted mean DGD limit of 0.1 bit period, or 10 ps [30].

The duration of a complete PSP estimate is proportional to the measurement rate and the number of measurements per estimate. The measurement rate is 10 Hz, limited by the speed of the liquid crystal polarization scrambler. Faster devices such as

lithium niobate waveguides or piezoelectrically stressed fiber devices are commercially available and would allow measurement rates above 10 kHz.

The choice of number of measurements depends upon the desired accuracy and the algorithm used. The eigenvector algorithm can be executed in less than a millisecond by a dedicated microprocessor. The nonlinear algorithm is not as fast, but yields greater precision. However, for a given precision, fewer measurements are needed, which may contribute to a faster overall speed.

3.2.4 Sign Ambiguity

As described so far, the PMD vector $\vec{\Omega}$ estimate has a sign ambiguity. A fundamental limitation is that the DOP ellipse cannot distinguish the slow and fast axes. One solution is to determine the sign initially by alternate means, and then track any subsequent variation of $\vec{\Omega}$ simply by assuming it varies continuously. That is, when two $\vec{\Omega}$ vectors of opposite sign are calculated, the one closest to the previously measured $\vec{\Omega}$ is always chosen.

Alternatively, the variation of the apparatus shown in Figure 3-4d resolves the ambiguity completely. If a fixed, known PMD is added at the receiver end, the total PMD seen by the polarimeter has a known offset. The sign is thus unambiguous as long as the PMD of the transmission line does not exceed the offset PMD. Figure 3-11 illustrates this in a two-dimensional space.

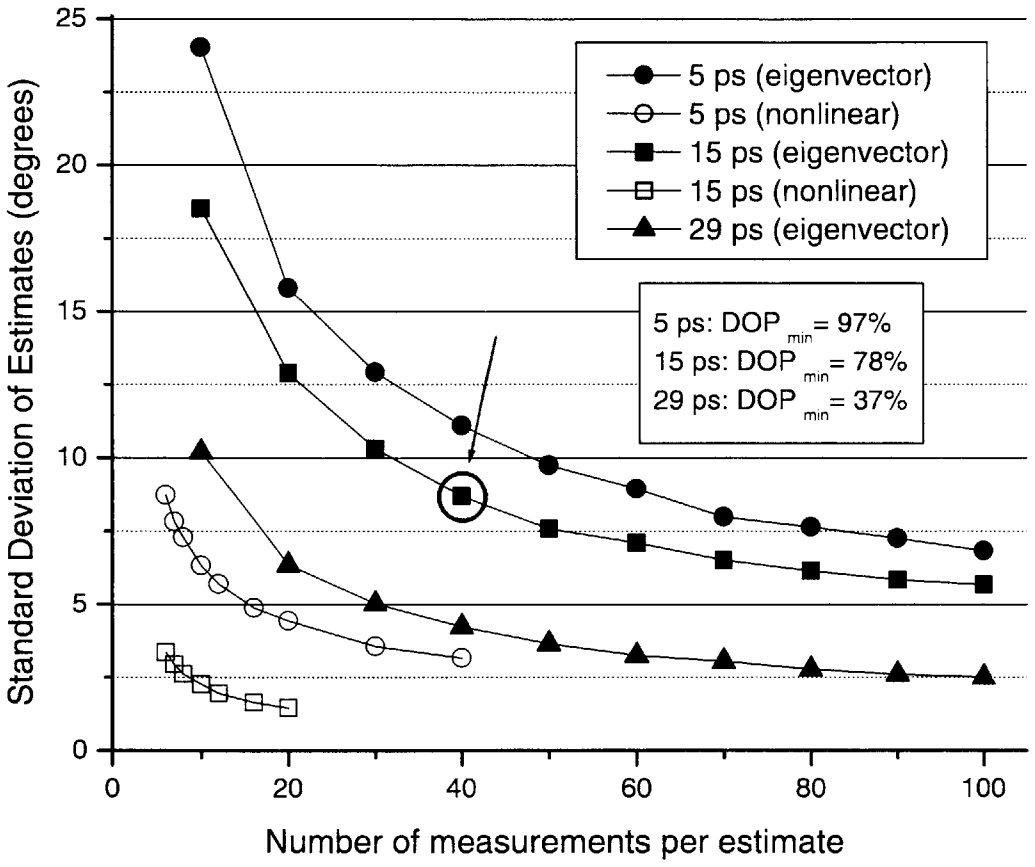

Figure 3-10: Standard deviation of the estimated PSP distance from the mean as a function of the number of measurements per estimate. Different DGD values using both eigenvector and nonlinear methods are shown. The inset table shows minimum DOPs corresponding to the DGDs. An arrow points to the conditions of the data displayed in Figures 3-8 and 3-9

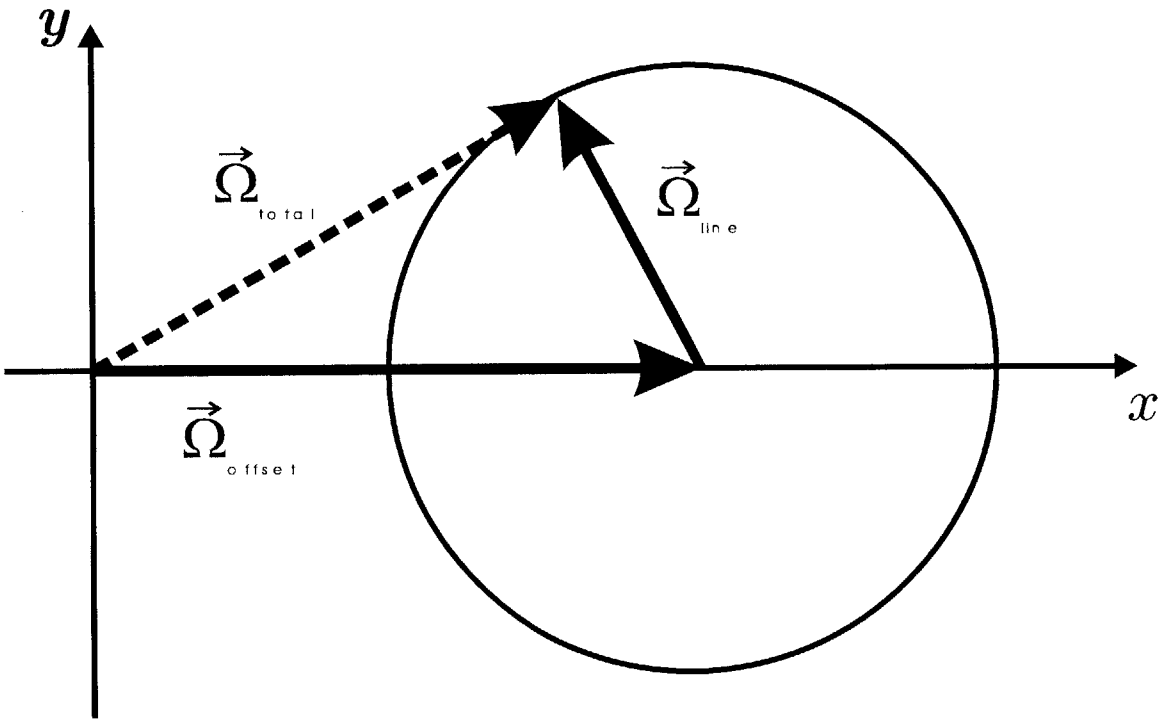

Figure 3-11: PMD vector $\vec{\Omega}_{line}$ offset by a fixed known offset $\vec{\Omega}_{offset}$. As long as $|\vec{\Omega}_{line}| \leq |\vec{\Omega}_{offset}|$, the resultant PMD vector $\vec{\Omega}_{total}$ will always be in the $+x$ region regardless of the $\vec{\Omega}_{line}$ orientation. Sign ambiguity is therefore absent.

3.3 Feedback-Free PMD Compensation

We now add PSP realignment to the above experiment. A challenge arises when using commercial polarization controllers. They are usually intended for use in feedback loops and are not precisely characterized at the factory. A method for calibrating the device is presented here. Great care must be taken in the process because even the slight motion of a fiber pigtail may cause errors in the expected polarization transformation of a pigtailed device.

3.3.1 Lookup Table Method

The realignment of the PSPs requires a fast and repeatable polarization transformer. The exact transformation induced by control voltages need not be predictable *a priori*. As long as this transformation is repeatable, it can be measured empirically during a calibration procedure. Both liquid crystal and squeezed fiber devices were tested. It was found that both are surprisingly repeatable. Even though they are fiber pigtailed, those devices can still give adequate results days after calibrating.

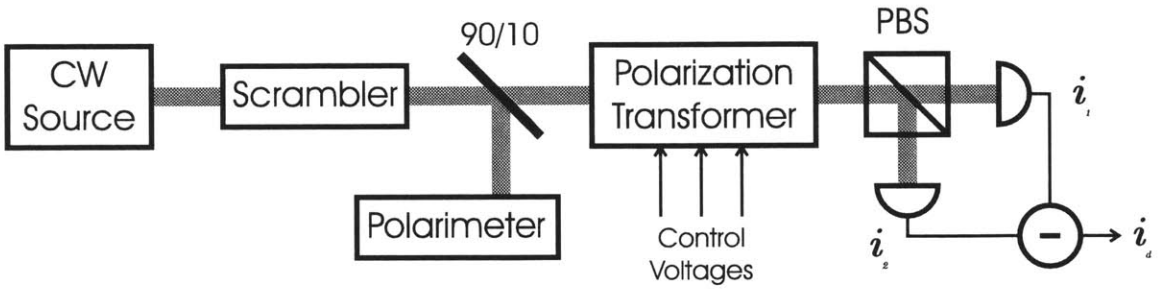

Figure 3-12: For a given set of control voltages, a computer controlled polarimeter measures random polarization states and corresponding detector difference currents i_d. It then predicts which measured polarization state would be transformed to be aligned with the PBS axes.

The goal of the calibration method is to determine, for a given set of applied control voltages, what incoming polarization state will be transformed to the linear state defined by the polarizing beamsplitter (PBS) at the output. A diagram of the method is shown in Figure 3-12. The SOP of a continuous wave (CW) source is modulated

by a scrambler. The signal SOP is transformed by the device to be calibrated, and then a projection in Stokes space is measured by a PBS with orientation $\hat{p}$. The photodetector currents i_1 and i_2 are related to the incoming SOP $\hat{s}$ by the expressions:

$$i_1 = \frac{1}{2}(1 + \hat{s} \cdot \hat{p}) \tag{3.6}$$

$$i_2 = \frac{1}{2}(1 - \hat{s} \cdot \hat{p}) \tag{3.7}$$

where i_1 and i_2 are normalized such that $(i_1 + i_2) = 1$. The difference current for an individual measurement $i_d = i_1 - i_2$ is then the projection itself: $\hat{s} \cdot \hat{p}$. Thus, for every SOP measurement $\hat{s}_j$ and detector difference current i_{dj}:

$$\hat{s}_j \cdot \hat{p} = i_{dj} \tag{3.8}$$

By collecting a set of m SOP measurements $\hat{s}_j$ into a matrix S, one can construct an overdetermined matrix equation:

$$S\hat{p} = \vec{i}_d \tag{3.9}$$

where $\vec{i}_d$ is the m-dimensional vector of corresponding difference current measurements, and $\hat{p}$ is a 3-vector defining the PBS orientation. S is composed of m 3-dimensional rows $\hat{s}_j$:

$$S = \begin{bmatrix} \hat{s}_1 \\ \hat{s}_2 \\ . \\ . \\ . \\ . \\ \hat{s}_m \end{bmatrix} \tag{3.10}$$

A least-squares approximation of $\hat{p}$ is then estimated by computing S^+, the pseudo-

inverse of S:

$$\hat{p} = S^{+}\vec{i}_d = (S^T S)^{-1} S^T \vec{i}_d \tag{3.11}$$

An advantage of this procedure is that the scrambled SOP never needs to coincide with the PBS axes exactly. Further, the scrambler need not be controlled with precision. The only requirement is that it randomizes the SOPs.

To fully calibrate a polarization transforming device, an estimate is computed for a variety of control voltage combinations. A lookup table consisting of voltages and corresponding PBS orientations is then created. With adequate coverage of the Poincaré sphere, for any incoming SOP, there exists in the table a voltage combination for which that SOP at the polarimeter coincides with the PBS axis at the output. Application of those voltages aligns the SOP with the PBS. For PMD compensation, the PBS is replaced with a local DGD device and a computed PSP is aligned to it in the above manner.

3.3.2 Compensation of Fixed PMD

An experiment demonstrating the use of a calibrated polarization controller in a dynamic compensator is constructed. It is similar to the configuration in Figure 3-4a. First order PMD is emulated, the PSPs are estimated using the nonlinear least-squares fit method, and the variable DGD compensator is replaced with a fixed polarization maintaining (PM) fiber. The experimental setup is shown in Figure 3-13. A DFB laser is modulated by a lithium niobate amplitude modulator which is driven by a 10 GHz oscillator. The polarization state is modulated by a scrambler, and a tunable DGD device emulates first order PMD.

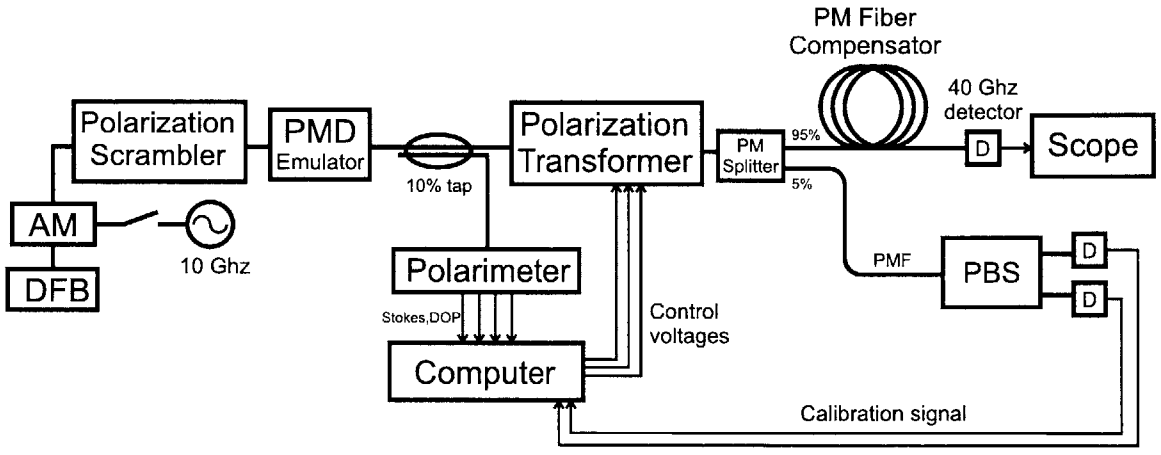

Figure 3-13: Experimental setup for PMD compensation demonstration. A polarization transformer aligns the principal states of a PMD emulator to a compensator. Calibration is performed with slow PBS detectors (D) and reconstructed pulses are detected by a 40 GHz photodetector. DFB: Distributed feedback laser. AM: Amplitude modulator.

The polarization state and DOP of the signal is monitored via a 10% tap coupler, and then rotated by the polarization transformer. A polarization maintaining (PM) coupler with a PBS and detectors allows calibration without removing the compensator.

During operation of the compensator, the emulator is set to 39.8 ps to match the PM fiber DGD and the amplitude modulator is turned on. The computer estimates the PSPs and sets the transformer to align them to the PBS using control voltages

found in the lookup table. To minimize hysteresis effects in the polarization controller, which is a piezoelectric device, the voltages are zeroed between iterations for both the calibration and compensation procedures.

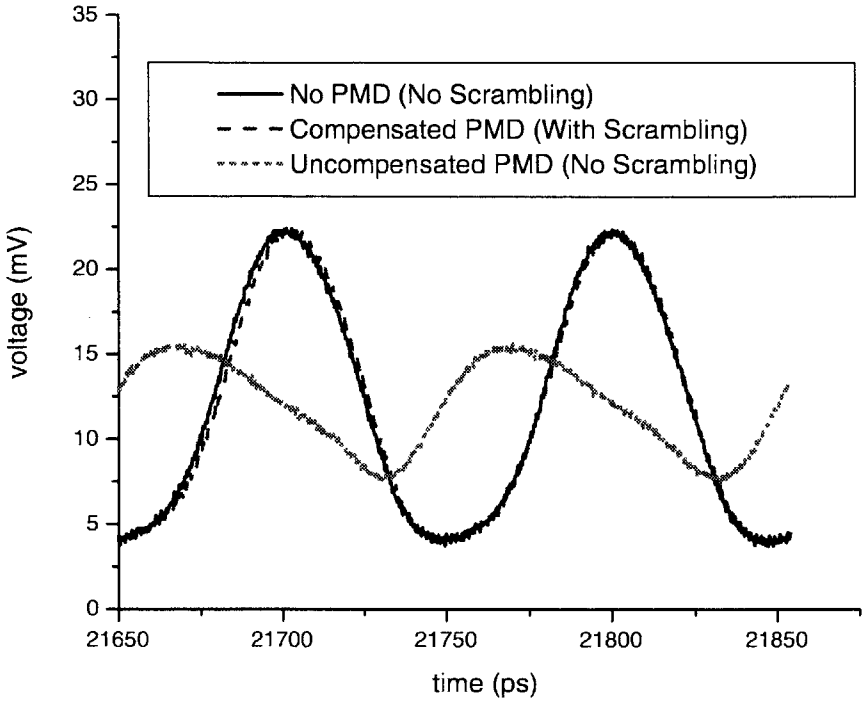

Figure 3-14: Averaged oscilloscope traces of pulses with no polarization scrambling, compensated PMD with scrambling, and uncompensated PMD without scrambling.

The reconstructed pulses are detected by a 40 GHz photodetector and displayed on a 50 GHz sampling scope. At this point, the alignment of PSPs to a fixed DGD fiber is demonstrated. However, if a variable DGD is available, the same least-squares fit parameter of the ellipsoid gives an estimate of DGD as well. Figure 3-14 shows averaged oscilloscope traces of the pulses under three different conditions: no PMD without scrambling, compensated PMD with scrambling, and uncompensated PMD without scrambling.

The accuracy of the lookup table is tested by having the scrambler generate random SOPs with a CW source, and measuring the polarization extinction ratio at the

PBS. A plot of more than 1000 extinction ratios measured for over one hour is shown in Figure 3-15, and a histogram is shown in Figure 3-16. The mean extinction ratio is -21.35 dB.

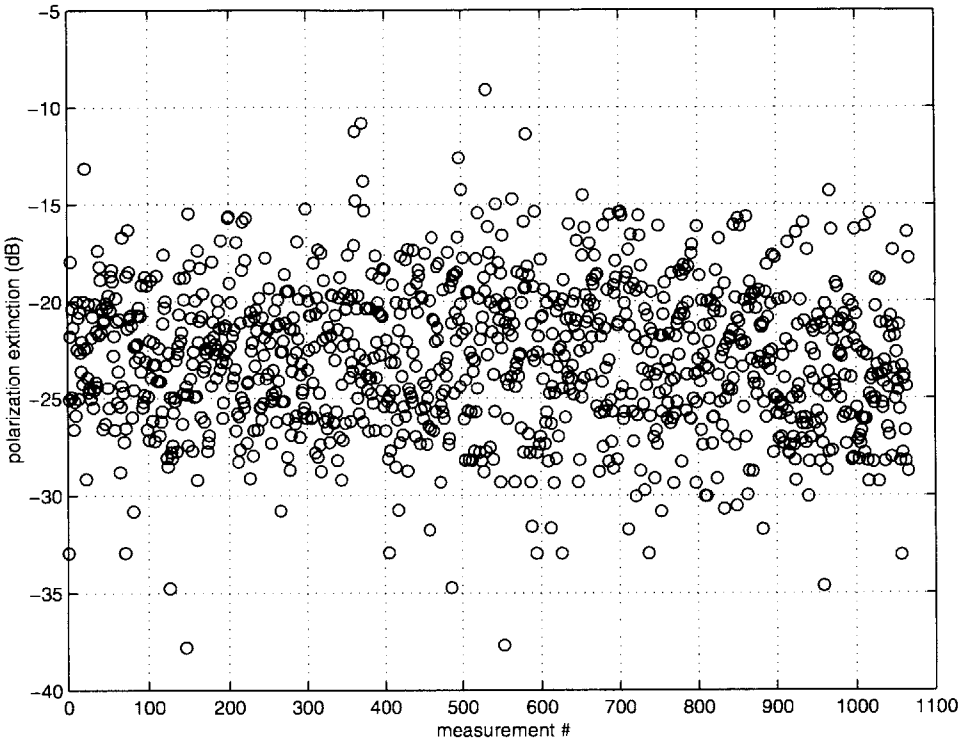

Figure 3-15: Measured extinction ratios. Randomly generated input polarization states are transformed by the calibrated polarization transformer using a lookup table.

A potential cause of error is incomplete coverage of the Poincaré sphere in the lookup table. The density of the coverage can be viewed in the plot of Figure 3-17. Points in the table are plotted on the upper and lower hemispheres, projected onto the $x - y$ plane. The table contains 1000 points. If evenly spaced, they would be separated by an arc distance of 7.3 degrees. Each point would then encompass an area corresponding to a -30 dB polarization extinction ratio.

To evaluate whether this is the dominant error mechanism, the data of Figures 3-15 and 3-16 are shown again in Figure 3-18. The extinction ratio of each point is plotted on a linear vertical axis. The horizontal axis is the distance between the randomly generated Stokes vector and the nearest point in the lookup table, which

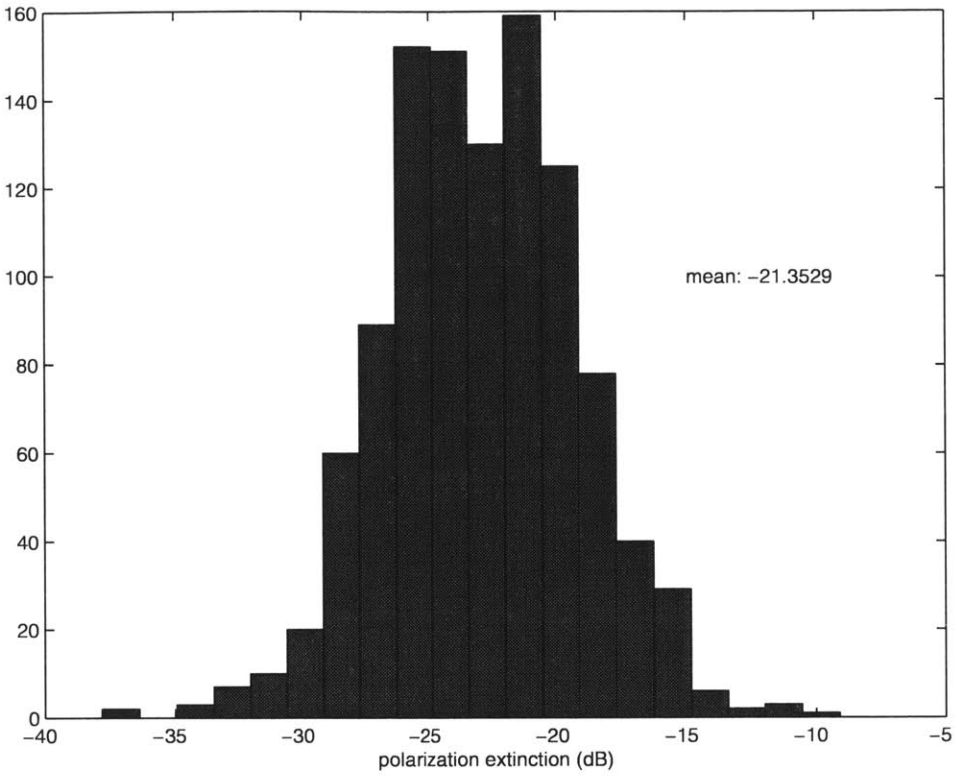

Figure 3-16: Histogram of measured extinction ratios for randomly generated input polarization states.

determines the controller voltages to be applied. A linear pattern through the origin would indicate a correlation between the two, and that errors are due to the lack of sufficient density in the table. Such a pattern is absent, however. The errors are more of a random nature. If coverage turned out to be a performance limitation, a process for filling in empty patches in the lookup table could be added to the calibration routine.

Another possible error source in a real system is long term drift of the polarization transformer or its pigtails. One would then devise a temperature controlled bulk optic device containing both the polarimeter and the transformer, or one could continuously re-calibrate the device *in situ*. The use of pulses and the presence of PMD during calibration should not adversely affect the calibration method, as long as adjustments for depolarization are taken into account.

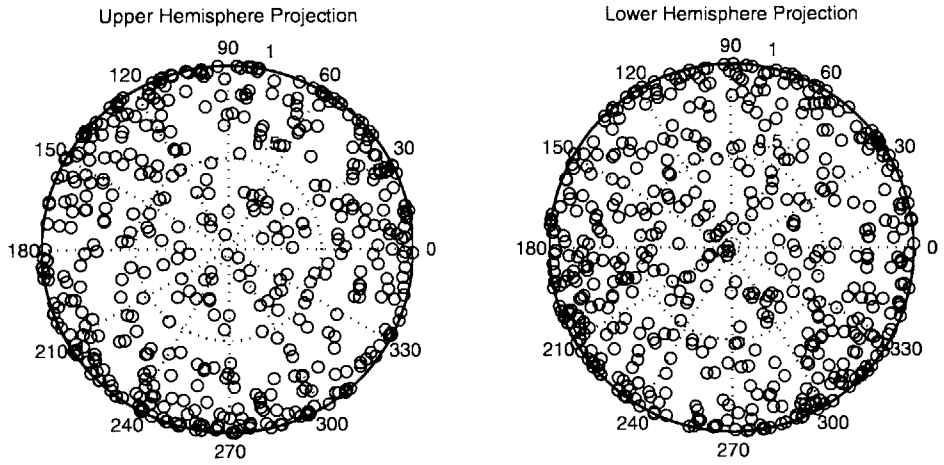

Figure 3-17: Lookup table coverage. Points in the lookup table are plotted on the Poincaré sphere. They are depicted here as projections onto the $x - y$ plane.

3.3.3 Slow Timing Jitter Due to Polarization Scrambling With Residual PMD

A performance measure of the PSP detection and realignment when combined is a histogram of the pulse's rising edge. Because of the polarization scrambling at the transmitter, residual PMD appears as timing jitter [31], as the scrambler constantly redistributes energy between the residual PSPs. Figure 3-19 illustrates this effect. The jitter caused by the scrambling adds a variance σ_s^2 approximately equal to $\tau_{res}^2/12$ (see Appendix B), where τ_{res} is the magnitude of the residual PMD.

Histograms of a rising pulse edge were measured on a 50 GHz sampling oscilloscope. With no scrambling, the inherent standard deviation was 2.91 ps. When the scrambling was turned on in the presense of the residual PMD, it grew to an average of 3.24 ps, indicating a residual PMD of 4.76 ps (see Figure 3-20).

Since both the PSP detection noise and the lookup table accuracy were both measured to be below -20 dB, overall errors are likely due to polarization dependent loss (PDL), which can cause systematic errors in the PSP detection. In a real system, PDL is of course undesirable for unrelated reasons and would be kept at a minimum.

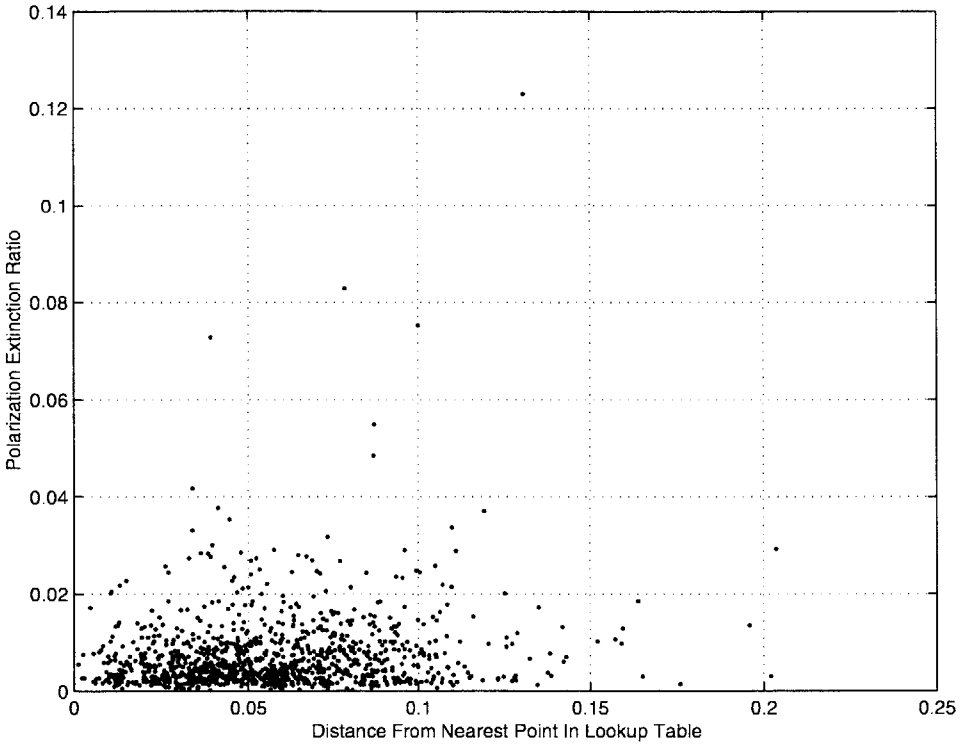

Figure 3-18: Plot of measured polarization extinction ratio of a randomly generated input polarization state versus the distance to the nearest point in a lookup table. The absence of a clear correlation indicates that the performance is not limited by the completeness of the lookup table.

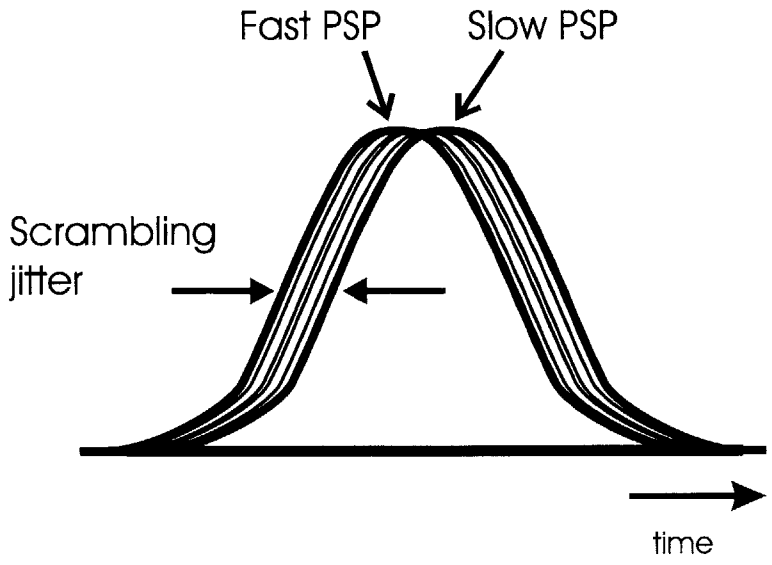

Figure 3-19: Polarization scrambling causes a slow timing jitter in the presence of small PMD remaining after compensation. The randomly varying excitation of the fast and slow PSPs make the pulse appear to shift back and forth in time.

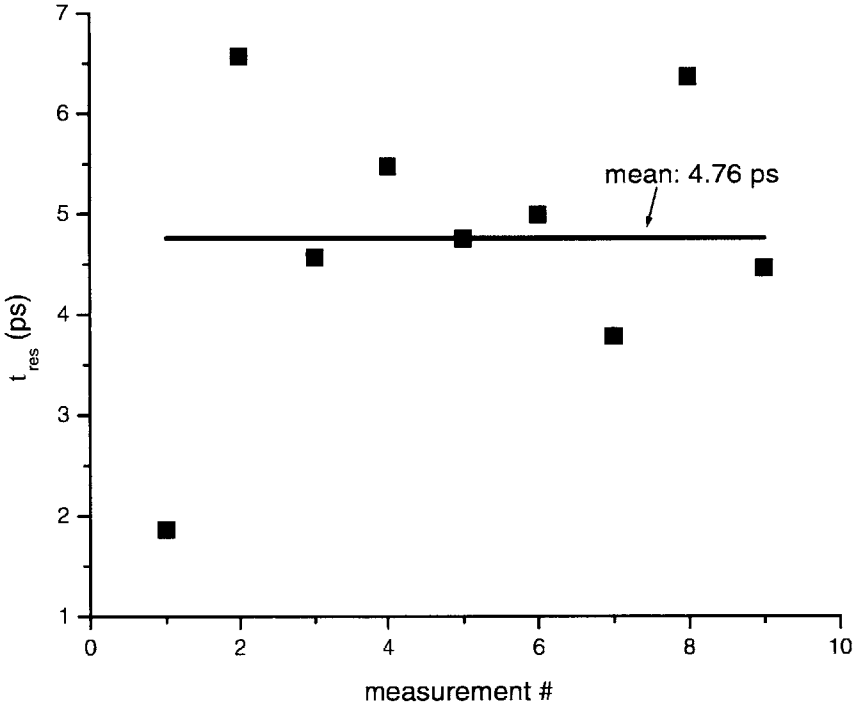

Figure 3-20: Measurements of residual PMD after compensation. Nine random PSP orientations are shown. Timing jitter due to polarization scrambling was evaluated by measuring oscilloscope histograms.

3.3.4 Characterizing PM Fiber DGD With Timing Jitter Measurements

An additional benefit of the scrambling timing jitter is that it provides a means of measuring fixed PMD with great accuracy. If a well calibrated variable PMD emulator is combined with a PMD device under test (DUT), one can use histogram measurements to characterize the DGD of the latter. The PM fiber serving as a fixed compensator was characterized in this way.

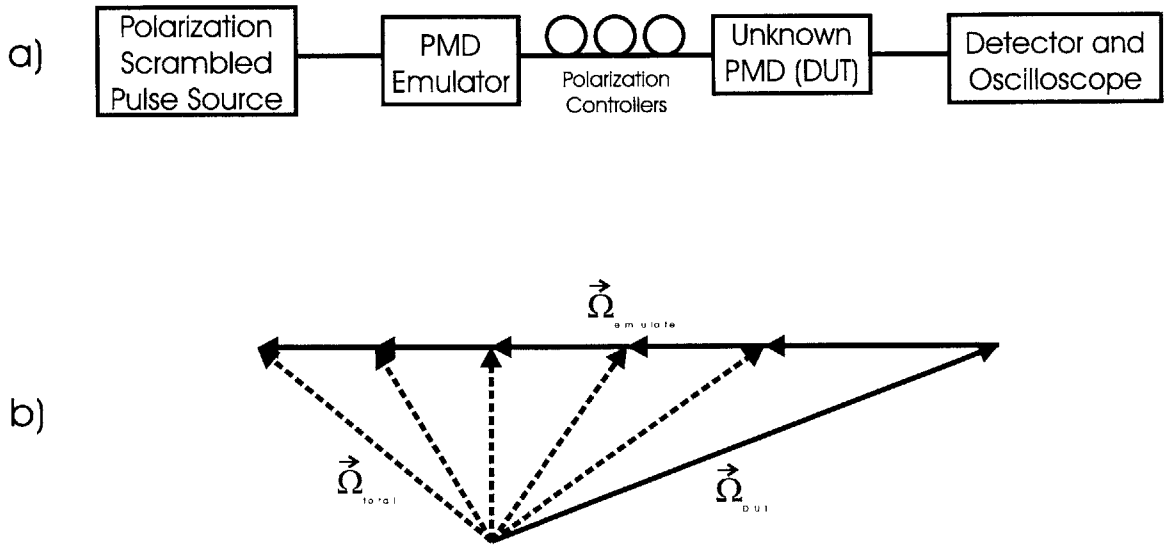

Figure 3-21: Use of scrambling jitter measurements to evaluate DGD. a) Schematic diagram. A polarization scrambled pulse source interrogates the PMD generated by an unknown device under test roughly aligned to a variable PMD emulator. Timing histograms are measured on an oscilloscope. b) Resultant PMD for various reference DGD values. The minimum $|\vec{\Omega}_{total}|$ occurs when $|\vec{\Omega}_{DUT}| \approx |\vec{\Omega}_{emulate}|$.

A schematic diagram of the method is shown in Figure 3-21a. A variable DGD emulator is placed in series with the device with unknown PMD. The PMD vectors of the two are coarsely aligned with manual polarization controllers. Histograms of pulse edges with scrambling jitter are then measured on the oscilloscope for a variety of emulated DGDs. Figure 3-21b illustrates the process in Stokes space. The PMD vectors $\vec{\Omega}_{emulate}$ and $\vec{\Omega}_{DUT}$ are roughly aligned, and to first order, the length of the resultant vector length $|\vec{\Omega}_{total}|$ is at a minimum when $|\vec{\Omega}_{emulate}| = |\vec{\Omega}_{DUT}|$. The

same applies to the corresponding histogram widths, which are measured by fitting Gaussian curves.

Figure 3-22 shows an example of widths plotted as a function of DGD. A fourth order polynomial fit reveals the center of the plot, and hence the value of $|\vec{\Omega}_{DUT}|$. For large resultant PMD $|\vec{\Omega}_{total}|$, the Gaussian approximation is poor, as seen in the inset of Figure 3-22. However, it is of little consequence because the symmetry axis of the curve is preserved.

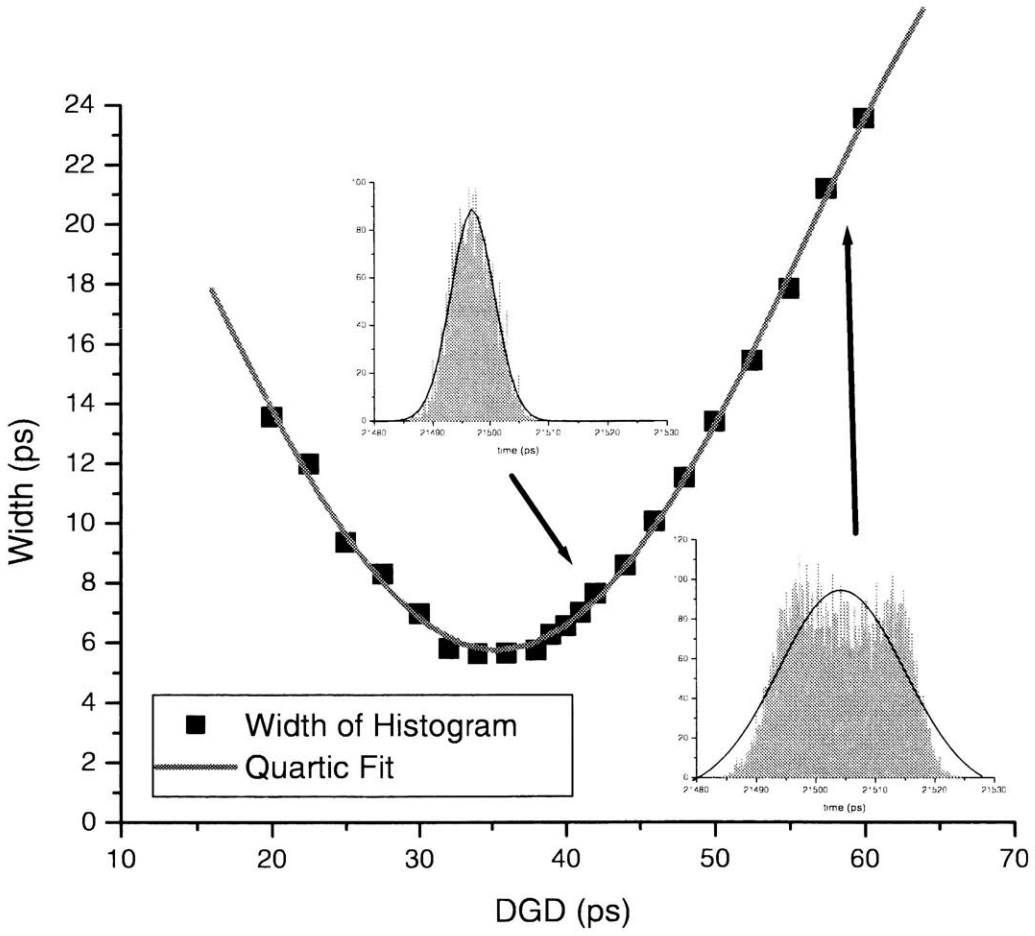

Figure 3-22: Example measurement of PM fiber DGD. Timing jitter induced by polarization scrambling is measured with oscilloscope histograms for different values of added PMD.

3.4 Summary of PMD Compensation Experiments

A simplified form of a PMD compensator has been demonstrated without feedback. The system speed is limited to an update rate of once per second because of polarimeter bandwidth of 2 kHz. The update rate can be scaled to accomodate millisecond scale fluctuations by choosing appropriate components and providing adequate computation power for the PSP characterization. In its current state, the technique characterizes and realigns PSPs without making any attempt to evaluate DGD. A completely feedback-free system would be desirable. In general, the signal pulse shape or spectrum must be known for this to be possible, and is a reasonable addition to the method. These future devlopements make the technique attractive for handling high speed fluctuations due to cable motion and rapidly switched optical networks.

Chapter 4

Short Pulse Generation With Frequency-Modulated DBR Laser and Long Chirped Fiber Bragg Grating

Chromatic dispersion is a linear optical phenomenon which, like PMD, generally causes pulse envelope broadening. However, in the demonstration presented in this chapter, the dispersive property of a fiber Bragg grating is utilized to create pulses, instead of destroying them.

The demonstration is of a picosecond optical pulse source consisting of a frequency modulated (FM) semiconductor laser with high modulation depth, and an ultra-long chirped fiber Bragg grating (FBG) with large group velocity dispersion (GVD). Unlike modelocked lasers [61, 67, 65], this source has a repetition rate which is not required to be synchronous with the laser cavity resonance. Because frequency modulation does not require gain switching, there is potential for very low timing jitter. The FBG also provides potential for higher pulse energies, lower background level, and more efficient use of the total laser energy output.

4.1 Ultra-Long Chirped Fiber Bragg Grating

FBGs [73] have been instrumental in the development of wavelength-division multiplexed (WDM) optical communication systems of recent years. Their low loss and environmental robustness have proven them to be effective filters for multiplexing and demultiplexing wavelength channels. Chirped FBGs have also been investigated for various other applications, including mode-locked fiber lasers [142]. Recently, another class of FBGs, ultra-long chirped FBGs, have been pursued.

4.1.1 Functionality

Chirped FBGs are designed to provide chromatic dispersion within the reflection band. By linearly chirping, or varying the periodicity of the grating, different frequencies are reflected at different positions within the grating. The result is a linear frequency dependence of the group delay.

Chirped FBGs are useful in a number of pulse compression applications, including mode-locked fiber lasers. For high capacity communications, it is desireable to compensate the dispersion of several channels at once so that one device ensures all pulses are compressed at the receiver. Because of aggressive efforts in the industry to increase system bandwidth, a system's wavelength channels can cover an enormous range. State of the art erbium doped fiber amplifiers now span 80 nm. Raman amplifiers make available wavelengths outside the erbium gain spectrum.

Dispersion compensation devices must then also cover a broad wavelength range. For a chirped FBG, the consequence is that it must be long if it is to satisfy the spectral width and dispersion magnitude requirements. This is clear from the relation between length L, dispersion D, and bandwidth $\Delta\lambda$ of a highly chirped FBG:

$$D \approx \frac{L}{c\Delta\lambda} \tag{4.1}$$

where c is the speed of the light in the fiber.

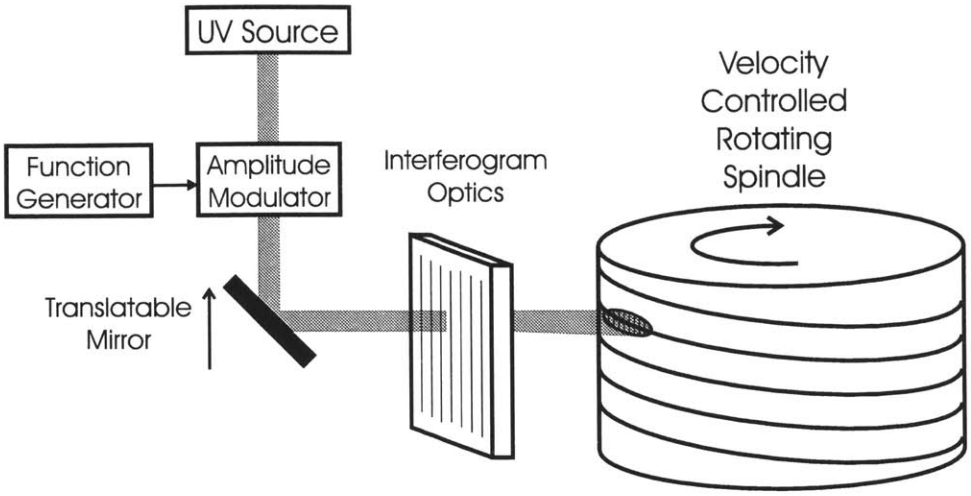

Figure 4-1: Ultra-long FBG fabrication technique developed at 3M Corporation.

4.1.2 Fabrication

The first long length FBGs were fabricated by Stubbe et al in 1995 [76]. Using a phase mask to create a grating through ultraviolet irradiation, the group irradiated one short section of a grating, translated the fiber, and then irradiated an adjacent short section. The process was continued until a 50 cm long FBG was constructed. The translation of the fiber was difficult because of the precision required. The stitching of sections must be accurate to a fraction of a wavelength. Regardless, other groups have developed the technique to the point where 2.5 m long FBGs were fabricated [77].

A different method developed at 3M Corporation by Brennan et al has proven to be more suited for even longer lengths. A 10 meter long chirped FBG was demonstrated in 1999 [71]. The unique fabrication technique involves mounting the fiber onto a spool with a helical groove (see Figure 4-1). The ultraviolet radiation illuminates a phase mask to create an interference pattern. The spool is rotated during the irradiation process while the UV beam is translated to follow the lateral shifting of the fiber position. The process is analagous to the threading of a screw. The illumination eventually reaches the entire length of fiber, whose length is limited only by how much fiber will fit on the spool. To prevent the grating from being smeared,

the ultraviolet light is amplitude modulated synchronously with the motion of the teeth in the fiber. While the spool is rotating, the ultraviolet beam is translated in the direction of the spool axis so that it follows the fiber in the helical groove.

To induce chirping of the grating, the rotational velocity of the spool is varied during irradiation. For acceptable optical performance, mechanical tolerances are excruciating. The velocity of the fiber must be stable to within one part per million. This requires, for example, the spool diameter to be true to within 250 nm [75].

4.2 Sinusoidal FM Modulation

One can generate an FM optical wave by applying a sinusoidally varying current to the mirror section of a 2-section distributed Bragg reflector (DBR) laser. The modulation rate is arbitrary, as long as it is much lower than the cavity's fundamental resonance. To convert the FM signal to a pulse stream, we attach an ultra-long chirped FBG at the laser output. The effect of the GVD from the FBG is that the up-chirped portion of the signal is compressed into pulses while the down-chirped portion is further chirped and dispersed into the background. With sinusoidal modulation and linear dispersion, the pulses contain approximately 40% of the total energy [61].

The experimental setup is shown in Figure 4-2. The laser is a 2-section InGaAsP DBR laser [63] fabricated at the Royal Institute of Technology in Kista, Sweden. It has a free spectral range of 205 GHz and is biased to operate at 1553 nm. We apply to the mirror section a 0.5 GHz current modulation, which dithers the center wavelength of the DBR reflector due to carrier induced index changes. The resulting optical signal is frequency modulated with a modulation index m of 52.5, defined

$$m = \Delta f / f_m \tag{4.2}$$

where the total sweep range $2\Delta f$ is 52.5 GHz, corresponding to 0.42 nm at 1553 nm. f_m is the modulation frequency 0.5 GHz. With higher modulation current, the bandwidth can be as wide as 0.76 nm, generating an index m of 95.

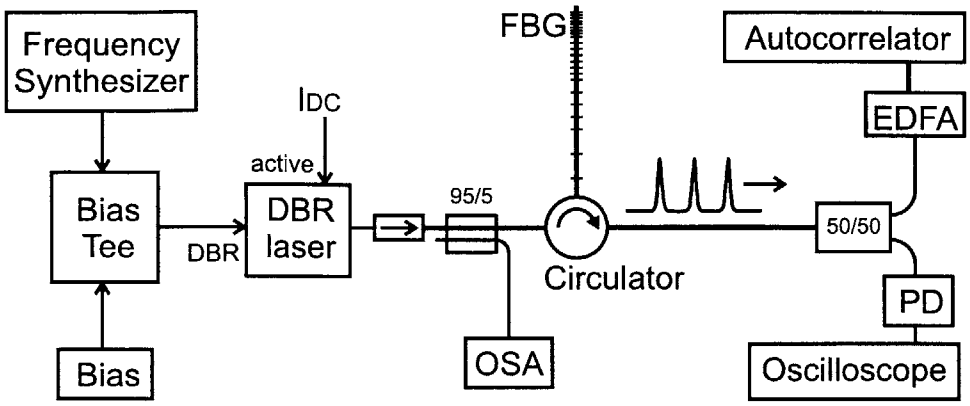

Figure 4-2: Experimental setup:DBR: Distributed Bragg Reflector; FBG: Fiber Bragg Grating; EDFA: Erbium Doped Fiber Amplifier; OSA: Optical Spectrum Analyzer; PD: Photodiode.

The output beam of the laser is coupled into a fiber, passed through a fiber pig-tailed isolator, and then tapped with a 95/5 coupler for optical spectrum monitoring. The light from the 95% port is then incident on a 3.86 meter long chirped FBG [71] manufactured at 3M Corporation in Austin, Texas. A circulator routes the FBG reflection to an output port, and upon reflection the frequency modulated light is converted to short pulses by the large dispersion of the FBG (-1360.8 ps/nm). A 50/50 coupler divides the light, half of which is characterized by an autocorrelator, the other half detected by a 24 GHz photodiode and high speed sampling oscilloscope. An erbium doped fiber amplifier (EDFA) is required for autocorrelation because the available power is small (approximately 0.15 mW average power) due to losses in the laser-fiber coupling and fiber connections.

The optical spectrum of the FM signal has a peak to peak width of 0.42 nm, shown in the inset of Figure 4-3, which also shows theoretical and measured autocorrelations. The suppression of the sidelobes predicted by the simulation is likely due to residual amplitude modulation. The FWHM is approximately 25 ps, roughly corresponding to a time-bandwidth product of unity. Harmonic distortion of the modulation signal is included in the simulation and can also account for a rise in background and degradation of pulse power efficiency. Given our bandwidth, FBG dispersion, and

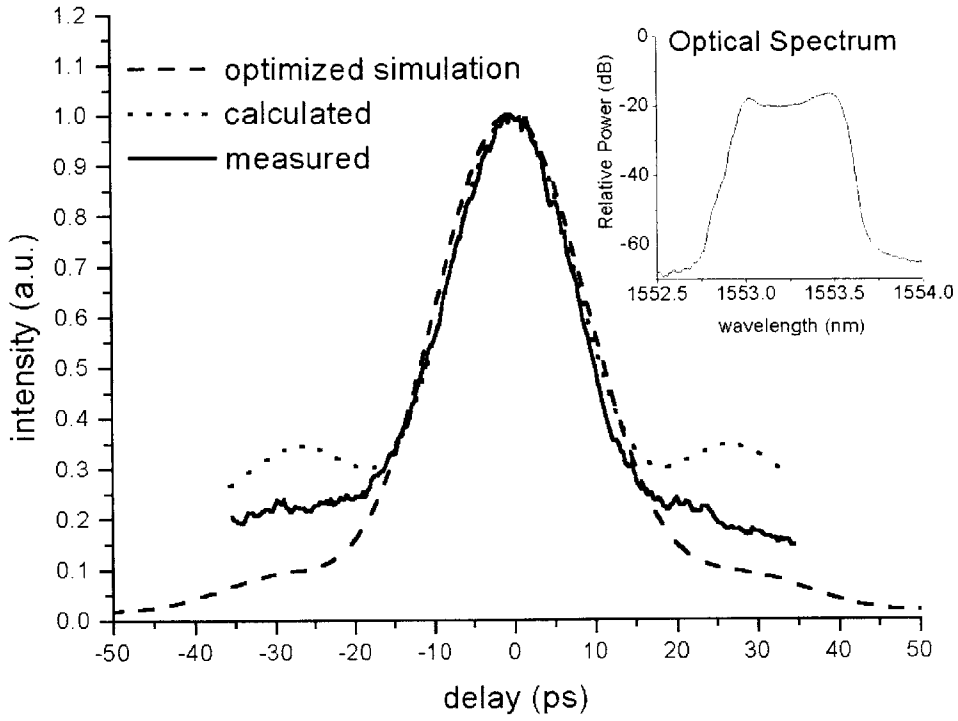

Figure 4-3: Measured and simulated autocorrelation traces.

fm, we estimate that 25% of the total power is in the pulse. This is consistent with estimates based on oscilloscope measurements. Figure 4-4 shows a sequence of autocorrelations as a function of bandwidth, with harmonic distortion included in both measured and simulated plots.

The shortest achievable pulse is limited by the free spectral range (FSR), which yields an inverse bandwidth of 4.9 ps. To further reduce sidelobes and overall background, amplitude modulation in the gain section can be induced. Alternatively, a sawtooth wave FM signal can replace the sinusoidal and induce only linear upchirping. High speed sawtooth waves can be generated by combining several RF harmonics with the correct amplitude and phase, or by using nonlinear electrical transmission lines for wave front distortion [70]. This would utilize the total power

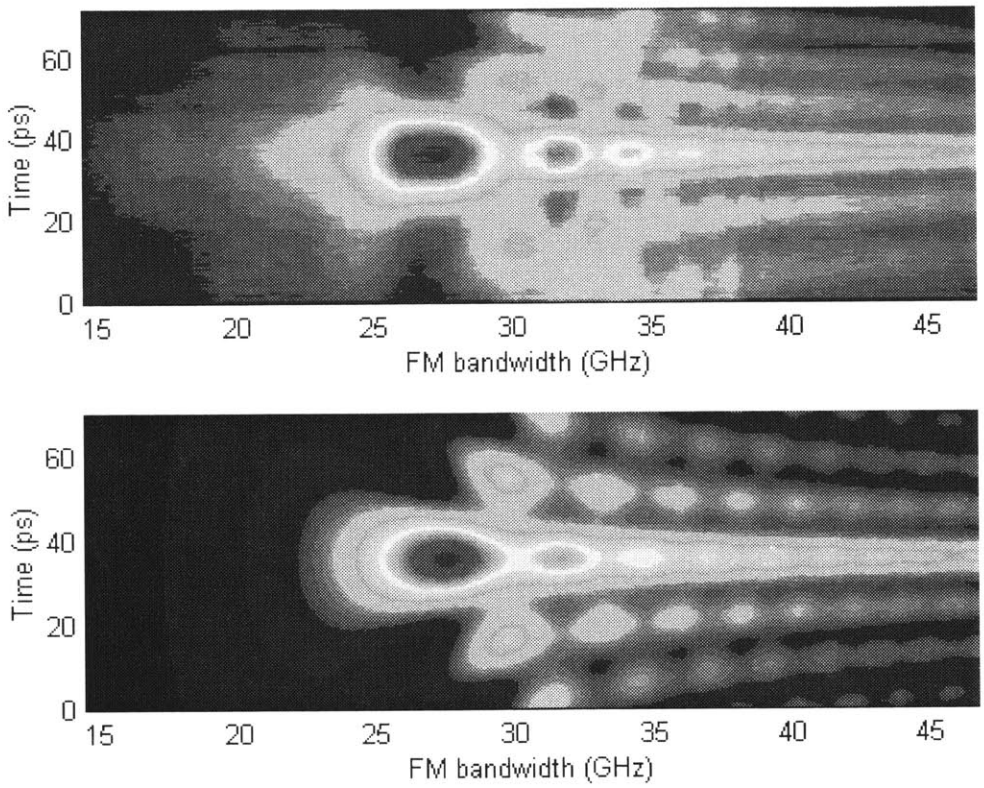

Figure 4-4: Autocorrelation traces with varying bandwidth and fixed dispersion. Top: experimental; bottom: calculated.

more efficiently, as well as remove high order chirp. Sawtooth wave generation is easily accomplished at lower repetition rates, however, requiring enormous dispersion delay which is best achieved with a long FBG as used here. An FBG is also advantageous in that its high order dispersion can be designed to match residual nonlinear chirp. Another limitation in a sawtooth wave experiment is in the bandwidth of the DBR tuning section itself. For this laser, the tuning signal rolls off at less than 1 GHz. A sawtooth with several harmonics would be filtered and rendered useless. Ideally, one should design a new laser with this particular application in mind.

Three features of this demonstration are notable: First, the wide frequency span and high modulation index is generated in a simple manner. It is possible to generate the chirp with external phase modulation, but it adds complexity [68] and is difficult in practice. Second, the laser is not modelocked. Modulating a single longitudinal mode laser is more stable, eliminates restrictions on repetition rates, and can potentially provide a low jitter pulse train for use in optical sampling. Third, the ultra-long FBG technology enables the use of low repetition rates which provide the option of more optimized modulation and dispersion shape to increase efficiency and reduce background.

Chapter 5

Time Domain Arbitrary Spectral Shaping of Pulsed Gyro Source

In Chapter 4 we explored a way of creating short time domain pulses using large chromatic dispersion. We now turn to a technique which utilizes the same ultra-long FBG to arbitrarily shape the optical frequency spectrum of a train of short pulses.

This demonstration is performed within the context of applying a mode-locked fiber laser as an optical source for a fiber optic gyroscope. Traditional sources emit amplified spontaneous emission which are desirable for their broad spectra and low coherence [112]. However, the Kerr effect causes errors in the rotation signal measured by the gyro. In this chapter we show how large chromatic dispersion reduces this error and enables convenient optimization of the spectral shape.

5.1 Kerr Error Reduction in Pulsed IFOG

Broad spectrum optical sources are important for applications such as Optical Coherence Tomography imaging (OCT) [109, 110, 111], wavelength division multiplexing (WDM) [115, 114, 116], and fiber sensors. A particular sensor, the Interferometric Fiber Optic Gyroscope (IFOG), benefits greatly from the broadness of a source spectrum because it reduces errors due to coherent Rayleigh scattering in the fiber coil [89].

Here we describe the IFOG sensor and the use of a mode-locked laser as a source.

5.1.1 IFOG Design

The IFOG is a sensor mainly consisting of a Sagnac loop. It measures rotation rate which induces a minute phase shift between two light signals counterpropagating within a loop of optical fiber. By interferometrically measuring the phase shift, the rotation rate can be measured. Applications include high precision inertial navigation for submarines and aircrafts as well as tasks such as airborn telescope stabilization.

A high performance IFOG must be carefully designed so that drift mechanisms are eliminated. One critical feature of a good design is called "reciprocity." This is not reciprocity in the strict electromagnetic sense [143], but instead refers to the two counterpropagating signals in the IFOG coil encountering exactly the same physical path lengths.

An environmentally stable design is important for low signal drift. For this reason, IFOGs have been developed to the point where in practice, it is a rule to follow the "Minimum Configuration" conditions. The following two sections discuss the importance of reciprocity and the Minimum Configuration.

Output Port of a Sagnac Loop

The Sagnac interferometer is shown in Figure 5-1. The input light is split by a 50/50 beam splitter and the two beams couple into a fiber loop and travel in opposite directions. Ideally, in the absence of rotation or other nonreciprocal effects, the two counterpropagating beams interfere constructively and destructively at output ports A and B respectively.

For an ideal lossless beamsplitter or waveguide coupler, the phase relation between reflected and transmitted light is exactly $\frac{\pi}{2}$. Errors in this relation occur in the nonideal case and drift slowly with environmental changes (See Appendix A).

As seen in Figure 5-1, both clockwise (CW) and counterclockwise (CCW) light experience the same phase while traveling through the loop, assuming no rotation.

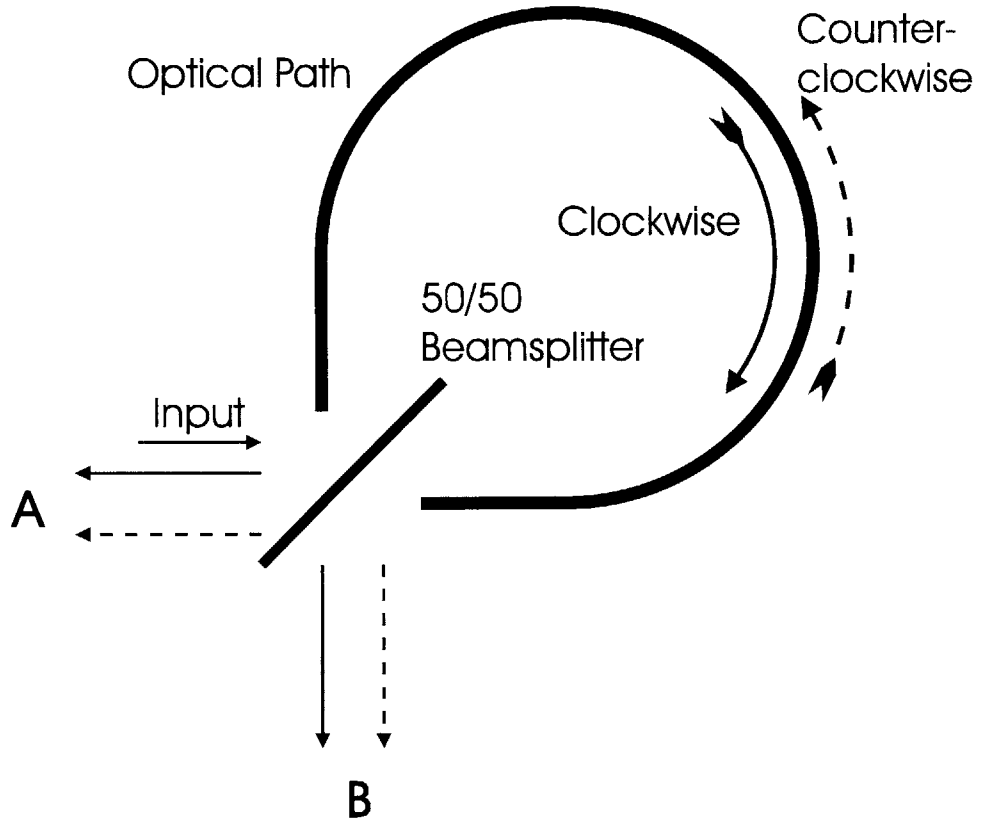

Figure 5-1: Sagnac loop interferometer. The clockwise (solid) and counter-clockwise (dashed) signals interfere at the 50/50 beamsplitter. Depending on the relative phase, the light can exit through port A or port B.

However, output A is the result of the interference between CW and CCW beams, each of which have experienced exactly one transmission t through the beamsplitter, and one reflection r:

$$CW : \phi_{total} = \phi_r + \phi_t \tag{5.1}$$

$$CCW : \phi_{total} = \phi_t + \phi_r \tag{5.2}$$

The total phases are identical for both CW and CCW cases.

At port B, on the other hand, CW sees two reflections and CCW experiences two transmissions:

$$CW : \phi_{total} = \phi_r + \phi_r \tag{5.3}$$

$$CCW : \phi_{total} = \phi_t + \phi_t \tag{5.4}$$

The total phases can drift independently.

Thus, when the phase between the reflection and transmission drifts with temperature, it causes the amplitude at port B to drift also. But at port A, both counterpropagating beams drift in phase simultaneously and the amplitude of the sum is unaffected. Port A is referred to as the reciprocal port.

Minimum Configuration

The first definition of the Minimum Configuration was given in [92](See Figure 5-2). It is clear that if environmental drift is a concern, only the reciprocal port can be used for output.

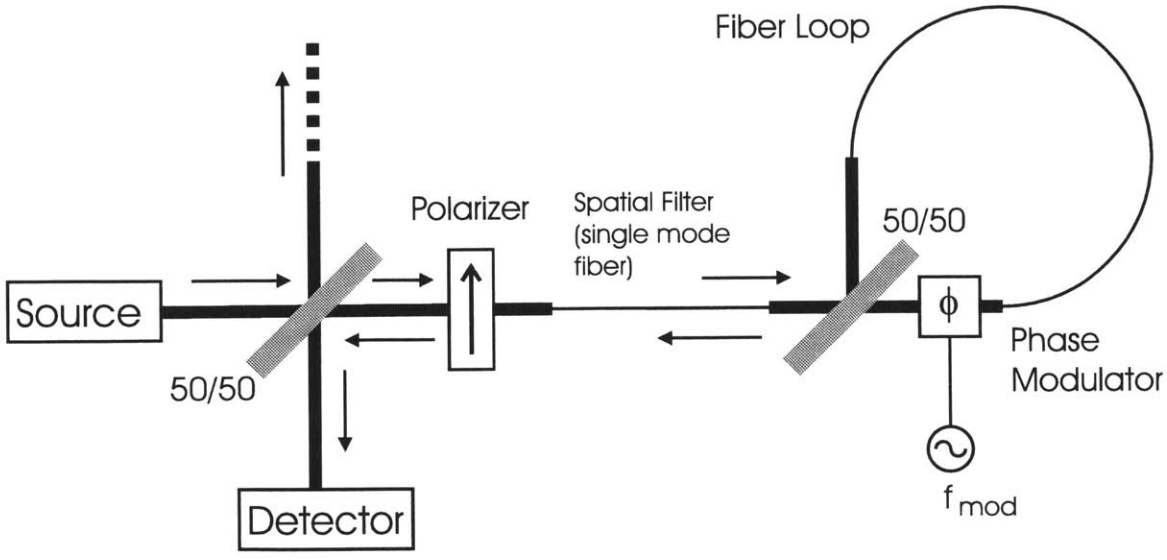

Figure 5-2: IFOG minimum configuration. The Sagnac loop signal is taken at the reflection port. A nonreciprocal phase modulation is applied within the loop for proper bias and sensitivity enhancement.

Two other conditions are set forth as well:

1. A single polarization mode in the fiber is required for true matching of optical path lengths. That is, a polarizer and spatial mode filter are required. This is to ensure that true interference of waves is achieved. Higher order spatial modes and lack of polarization matching causes interference fringes to be unstable.

2. A method of biasing is used so that rotation detection is linear and unambiguous. The most common method of bias is to insert a phase modulator at one end of the fiber loop. This time varying phase modulation is equivalent to time varying rotation if it is fast enough to be comparable to the transit time of the light in the loop. Other methods are sometimes used in gyro designs which do not exactly follow the Minimum Configuration [101, 102].

It is pointed out in [92] that the Minimum Configuration may be violated under conditions where thermal drift is not an issue.

5.1.2 Pulse Excited IFOG With Pulse Stretching

In this section the pulse excited IFOG is introduced. The pulse source is advantageous in its ability to produce a wide spectrum and high average power at the same time. It also opens the door to new methods of stabilizing mean wavelength, reducing sidelobes in coherence function, and reducing shot noise via optical squeezing.

When using a short pulse source in an IFOG, the high peak intensities of the pulses cause nonlinear phase shift in the gyro coil due to the Kerr effect. This alone would not be an inherent problem. But if the Sagnac interferometer's Y-splitter output power ratio is not perfectly 50/50, then the counter-propagating radiations experience different nonlinear phase shifts resulting in a bias offset. Small random variations of the splitting ratio result in errors.

Figure 5-3 shows the experimental setup. An Additive Pulse Modelocked (APM) erbium doped fiber laser [129] is used as a source in a standard IFOG configuration [92]. A 25.2 km spool of Corning SMF28 can be inserted between the fiber laser and the rest of the gyro. A variable attenuator is also inserted so that the input power can be adjusted. With the variable attenuator one can check on any power

dependent error present in the gyro output signal. The backward pumped erbium fiber has dual purpose: First, it acts as an amplifier to increase the power of the pulse source. When the APM laser is turned off, it is then a CW fluorescence source which can be used for direct comparison.

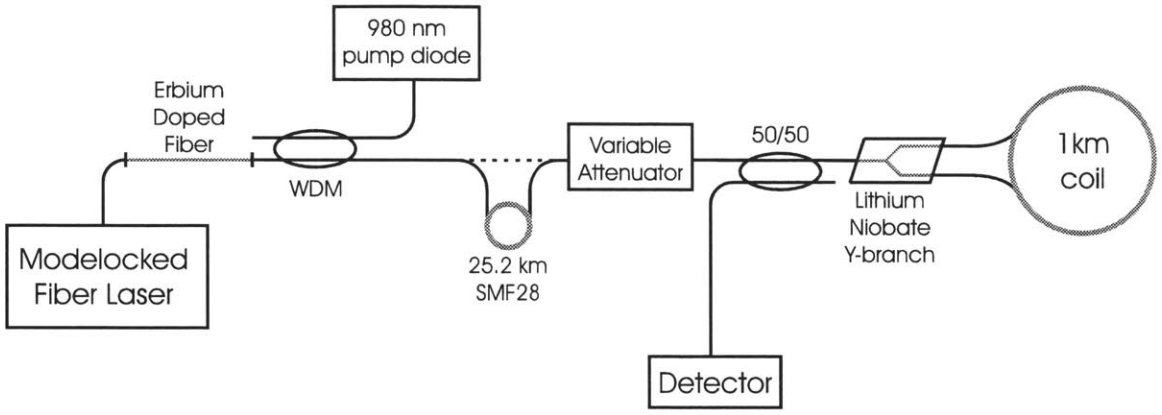

Figure 5-3: Experimental setup of pulsed gyro. A mode-locked fiber laser excites a standard IFOG minimum configuration. The pulses are amplified and stretched by 25.2 km of standard single mode fiber before entering the Sagnac loop. A phase modulator is built into the lithium niobate splitter for detection.

Figure 5-4 illustrates the power dependence of the Kerr induced error signal. When the erbium fluorescence is used as a CW source, there is no detectable error. With the pulsed laser as a source, however, there is a large power dependent error. This is reduced by inserting a long length of SMF28 fiber to stretch the pulses so that their widths are on the order of τ, where $\frac{1}{\tau}$ is the repetition rate.

The amount of pulse stretching via chirping can be increased by using a laser with a wider optical bandwidth, a longer spool of fiber, or another more dispersive element such as a dispersion compensating fiber grating. This technique can stretch the pulses so much that they would be virtually indistinguishable from a truly CW source. With this pseudo-CW source, an IFOG can benefit from the high power and wide spectral widths of mode-locked lasers, without sacrificing in Kerr bias error.

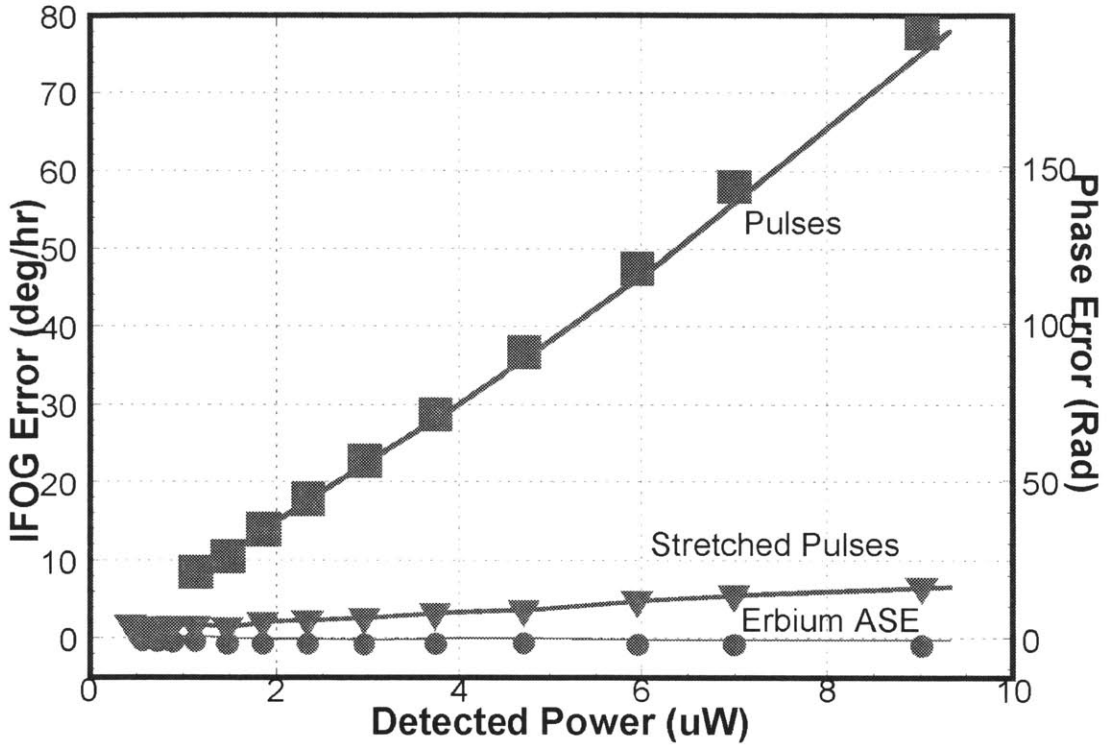

Figure 5-4: Optical power dependence of IFOG bias error for pulse source, stretched pulse source, and erbium ASE.

5.2 Time Domain Spectral Shaping Technique

5.2.1 Spectral Shaping Methods and Applications

Broad spectrum pulses are used in many applications, and in several of these, the spectral shape impacts system performance [141]. For example, a broad Gaussian spectrum and narrow coherence function provide optimal image resolution in optical coherence tomography (OCT). Typical spectra of pulses used in OCT contain ripples that cause sidelobes in the coherence function and thus limit spatial resolution [111]. Similar characteristics are desired for interferometric fiber optic gyroscope (IFOG) sources, since a narrower coherence function reduces the rotation rate sensing er-

ror caused by coherent Rayleigh backscattering [90]. IFOGs also require the mean wavelength of the source to be stable.

In other applications, one may record information in the pulse spectrum by altering the amplitude or phase of various spectral bands comprising the pulse. In optical communications, chirped pulse wavelength division multiplexing (CPWDM) may utilize a pulsed laser source and a single modulator to encode data onto several wavelength channels, whose wavelength-location and channel-spacing are electronically defined and therefore quickly reconfigurable [115, 116]. CPWDM may become a cost effective alternative to traditional wavelength division multiplexing. Pulse spectral shaping is also used in code-division multiple access (CDMA), which provides multi-access communications in optical networks by introducing channel specific code sequences in pulse spectra that can be used for channel discrimination [117].

Several investigators have proposed and demonstrated that fiber Bragg gratings (FBGs) can be used as spectral filters of controllable phase and amplitude [79]. Specialized FBGs have been fabricated for pattern generation and recognition (CDMA) [80, 81], pulse rate multiplication from 10 GHz to 40 GHz [82], pulse envelope transformation into rectangular pulses [83], and for optimization of pulse detection with matched filters [84]. In these demonstrations, the spectral filter was written directly into the FBG; to alter a filter function, one would need to fabricate another FBG and implement it into the optical system.

In some cases, time domain spectral shaping (TDSS) may be an attractive alternative, since the filter functions are readily configurable and real time spectral encoding is possible. TDSS employs large amounts of group velocity dispersion (GVD) to temporally stretch, or chirp, a short pulse. During stretching, the pulse enters a regime that is the time domain analog of Fraunhofer diffraction [85]. In this regime, the pulse envelope is proportional to the pulse spectrum, which is the Fourier transform of the original unstretched envelope. Since the individual frequency components are distributed within the stretched envelope, they can be isolated temporally and modulated in amplitude or phase without the use of optical filters. TDSS can be used to implement fixed filters, like previous FBG work, as well as variable spectral shaping

as needed in CPWDM and variable route CDMA systems.

5.2.2 Time Domain Spectral Shaping With Ultra-Long Fiber Bragg Grating

In previous TDSS experiments, mode-locked laser pulses were stretched with several kilometers of standard single mode fiber (SMF) to several nanoseconds for CPWDM, reducing nonlinear bias in an IFOG [100] [115], and for time domain spectral measurements [118]. Outside the laboratory, however, TDSS with a bulky spool of SMF as a pulse stretcher is impractical.

Here we demonstrate the use of a linearly-chirped ultra-long FBG to chromatically disperse a pulse for subsequent TDSS [119]. We utilize a compact and robust chirped FBG packaged with a circulator; the package volume is smaller than the SMF spool by a factor of 8.7 and lighter in weight by a factor of 9.3. Until recently, FBGs were too short to provide enough GVD over a sufficient bandwidth for use in TDSS systems. Now FBGs of several meters in length are available [77, 71]. While reflection bands are generally not as wide and smooth compared to SMF, long length FBG fabrication technology will likely continue to improve and yield gratings with reflection profiles of quality comparable to SMF. After stretching the pulse with the FBG, we implement complex and arbitrary spectral shaping by suppressing select frequency components of the spectrum. Such filters can remove spectral ripple and sidelobes to generate flattened or Gaussian spectra, control the mean wavelength, or encode data.

For the demonstration we use a linearly chirped 3.86-meter-long FBG manufactured at 3M Corporation [71]. The bandwidth is approximately 28 nm, which provides 1360 ps/nm dispersion. The setup is shown in Figure 5-5. A passively mode-locked erbium doped fiber laser (EDFL) with two output ports, "rejection" and "variable", provides a train of broad spectrum pulses (70 nm wide) at a repetition rate of 30.7 MHz (32.6 ns period) [141]. Spectra of the rejection port and its reflection from the FBG are shown in Figure 5-6. The FBG spectral response is nearly identical to the reflected spectrum. The EDFL rejection port emits chirped pulses on the order of

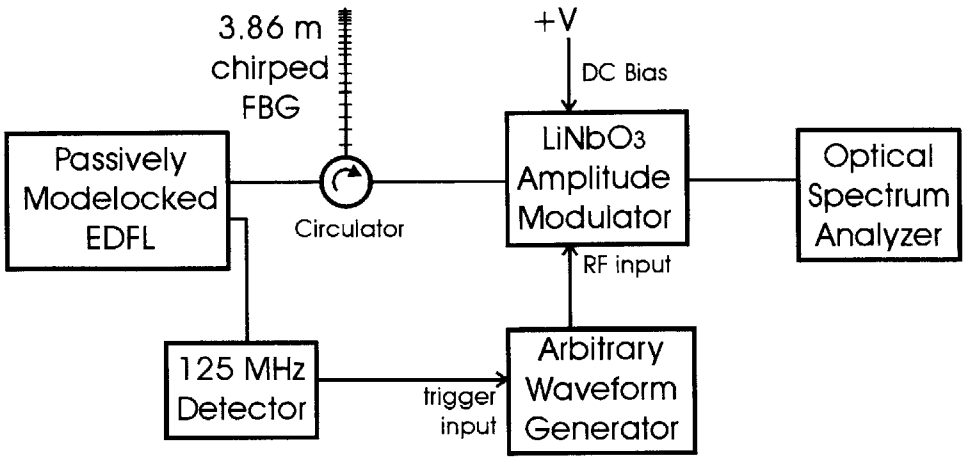

Figure 5-5: Setup for time domain spectral shaping experiment. Pulses from a modelocked fiber laser are chirped by an ultra-long fiber Bragg grating. Spectral shaping is performed by an amplitude modulator driven by an arbitrary waveform generator synchronized with the pulse train. An optical spectrum analyzer measures the spectrum.

3 ps in width; the exact initial chirp and width are overshadowed by the enormous dispersion provided by the FBG. The variable output port is coupled to a 125 MHz detector that triggers the arbitrary waveform generator (ArbWG). The pulses are routed via a circulator into the FBG, which reflects effectively a 24 nm wide window of light centered at 1550 nm (Figure 5-6) and provides a total delay of 32.6 ns between the short and long wavelength reflected light. Due to cladding mode losses, the 5 dB bandwidth of the FBG is limited to 24 nm. Pulses stretched to 32 ns are shown in Figure 5-7. The spike at the front of the pulse is a small reflection between the FBG and the circulator and the smaller ripples are due to variations in grating reflectivity and artifacts of detection electronics. After stretching pulses with the FBG, a circulator routes them to a lithium niobate amplitude modulator driven by a 1 GHz internally clocked ArbWG, which can be programmed for several waveforms. The optical spectrum is then observed on an optical spectrum analyzer.

In one case, we generate a Gaussian-shaped spectrum for OCT and IFOG ap-

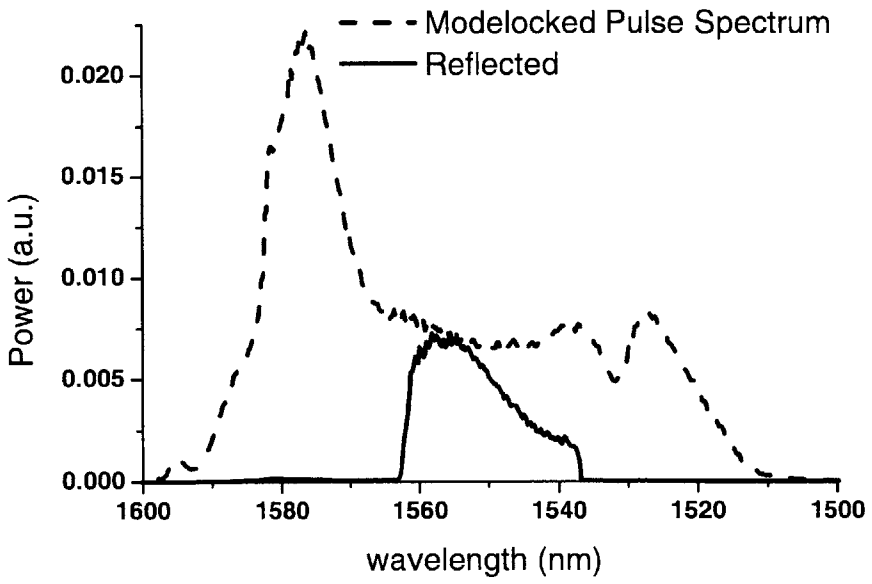

Figure 5-6: FBG input spectrum and reflected output spectrum.

plications. Figure 5-8 shows the spectrum with and without the ArbWG program activated. The untreated spectrum contains deep ripples due to birefringence in the FBG and the polarizing waveguide in the amplitude modulator. In future experiments, a FBG made with polarization maintaining fiber may be used. Even without polarization control, we can manually program a modulation signal to suppress the ripples, resulting in a much smoother spectrum. The signal applied to the ArbWG is thus proportional to the difference between a Gaussian function and the dashed curve in Figure 5-8. An appropriate algorithm can generate a further optimized signal. A reduction of average power will always be observed, in this case 4.0 dB, when the filter program is activated. Although modulation is applied, TDSS cannot generate new frequencies in the limit that the modulation bandwidth is much smaller than the optical spectral width. Thus, as with ordinary optical filters, this technique can only suppress frequency components and not create new ones.

The filter resolution $\Delta\lambda$ of the technique is dependent upon the temporal resolu-

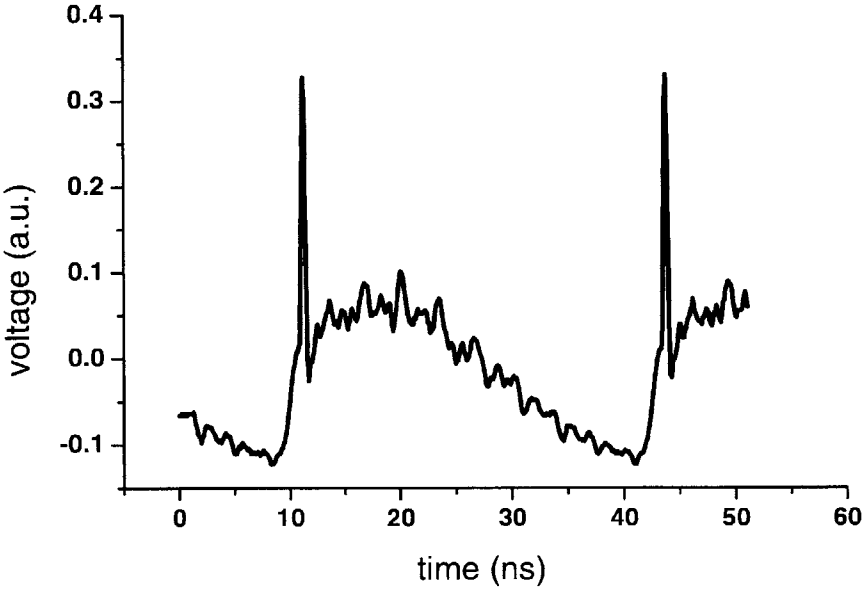

Figure 5-7: Oscilloscope trace of pulse after being stretched by the FBG. The time domain shape is similar to the output spectrum of Figure 5-6.

tion of the ArbWG, the bandwidth and the length of the FBG:

$$\Delta\lambda = \frac{W}{\tau}\tau_0 \tag{5.5}$$

where W is the pulse spectral width, τ is the delay induced by the FBG, and τ_0 is the temporal resolution of the ArbWG. In our experiment τ_0 is 1 nanosecond, yielding a theoretical resolution $\Delta\lambda$ of 0.7 nm. The repetition rate of the pulse source also places a limit of 32.6 nanoseconds on the maximum possible stretching. To measure the resolution, the narrowest possible optical notch filter was programmed into the ArbWG. The resulting filter shape, shown in Figure 5-9, reveals a 3 dB resolution bandwidth of 0.85 nm.

An analogous technique to TDSS has been demonstrated with femtosecond pulses and a spatial light modulator [117], where programmable modulation is performed in the spatial domain. Although it is not demonstrated here, TDSS is also effective in

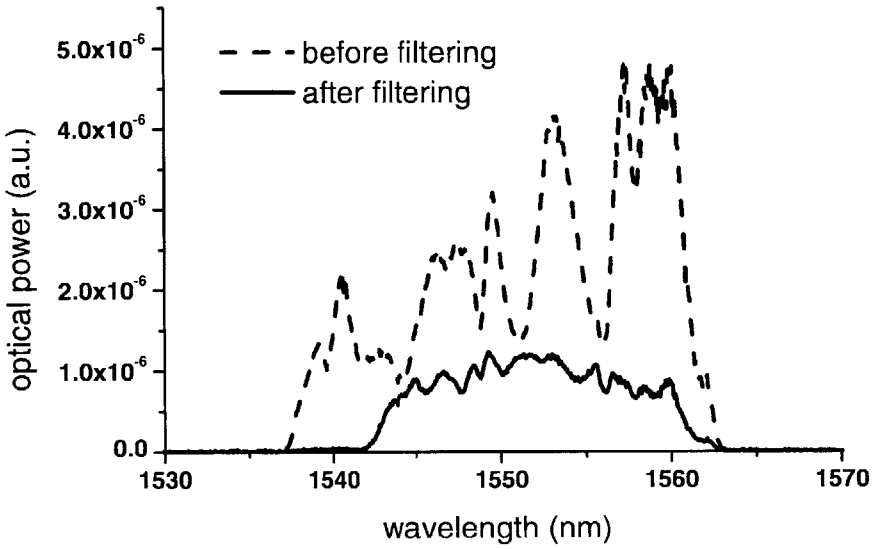

Figure 5-8: Arbitrary reshaping of irregular spectrum.

removing nonlinear chirp by phase modulation of frequency components [120, 121], done by replacing the amplitude modulator with a phase modulator. An advantage of TDSS is that all the optical components are fiber compatible, whereas the spatial domain method requires careful alignment of bulk optical components. The spatial technique, however, has no dependence on repetition rate. In telecommunications, TDSS is best suited for applications such as CPWDM and CDMA, where channel count and reconfigurability can compensate for low bit rate. For IFOGs, where superluminescent diodes and erbium fiber fluorescence sources are standard, the use of the modelocked laser provides an advantage because its spectrum is not limited by the spectral width of the gain medium [111]. Additionally, modelocked lasers enable supercontinuum generation for even wider bandwidth [122, 123, 124].

Ultra-long FBGs may expand the applications of TDSS, since pulse compression that is matched to the stretching function is possible. In general, dispersion compensating fiber does not inversely match the high order dispersion of SMF over a wide bandwidth, so effective pulse stretching and recompression are not possible. But FBG

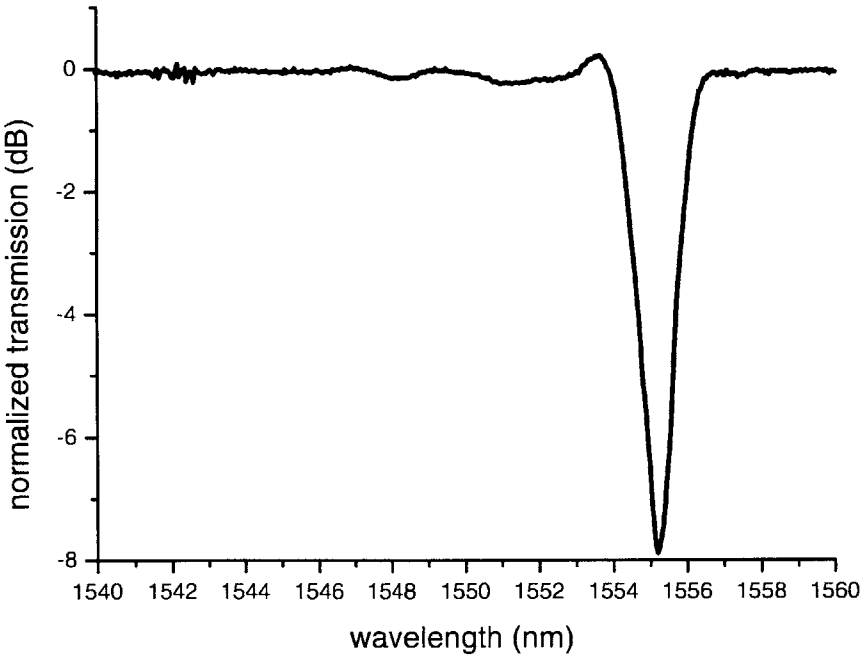

Figure 5-9: Notch filter response implemented with the arbitrary waveform generator.

may be fabricated as matched filter pairs [84].

This demonstration implements arbitrarily shaped optical filters, which are electronically programmable and can be tailored to produce nearly any desired spectrum from a broad input spectrum. The programmable nature of this technique is advantageous because source spectra can vary from laser to laser, and sometimes day to day for the same laser. The use of an FBG instead of several kilometers of SMF illustrates that TDSS can be implemented with more compact and robust devices. Future experiments with longer length and higher quality FBGs may demonstrate smaller spectral resolution TDSS for more complex filter shapes and added functionality.

Chapter 6

Conclusions and Future Work

6.1 PMD

It is interesting to note that after years of highly aggressive research and development, there does not yet exist a solid commercially available solution to PMD. Although this year (2000) there have been products released for evaluation by system manufacturers, there has been no indication that these tests were a resounding success. So despite the numerous techniques that have been proposed and demonstrated in conference and journal papers, the transition from the laboratory to the field has proven to be a barrier. Without having attempted to design a commercial product oneself, one can speculate that part of the difficulty is devising an adaptive system that is rigorous enough to comply with standard telecom outage rates, which are painfully stringent. It is not immediately obvious, for example, what feedback algorithm will most gracefully handle polarization controller resets, or whether degree of polarization or RF subharmonics provide the best feedback signals.

Even if feedback based PMD compensators are successful in the field, the next hurdle is clearly high order PMD. For long-haul systems within which PMD compensators are placed periodically, if only first order PMD is compensated, the high order PMD will still continue to accumulate [28]. High order PMD inherently contains more degrees of freedom and can only make the feedback problem more difficult. Hence, the motivation for investigating feedback-free techniques is highlighted by the

future direction of PMD compensation work. Although it entails using devices that may contain hysteresis and temperature instabilities, it is entirely conceivable that a feedback-free method may turn out to be more practical in the long run.

One might expect that a single high order compensator would be required for each set of WDM channels. This would be true for point to point links. However, an ongoing trend in optical communications is leading toward switched mesh networks. This implies that at any given node, the signal at a particular wavelength channel need not originate at the same point for very long. The path may be switched at any given moment, and the PMD compensator must adapt within several milliseconds for the switch to be minimally disruptive. It would be difficult for a single comprehensive compensator to adapt to one channel without disturbing the others.

If one were to consider longer term solutions several years down the road, soliton propagation looks to be most promising [33, 34]. The soliton, whether dispersion-managed or not, creates its own nonlinear potential well and is naturally resistant to spreading from either GVD or PMD. But even with nonlinear effects combating PMD, a hybrid solution involving compensators may eventually be the favored method.

6.2 Ultra-Long FBG Applications

Chirped FBGs have several advantages over other dispersive devices such as low nonlinearity and natural fiber compatibility. A notable feature of FBGs, however, which distinguishes them from other dispersive devices is the ripple in their frequency dependent delay. The ultra-long FBG used in this thesis was a first generation prototype, and has served well in experimental demonstrations despite the measurable ripple. Design and manufacturing techniques continually advance, as the device is being developed at 3M Corporation for commercial deployment in telecom systems. As it improves further, it will be seen in more telecom systems and other applications.

The application of ultra-long FBGs to spectral shaping, while benefiting from reduced ripple, is primarily limited by other factors. Future modelocked lasers which are environmentally stable will make the technique much more practical. It is also fea-

sible only with a low repetition rate laser. Ways of shaping spectra of high repetition rate lasers would also be of great interest.

For the pulse generation technique, smaller delay ripple will help reduce background radiation and yield shorter pulses. In addition to FBG improvements, a fast sawtooth FM signal could be applied to the DBR and could remove nearly all background radiation. The limiting factor here, though, is the tuning speed of the DBR laser. They are designed for sub-gigahertz wavelength switching, and not multi-gigahertz modulation. Therefore, even if a fast sawtooth signal were generated, the harmonics would not be seen. If the DBR section were redesigned to accept much faster signals, then not only could a sawtooth work, but a faster repetition rate could be used and hence a shorter FBG could work as well.

6.3 Summary

Optical pulse propagation has been and will continue to be an area of study in both scientific and technological contexts. Because of the recent Internet explosion, much emphasis has been on the impact on communications. But sensing applications such as fiber gyroscopes and optical coherence tomography will still be of interest even after the Internet boom dissipates. But regardless of economic cycles, the topics of dispersion and polarization, while not new, have been and will continue to present the research community with exciting new challenges.

Appendix A

Scattering Matrix of a Lossy Beamsplitter or Coupler

In practice, a Sagnac interferometer requires either a 50/50 beamsplitter or a 50/50 waveguide directional coupler. Such devices are not perfectly lossless in reality. The phase characteristics are important in a Sagnac interferometer, and it is necessary to understand them in the nonideal cases. In this appendix we shall apply the scattering matrix formalism. Since the treatments for beamsplitters and waveguide couplers are identical, we refer only to the beamsplitter.

A beamsplitter can be represented by a 2×2 scattering matrix **S** (see [143]):

$$\mathbf{S} = \begin{bmatrix} S_{11} & S_{12} \\ S_{21} & S_{22} \end{bmatrix} \tag{A.1}$$

One can write:

$$\mathbf{b} = \mathbf{Sa} \tag{A.2}$$

where

$$\mathbf{a} \equiv \begin{bmatrix} a_1 \\ a_2 \end{bmatrix} \tag{A.3}$$

$$\mathbf{b} \equiv \begin{bmatrix} b_1 \\ b_2 \end{bmatrix} \tag{A.4}$$

(A.5)

a_1 and a_2 are the input beams, and b_1 and b_2 are the output beams as shown in Figure A-1

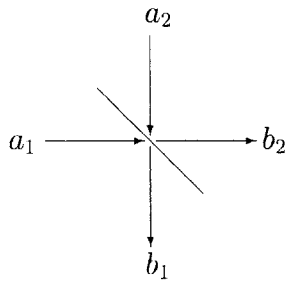

Figure A-1: Beamsplitter input and output ports.

Reciprocity requires **S** to by symmetric. This removes a degree of freedom by means of the restriction:

$$S_{12} = S_{21} \tag{A.6}$$

If we choose appropriate reference planes, and $|S_{11}| = |S_{22}|$, we can write:

$$\mathbf{S} = \begin{bmatrix} -r & jt \\ jt & -r \end{bmatrix} \tag{A.7}$$

Here, we have made use of the knowledge that for a lossless beamsplitter, the phase between reflection and transmission is exactly $\frac{\pi}{2}$. Because this is a passive device, we can restrict r and t further by starting with:

$$|\mathbf{b}|^2 \leq |\mathbf{a}|^2 \tag{A.8}$$

If Equation A.8 were not satisfied, we would have gain and that is clearly not the case. Substituting Equation A.2,

$$|\mathbf{Sa}|^2 \leq |\mathbf{a}|^2 \tag{A.9}$$

which leads to

$$\mathbf{a}^+[\mathbf{1} - \mathbf{S}^+\mathbf{S}]\mathbf{a} \geq 0 \tag{A.10}$$

For Equation A.10 to hold, the matrix $[\mathbf{1}-\mathbf{S}^+\mathbf{S}]$ must be positive semidefinite. Equivalently, the eigenvalues must be nonnegative. We shall use this to determine the limits on the phase relation between r and t in the lossy case.

From Equation A.7, we have

$$[\mathbf{1} - \mathbf{S}^+\mathbf{S}] = \begin{bmatrix} 1-(|r|^2+|t|^2) & -jtr^* + jt^*r \\ jt^*r - jtr^* & 1-(|r|^2+|t|^2) \end{bmatrix} \tag{A.11}$$

Let

$$L = 1-(|r|^2+|t|^2) \tag{A.12}$$

For the 2×2 matrix the eigenvalues are given by the quadratic formula:

$$\lambda_\pm = L \pm \sqrt{2|r|^2|t|^2 - (t^{*2}r^2 + t^2r^{*2})} \tag{A.13}$$

In order to ensure nonnegative λ's, we impose that

$$L \geq \sqrt{2|r|^2|t|^2 - (t^{*2}r^2 + t^2r^{*2})} \tag{A.14}$$

Now if we set r to be real and allow t have a phase ϕ:

$$r = r_0 \tag{A.15}$$

$$t = t_0 e^{j\phi} \tag{A.16}$$

This leads to

$$L^2 \geq 2r_0^2 t_0^2 [1 - \cos(2\phi)] \tag{A.17}$$

and finally substituting for L,

$$\cos(2\phi) \geq \frac{2(r_0^2 + t_0^2) - (1 + r_0^4 + t_0^4)}{2r_0^2 t_0^2} \tag{A.18}$$

As a check, one can confirm that for the perfectly lossless case, that is, when $r_0 = t_0 = \frac{1}{\sqrt{2}}$, then

$$\cos(2\phi) \geq 1 \tag{A.19}$$

and ϕ can only be 0. Therefore, the total phase between reflection and transmission for a lossless beamsplitter can only be $\frac{\pi}{2}$.

Appendix B

Timing Jitter Due to Polarization Scrambling and Residual PMD

As described in section 3.3.3, polarization scrambling causes a timing jitter at the receiver if there is small PMD in the transmission line. Here, we derive the resulting timing jitter variance [35].

We first express the output electric field of a PMD medium with residual DGD τ_{res}, which is small compared with the inverse bandwidth of the input pulse shape $a_0(t)$:

$$\vec{E}_{out}(t) = \begin{bmatrix} ua_0(t + \frac{\tau_{res}}{2}) \\ va_0(t - \frac{\tau_{res}}{2}) \end{bmatrix} \tag{B.1}$$

u and v are normalized amplitudes such that

$$|u|^2 + |v|^2 = 1 \tag{B.2}$$

Intensities are defined in terms of $\vec{E}_{out}$ and $a_0(t)$:

$$I_{out}(t) = |\vec{E}_{out}|^2 \tag{B.3}$$

$$I_0(t) = |a_0(t)|^2 \tag{B.4}$$

We then rewrite $I_{out}(t)$ by plugging B.1 into B.3:

$$
\begin{aligned}
I_{out}(t) &= |u|^2 \left| a_o\left(t + \frac{\tau_{res}}{2}\right)\right|^2 + |v|^2 \left| a_o\left(t - \frac{\tau_{res}}{2}\right)\right|^2 && \text{(B.5)}\\
&\approx |u|^2 \left| a_0(t) + \frac{\tau_{res}}{2} a_0'(t)\right|^2 + |v|^2 \left| a_0(t) - \frac{\tau_{res}}{2} a_0'(t)\right|^2 && \text{(B.6)}\\
&= (|u|^2 + |v|^2)\left(|a_0(t)|^2 + \left|\frac{\tau_{res}}{2} a_0'(t)\right|^2\right) + \\
&\quad \frac{\tau_{res}}{2}\left(|u|^2 - |v|^2\right)[2a_0(t)a_0'(t)] && \text{(B.7)}\\
&\approx I_0(t) + \frac{\tau_{res}}{2}\left(|u|^2 - |v|^2\right) I_0'(t) && \text{(B.8)}
\end{aligned}
$$

A first order approximation is made in B.6, and B.2 and B.4 are used to simplify B.8. τ_{res}^2 terms are dropped, and $I_0'(t)$ is substituted for $2a_0(t)a_0'(t)$.

Next, we notice from B.8 that the apparent shift τ_{shift} is the coefficient of $I_0'(t)$:

$$\tau_{shift} = \frac{\tau_{res}}{2}\left(|u|^2 - |v|^2\right) \tag{B.9}$$

In Poincaré space, the quantity $|u|^2 - |v|^2$ corresponds to the z component of the polarization state. The z component is also the cosine of the azimuthal angle from the z axis:

$$z = |u|^2 - |v|^2 = cos(\theta) \tag{B.10}$$

Therefore:

$$\tau_{shift} = \frac{\tau_{res}}{2} cos(\theta) \tag{B.11}$$

For good scrambler which randomizes the polarization state to spread it evenly about the Poincaré sphere, the mean θ is intuitively $\pi/2$ and the mean z is similarly 0.

$$\langle \tau_{shift} \rangle = \frac{\tau_{res}}{2} \langle cos(\theta) \rangle = \frac{\tau_{res}}{2} \langle z \rangle = 0 \tag{B.12}$$

To calculate the σ_{shift}^2, the variance of τ_{shift}, we use the probability density function for the azimuth θ:

$$p_\theta(\theta') = \frac{sin(\theta')}{2} \tag{B.13}$$

σ^2_{shift} is thus computed:

$$\sigma^2_{shift} = \left\langle \tau^2_{shift} \right\rangle = \left(\frac{\tau_{res}}{2}\right)^2 \int_0^{\pi} cos^2(\theta) p_\theta(\theta) d\theta \tag{B.14}$$

$$= \left(\frac{\tau_{res}}{2}\right)^2 \frac{1}{2} \int_0^{\pi} cos^2(\theta) sin(\theta) d\theta \tag{B.15}$$

$$= \frac{\tau^2_{res}}{12} \tag{B.16}$$

The variance σ^2_{shift} and the square of the associated residual PMD τ_{res} are thus related by a factor of 12.

Appendix C

List of Acronyms

AC Autocorrelation

AM Amplitude Modulator

APM Additive Pulse Modelocked

ArbWG Arbitrary Waveform Generator

ASE Amplified Spontaneous Emission

CCW Counter-Clockwise

CDMA Code-Division Multiple Access

CPWDM Chirped Pulse Wavelength Division Multiplexing

CW Clockwise

CW Continuous Wave

D Detector

DBR Distributed Bragg Reflector

DC Direct Current

DFB Distributed Feedback

DGD Differential Group Delay

DOP Degree Of Polarization

DUT Device Under Test

EDF Erbium Doped Fiber

EDFA Erbium Doped Fiber Amplifier

EDFL Erbium Doped Fiber Laser

FBG Fiber Bragg Grating

FM Frequency Modulated

FSR Free Spectral Range

FWHM Full Width Half Maximum

GVD Group Velocity Dispersion

IFOG Interferometric Fiber Optic Gyroscope

JME Jones Matrix Eigenanalysis

LED Light Emitting Diode

MMM Müller Matrix Method

NRZ Non Return to Zero

OCT Optical Coherence Tomography

OSA Optical Spectrum Analyzer

P-APM Polarization Additive Pulse Modelocked

PBS Polarizing Beamsplitter

PD Photodiode

PDL Polarization Dependent Loss

PM Polarization Maintaining

PMD Polarization Mode Dispersion

PMDC Polarization Mode Dispersion Compensator

PMF Polarization Maintaining Fiber

PSP Principal State of Polarization

RF Radio Frequency

SLD Superluminescent Diode

SLM Spatial Light Modulator

SMF Single Mode Fiber

SOP State of Polarization

SP-APM Stretched Pulse Additive Pulse Modelocked

TDSS Time Domain Spectral Shaping

UV Ultraviolet

WDM Wavelength Division Multiplexed

Bibliography

PMD Background

[1] H. A. Haus, "Group velocity, energy, and polarization mode dispersion," *Journal of the Optical Society of America B-Optical Physics*, vol.16, no.11, Nov. 1999, pp.1863-7.

[2] R. M. Jopson, L. E. Nelson, H. Kogelnik, "Measurement of Second-Order Polarization-Mode Dispersion Vectors in Optical Fibers," *IEEE Photonics Technology Letters*, vol. 11, no. 9, September, 1999.

[3] L. E. Nelson, R. M. Jopson, H. Kogelnik, G. J. Foschini, "Measurement of Depolarization and Scaling Associated with Second-Order Polarization Mode Dispersion in Optical Fibers," *IEEE Photonics Technology Letters*, vol. 11, no. 12, pp. 1614-6, December, 1999.

[4] Poole, C. D. and Wagner, R. E., "Phenomenological approach to polarization dispersion in long single-mode fibers," *Electronics Letters*, vol. 22, pp. 1029-30, 1986.

[5] Poole, C. D., Winters, J. H., Nagel, J. A., "Dynamical equation for polarization dispersion," *Optics Letters*, vol. 16, no. 6, pp. 372-4, 1991.

[6] Poole, C. D. and Giles, C. R., "Polarization-dependent pulse compression and broadening due to polarization dispersion in dispersion-shifted fiber," *Optics Letters*, vol. 13, no. 2, pp. 155-7, 1988.

[7] Poole, C. D., "Statistical treatment of polarization dispersion in single-mode fiber," *Optics Letters*, vol. 13, no. 8, pp. 687-9, 1988.

[8] Poole, C. D., Tkach, R. W., Chraplyvy, A. R., Fishman, D. A., "Fading in Lightwave Systems Due to Polarization-Mode Dispersion," *IEEE Photonics Technology Letters*, vol. 3, no. 1, pp. 68-70, 1991.

[9] Poole, C. D., Foschini, G. J., "Statistical Theory of Polarization Dispersion in Single Mode Fibers," *Journal of Lightwave Technology*, vol. 9, no. 11, pp. 1439-56, 1991.

[10] Poole, C. D. and Nagel, J., "Polarization Effects in Lightwave Systems," Chapter 6 of *Optical Fiber Telecommunications IIIA*, I. P. Kaminow and T. L. Koch, ed., copyright ©1997 by AT&T, reproduced by permission of Academic Press. All rights reserved.

[11] J. P. Gordon, H. Kogelnik, "PMD fundamentals: Polarization mode dispersion in optical fibers," *Proceedings of the National Academy of Sciences*, vol. 97, no. 9, April 25, 2000, pp. 4541-4550.

[12] Heffner, B. L., "Deterministic, Analytically Complete Measurement of Polarization-Dependent Transmission Through Optical Devices," *IEEE Photonics Technology Letters*, vol. 4, no. 5, pp. 451-4, May, 1992.

[13] J. Cameron, X. Bao, J. Stears, "Time evolution of polarization-mode dispersion for aerial and buried cables," OFC'98 Technical Digest, WM51, pp. 240-1, San Jose, February, 1998.

[14] Bülow, H., Baumert, W., Schmuck H., Mohr, F., Schulz, T., Küppers, F., Weiershausen, W., "Measurement of the Maximum Speed of PMD Fluctuation in Installed Field Fiber," OFC'99 Proceedings, WE4, February, 1999, San Diego, CA.

[15] R. C. Jones, "New Calculus for the Treatment of Optical Systems I. Description and Discussion of the Calculus," *J. Optical Soc. Amer.*, vol. 31, pp. 488-93, 1941.

[16] R. C. Jones, "A new calculus for the treatment of optical systems. VI. Experimental determination of the matrix," *J. Optical Soc. Amer.*, vol. 37, pp. 110-2, 1947.

[17] Shurcliffe, W. A. *Polarized Light.* Oxford University Press, 1962.

[18] M. Born, E. Wolf, *Principles of Optics*, Pergamon Press, New York, 1965.

[19] H. Poincaré, "Théorie Mathcématique de la Lumière," Paris, Georges Carré, ed., Vol. 2, (1892) Chap 12.

[20] N. Gisin, J. Von der Weid, J. Pellaux, "Polarization mode dispersion of short and long single-mode fibers," *IEEE J. Lightwave Tech*, vol. LT-9, pg 821-7, 1991.

[21] B. L. Heffner, "Automated Measurement of Polarization Mode Dispersion Using Jones Matrix Eigenanalysis," *IEEE Photonics Technology Letters*, vol. 4, no. 9, Sep. 1992, pp. 1066-9.

[22] B. L. Heffner, "Accurate, Automated Measurement of Differential Group Delay Dispersion and Principal State Variation Using Jones Matrix Eigenanalysis," *IEEE Photonics Technology Letters*, vol. 5, no. 7, Jul. 1993, pp. 814-7.

[23] H. Sunnerud, B. Olsson, P. A. Andrekson, "Measurement of Polarization Mode Dispersion Accumulation Along Installed Optical Fibers," *IEEE Photonics Technology Letters*, vol. 11, no. 7, Jul. 1999, pp. 860-2.

[24] F. Corsi, A. Galtarossa, L. Palmieri, M. Schiano, T. Tambosso, "Continuous-Wave Backreflection Measurement of Polarization Mode Dispersion," *IEEE Photonics Technology Letters*, vol. 11, no. 4, April, 1999, pp. 451-3.

[25] B. Huttner, B. Gisin, N. Gisin, "Distributed PMD Measurement with a Polarization-OTDR in Optical Fibers," *Journal of Lightwave Technology*, vol. 17, no. 10, Oct. 1999, pp. 1843-8.

[26] D. Andresciani, F. Curti, F. Matera, B. Daino, "Measurement of the group-delay difference between the principal states of polarization on a low-birefringence terrestrial fiber cable," *Optics Letters*, vol. 12, no. 10, October, 1987, pg. 844-6.

[27] Poole, C. D., Bergano, N. S., Wagner, R. E., and Schulte, H. J., "Polarization Dispersion and Principal States in a 147-km Undersea Lightwave Cable," *Journal of Lightwave Technology*, vol. 6, no. 7, pp. 1185-90, 1988.

[28] J. M Fini, H. A. Haus, "Accumulation of Polarization Mode Dispersion in Cascades of Compensated Optical Fibers," to appear in *IEEE Photonics Technology Letters*, Feb. 2000.

[29] Hernday, P., "Polarization Measurements," Chapter 6 of *Fiber Optic Test and Measurement*, D. Derickson, ed., Prentice Hall, 1998.

[30] H. Bülow, "System Outage Probability Due to First- and Second-Order PMD," *IEEE Photonics Technology Letters*, vol. 10, no. 5, May, 1998.

[31] L. E. Nelson, R. M. Jopson, H. Kogelnik, J. P. Gordon, "Measurement of polarization mode dispersion vectors using the polarization-dependent signal delay method," *Optics Express*, vol.6, no.8, 10 April 2000.

[32] N. Gisin, J. P. Pellaux, "Polarization mode dispersion: time versus frequency domains," *Optics Communications*, vol. 89, no. 2,3,4, 1 May 1992, pp. 316-23.

[33] Y. Chen, H. A. Haus, "Manakov solitons and polarization mode dispersion," *Chaos*, vol.10, no.3, Sept. 2000, pp.529-38.

[34] C. R. Menyuk, "Polarization mode dispersion in optical communication systems," *Conference on Lasers and Electro-Optics (CLEO 2000), Technical Digest, Postconference Edition*, Opt. Soc. America. 2000, pp.58.

[35] Private discussion with J. M. Fini.

PMD Compensation

[36] Hakki, B. W., "Polarization mode dispersion compensation by phase diversity detection," *IEEE Photonics Technology Letters*, vol.9, no.1, pp. 121-3, 1997.

[37] Heismann, F., Fishman, D. A., and Wilson, D. L., "Automatic Compensation of First-Order Polarization Mode Dispersion in a 10 Gb/s Transmission System," ECOC'98 Proceedings, pp 529-30, September 1998, Madrid, Spain.

[38] C. Glingener, A. Schöpflin, A. Färbert, G. Fischer, R. Noé, D. Sandel, S. Hinz, M. Yoshida-Dierolf, V. Mirvoda, G. Feise, H. Herrmann, R. Ricken, W. Sohler, F. Wehrmann, "Polarization mode dispersion compensation at 20 Gb/s with a compact distributed equalizer in $LiNbO_3$," OFC'99 Postdeadline Proceedings, PD29, February, 1999, San Diego, CA.

[39] F. Roy, C. Francia, F. Bruyère, D. Penninckx, "A simple dynamic polarization mode dispersion compensator," OFC'99 Proceedings, PD29, February, 1999, San Diego, CA.

[40] Chbat, M. W., Soigné, J-P., Fuerst, T., Anthony, J. T., Lanne, S., Février, H., Desthieux, B. M., Bush, A. H., and Penninckx, D., "Long Term Field Demonstration of Optical PMD Compensation on an Installed OC-192 Link," OFC'99 Postdeadline Proceedings, PD12, February, 1999, San Diego, CA.

[41] S. Lee, R. Khosravani, J. Peng, V. Grubsky, D. S. Starodubov, A. E. Willner, J. Feinberg, "Adjustable Compensation of Polarization Mode Dispersion Using a High-Birefringence Nonlinearly Chirped Fiber Bragg Grating," *IEEE Photonics Technology Letters*, vol. 11, no. 10, October, 1999, pp. 1277-9.

[42] M. Karlsson, H. Sunnerud, P. A. Andrekson, "A comparison of different PMD-compensation techniques," *European Conference on Optical Communications*, Munich, Germany, Aug. 2000, paper 4.2.2.

[43] H. Bülow, "PMD mitigation techniques and their effectiveness in installed fiber," *OFC 2000*, Baltimore, MD, March, 2000, paper ThH1.

[44] M. Romagnoli, P. Franco, R. Corsini, A. Schiffini, M. Midrio, "Time domain Fourier optics for polarization-mode dipsersion compensation," *Optics Letters*, vol. 24, no. 17, 1 Sep. 1999, pp. 1197-9.

[45] T. Takahashi, T. Imai, M. Aiki, "Automatic compensation technique for timewise fluctuating polarisation mode dispersion in in-line amplifier systems," *Electronics Letters*, vol. 30, no. 4, February 17, 1994, pg. 348-9.

[46] J. Nagel, L. Garrett, "Time variations of PMD- Field measurements," OSA Annual Meeting 2000, Providence, RI, Invited paper ThGG3.

[47] J. A. Nagel, M. W. Chbat, L. D. Garrett, J. P. Soigné, N. A. Weaver, B. M. Desthieux, H. Bülow, A. R. McCormick, R. M. Derosier, "Long-term PMD mitigation at 10 Gb/s and time dynamics over high-PMD installed fiber," *European Conference on Optical Communications*, Munich, Germany, Aug. 2000, paper 4.2.1.

[48] D. A. Watley, K. S. Farley, W. S. Lee, g. Bordogna, B. J. Shaw, A. P. Hadjifotiou, "Field evaluation of an optical PMD compensator using an installed 10 Gbit/s system," *Optical Fiber Communications 2000*, March, 2000, paper ThB6, pg. 37-9, vol 3.

[49] F. Roy, C. Francia, F. Bruyère, D. Penninckx, "A simple dynamic polarization mode dispersion compensator," *Optical Fiber Communications 1999*, February, 1999, paper TuS4, pg. 275-8.

[50] C. Francia, F. Bruyère, J.-P. Thiéry, D. Penninckx, "Simple dynamic polarisation mode dispersion compensator," *Electronics Letters*, vol. 35, no. 5, March 4th, 1999, pp. 414-5.

[51] R. Noé, D. Sandel, M. Yoshida-Dierolf, S. Hinz, V. Mirvoda, A. Schöpflin, C. Glingener, E. Gottwald, C. Scheerer, G. Fischer, T. Weyrauch, W. Haase, "Polarization Mode Dispersion Compensation at 10, 20, and 40 Gb/s with Various

Optical Equalizers," *Journal of Lightwave Technology*, vol. 17, no. 9, September, 1999, pg. 1602-16.

[52] F. Heismann, M. S. Whalen, "Fast automatic polarization control system," *IEEE Photonics Technology Letters*, vol.4, no.5, May 1992, pp.503-5.

[53] A. Weber, B. L. Heffner, D. W. Dolfi, P. Chou, "Reset-free system for real-time polarization control and synthesis," *Applied Optics*, vol.31, no.34, 1 Dec. 1992, pp.7180-2.

[54] M. Shtaif, A. Mecozzi, M. Tur, J. A. Nagel, "A Compensator for the Effects of High-Order Polarization Mode Dispersion in Optical Fibers," *IEEE Photonics Technology Letters*, vol. 12, no. 4, April, 2000, pp. 434-6.

[55] N. S. Bergano, C. R. Davidson, F. Heismann, "Bit-synchronous polarization and phase modulation improves the performance of optical amplifier transmission systems," OFC'96. Optical Fiber Communication. Vol.2. 1996 Technical Digest Series. Conference Edition (IEEE Cat. No.96CH35901). Opt. Soc. America. 1996, pp.70. Washington, DC, USA.

[56] N. S. Bergano, C. R. Davidson, F. Heismann, "Bit-synchronous polarisation and phase modulation scheme for improving the performance of optical amplifier transmission systems," *Electronics Letters*, vol. 32, no. 1, 4 Jan. 1996, pp.52-4.

[57] F. Bruyere, O. Audouin, V. Letellier, B. Bassier, P. Marmier, "Demonstration of an optimal polarization scrambler for long-haul optical amplifier systems," *IEEE Photonics Technology Letters*, vol. 6, no. 9, Sept. 1994, pp.1153-5.

[58] N. S. Bergano, C. R. Davidson, "Polarization-scrambling-induced timing jitter in optical-amplifier systems," OFC '95 Optical Fiber Communication. Summaries of Papers Presented at the Conference on Optical Fiber Communication. Vol.8. 1995 Technical Digest Series. Postconference Edition. Opt. Soc. America. 1995, pp.122-3. Washington, DC, USA.

[59] P. C. Chou, J. M. Fini, H. A. Haus, "Real-Time Principal State Characterization for Feedback-Free PMD Compensation," submitted to *IEEE PTL.*

[60] H. Sunnerud, M. Karlsson, P. A. Andrekson, "Analytical Theory for PMD-Compensation," *IEEE Photonics Technology Letters*, vol. 12, no. 1, Jan. 2000, pp. 50-2.

Frequency Modulation of Lasers

[61] D. J. Kuizenga, A. E. Siegman, "FM-Laser Operation of the Nd:YAG laser," *IEEE Journal of Quantum Electronics*, vol. QE-6, no. 11, pp. 673-7, 1970.

[62] A. E. Siegman, *Lasers.* Mill Valley, CA: University Science Books, 1993.

[63] O. Kjebon, R. Schatz, S. Lourdudoss, S. Nilsson, B. Stålnacke, L. Bäckbom "30 GHz direct modulation bandwidth in detuned loaded InGaAsP DBR lasers at 1.55μm wavelength," *Electronics Letters*, vol. 33, no. 6, p. 488-9, 1997.

[64] S. E. Harris, R. Targ, "FM oscillation of the He-Ne laser," *Applied Physics Letters*, vol. 5, no. 10, pp. 202-4, 1964.

[65] S. R. Chinn, E. A. Swanson, "Passive FM Locking and Pulse Generation from 980-nm Strained-Quantum-Well Fabry-Perot Lasers," *IEEE Photonics Technology Letters*, vol. 5, no. 9, pp. 969-71, 1993.

[66] L. F. Tiemeijer, P. I. Kuindersma, P. J. A. Thijs, G. L. J. Rikken, "Passive FM Locking in InGaAsP Semiconductor Lasers," *IEEE Journal of Quantum Electronics*, vol. 25, no. 6, pp. 1385-92, 1989.

[67] R. Nagar, D. Abraham, N. Tessler, A. Fraenkel, G. Eisenstein, E. P. Ippen, U. Koren, G. Raybon, "Frequency-modulation mode locking of a semiconductor laser," *Optics Letters*, vol. 16, no. 22, pp. 1750-2, 1991.

[68] T. Kobayashi, H. Yao, K. Amano, Y. Fukushima, A. Morimoto, T. Sueta, "Optical Pulse Compression Using High-Frequency Electrooptic Phase Modulation," *IEEE Journal of Quantum Electronics*, vol. 24, no. 2, pp. 382-7, 1988.

[69] A. E. Willner, M. Kuznetsov, I. P. Kaminow, U. Koren, T. L. Koch, C. A. Burrus, G. Raybon, "Multigigahertz Bandwidth FM Response of Frequency Tunable Two-Electrode DFB Lasers," *IEEE Photonics Technology Letters*, vol. 1, no. 11, pp. 360-3, 1989.

[70] M. J. W. Rodwell, M. Kamegawa, R. Yu, M. Case, E. Carman, K. S. Giboney, "GaAs Nonlinear Transmission Lines for Picosecond Pulse Generation and Millimeter-Wave Sampling," *IEEE Transactions on Microwave Theory and Techniques*, vol. 39, no. 7, pp. 1194-1204, 1991.

Fiber Bragg Gratings

[71] J. F. Brennan III, D. L. LaBrake, "Realization of >10-m-long chirped fiber Bragg gratings," *Technical Digest of Bragg Gratings, Photosensitivity, and Poling in Glass Waveguides*, Optical Society of America, p. 35-7, 1999.

[72] K. O. Hill, Y. Fujii, D. C. Johnson, B. S. Kawasaki, "Photosensitivity in optical fiber waveguides: Application to reflection filter fabrication," *Applied Physics Letters*, vol. 32, pp. 647-9, 1978.

[73] B. S. Kawasaki, K. O. Hill, D. C. Johnson, Y. Fujii, "Narrow-band Bragg reflectors in optical fibers," *Optics Letters*, vol. 3, pp. 66-8, 1978.

[74] G. Meltz, W. W. Morey, W. H. Glenn, "Formation of Bragg gratings in optical fibers by a transverse holographic method," *Optics Letters*, vol. 14, pp. 823-5, 1989.

[75] J. F. Brennan III, "Long-length fiber Bragg gratings usher in a new era," *Lightwave Magazine*, vol. 17, no. 3, March, 2000.

[76] A. Asseh, H. Storoy, B. E. Sahlgren, S. Sandgren, R. A. H. Stubbe, "A writing technique for long fiber Bragg gratings with complex reflectivity profiles," *Journal of Lightwave Technology*, vol.15, no.8, pp.1419-23, 1997.

[77] H. Rourke, B. Pugh, S. Kanellopoulos, V. Baker, B. Napier, D. Greene, D. Goodchile, J. Fells, R. Epworth, A. Collar, C. Rogers, "Fabrication of extremely long fibre gratings by phase matched concatenation of multiple short sections," *Technical Digest of Bragg Gratings, Photosensitivity, and Poling in Glass Waveguides*, (Optical Society of America, Washington, D. C., 1999),p. 32.

[78] Rourke, H. N., Baker, S. R., Byron, K. C., Baulcomb, R. S., Ojha, S. M., and Clements, S., "Fabrication and characterisation of long, narrowband fibre gratings by phase mask scanning," *Electronics Letters*, vol. 30, no. 16, pp. 1341-2, 1994.

[79] L. R. Chen, S. D. Benjamin, P. W. E. Smith, J. E. Sipe, S. Juma, "Ultrashort pulse propagation in multiple-grating fiber structures," *Optics Letters*, vol.22, no.6, 15 March 1997, pp.402-4.

[80] H. Geiger, A. Fu, P. Petropoulos, M. Ibsen, D. J. Richardson, R. I. Laming, "Demonstration of a simple CDMA transmitter and receiver using sampled fibre gratings," *24th European Conference on Optical Communication ECOC '98.*

[81] A. Grunnet-Jepsen, a. E. Johnson, E. S. Maniloff, T. W. Mossberg, M. J. Munroe, J. N. Sweetser, "Demonstration of All-Fiber Sparse Lightwave CDMA Based on Temporal Phase Encoding," *IEEE Photonics Technology Letters*, vol. 11, no. 10, pg 1283-5, October, 1999.

[82] P. Petropoulos, M. Ibsen, D. J. Richardson, "GHz-repetition-rate pulse multiplication using a sampled fiber Bragg grating," Summaries of papers presented at the Conference on Lasers and Electro-Optics. Postconference Edition. CLEO '99. Conference on Lasers and Electro-Optics (IEEE Cat. No.99CH37013). Opt. Soc. America. 1999, pp.220. Washington, DC, USA.

[83] P. Petropoulos, M. Ibsen, D. J. Richardson, "Rectangular pulse generation based on pulse reshaping using a superstructured fiber Bragg grating," *Technical Digest of Bragg Gratings, Photosensitivity, and Poling in Glass Waveguides*, (Optical Society of America, Washington, D. C., 1999), p. 186-8.

[84] H. Geiger, M. Ibsen, R. I. Laming, "Optimum receivers with fiber gratings," OFC '98. Optical Fiber Communication Conference and Exhibit. Technical Digest. Conference Edition. 1998 OSA Technical Digest Series Vol.2 (IEEE Cat. No.98CH36177). Opt. Soc. America. 1998, pp.152-4. Washington, DC, USA.

[85] M. A. Muriel, J. Azaña, A. Carballar, "Real-time Fourier transformer based on fiber gratings," *Optics Letters*, vol.24, no.1, 1 Jan. 1999, pp.1-3.

[86] M. A. Putnam, M. L. Dennis, I. N. Duling III, C. G. Askins, and E. J. Friebele, "Broadband square-pulse operation of a passively mode-locked fiber laser for fiber Bragg grating interrogation," *Optics Letters*, vol. 32, no. 2, p. 138-40, 1998.

Fiber Optic Gyroscopes

[87] K. Böhm, P. Russer, E. Weidel, and R. Ulrich, "Low-Noise Fiber-Optic Gyroscope," *Optics Letters*, vol. 6, p. 64-6, 1981.

[88] R. A. Bergh, H. C. Lefevre, H. J. Shaw, "All-Single-Mode Fiber-Optic Gyroscope," *Optics Letters*, vol. 6, p. 198-200, 1981.

[89] H. Lefèvre, *The Fiber-optic Gyroscope.* Boston: Artech House, 1993.

[90] W. K. Burns, ed., *Optical Fiber Rotation Sensing* (Academic Press, San Diego, CA, 1994).

[91] Sagnac, G., "L'éther lumineux démontré par l'effet du vent relatif d'éther dans un interféromètre en rotation uniforme," Comptes rendus de l'Académie des Sciences, Vol. 95, 1913, pp. 708-710. Sagnac, G., "Sur la preuve de la réalité de

l'éther lumineux par l'expérience de l'interférographe tournant," Comptes rendus de l'Académie des Sciences, Vol. 95, 1913, pp. 1410-1413.

[92] S. Ezekiel and H. J. Arditty, "Fiber-Optic Rotation Sensors," *Fiber-Optic Rotation Sensors and Related Technologies*, pp.2-26, 1982.

[93] S. Ezekiel, J. L. Davis, R. W. Hellwarth, "Intensity Dependent Nonreciprocal Phase Shift in a Fiberoptic Gyroscope," Springer Series in Optical Sciences, vol. 32, p. 332-6, 1982.

[94] K. Petermann, "Intensity-Dependent Nonreciprocal Phase Shift in Fiber-Optic Gyroscopes for Light Sources With Low Coherence," *Optics Letters*, vol. 7, no. 11, p. 563-5, 1982.

[95] A. E. Kaplan and P. Meystre, "Large Enhancement of the Sagnac Effect in a Nonlinear Ring Resonator and Related Effects," Springer Series in Optical Sciences, vol. 32, p. 375-85, 1982.

[96] R. A. Bergh, B. Culshaw, C. C. Cutler, H. C. Lefevre, and H. J. Shaw, "Source statistics and the Kerr effect in fiber-optics gyroscopes," *Optics Letters*, vol. 7, no. 11, p. 563-5, 1982.

[97] R. A. Bergh, H. C. Lefevre, and H. J. Shaw, "Compensation of the optical Kerr effect in fiber-optic gyroscopes," *Optics Letters*, vol. 7, no. 6, p. 282-4, 1982.

[98] K. A. Fesler, M. J. F. Digonnet, B. Y. Kim, H. J. Shaw, "Stable fiber-source gyroscopes," *Optics Letters*, vol. 15, no. 22, p. 1321-3, 1990.

[99] J. L. Wagener, M. J. F. Digonnet, H. J. Shaw, "A High-Stability Fiber Amplifier Source for the Fiber Optic Gyroscope," *IEEE Journal of Lightwave Technology*, vol. 15, no. 9, p. 1689-94, 1997.

[100] P. C. Chou, H. A. Haus, and O. M. Laznicka, "Pulse excited interferometric fiber-optic gyroscope," *Conference on Lasers and Electro-Optics 1998 Technical Digest Series*, paper CWR5, p. 313-4, 1998.

[101] C. R. Doerr, K. Tamura, M. Shirasaki, H. A. Haus, and E. P. Ippen, "Orthogonal polarization fiber gyroscope with increased stability and resolution," *Applied Optics*, vol. 33, pp. 8062-8, 1994.

[102] H. P. Yuen, V. W. S. Chan, "Noise in homodyne and heterodyne detection," *Optics Letters*, vol. 8, p. 177, 1983.

[103] H. A. Haus, K. Bergman, and Y. Lai, "Fiber gyro with squeezed radiation," *Journal of the Optical Society America B*, vol. 8, p. 1952-7, 1991.

[104] R. C. Youngquist, L. F. Stokes, and H. J. Shaw, "Effects of Normal Mode Loss in Dielectric Waveguide Directional Couplers and Interferometers," *IEEE Journal of Quantum Electronics*, vol. QE-19, pp. 1888-96, 1983.

[105] H. Chou and S. Ezekiel, "Wavelength stabilization of broadband semiconductor light sources," *Optics Letters*, vol. 10, no. 12, p. 612-4, 1985.

[106] C. R. Doerr, M. Shirasaki, and H. A. Haus, "Dispersion of pulsed squeezing for reduction of sensor nonlinearity," *Optics Letters*, vol. 17, no. 22, p. 1617-9, 1992.

[107] C. C. Cutler, S. A. Newton, and H. J. Shaw, "Limitation of rotation sensing by scattering," *Optics Letters*, vol. 5, no. 11, p. 488-90, 1980.

[108] C. R. Doerr, "Toward a Noise-Free Interferometric Fiber Optic Gyroscope," MIT PhD Thesis, 1994.

Spectral Shaping

[109] G. J. Tearney, M. E. Brezinski, B. E. Bouma, S. A. Boppart, C. Pitris, J. F. Southern, J. G. Fujimoto, "In vivo endoscopic optical biopsy with optical coherence tomography," *Science*, vol. 276, no. 5321, p.2037-9, 1997.

[110] U. Morgner, W. Drexler, F. X. Kartner, X. D. Li, C. Pitris, E. P. Ippen, J. G. Fujimoto, "Spectroscopic optical coherence tomography," *Optics Letters*, vol. 25, no. 2, pp. 111-3, January, 2000.

[111] W. Drexler, U. Morgner, F. X. Kärtner, C. Pitris, S. A. Boppart, X. D. Li, E. P. Ippen, J. G. Fujimoto, "In vivo ultrahigh-resolution optical coherence tomography," *Optics Letters*, vol. 24, no. 17, pp. 1221-3, September, 1999.

[112] G. A. Alphonse, N. Morris, M. G. Harvey, D. B. Gilbert, J. C. Connolly, "New high-power single-mode superluminescent diode with low spectral modulation,," *Conference on Lasers and Electro-Optics 1996 Technical Digest Series*, paper CTul3, p. 107-8, 1996.

[113] A. M. Weiner, D. E. Learid, J. S. Patel, J. R. Wullert, II, "Programmable shaping of femtosecond optical pulses by use of 128-element liquid crystal phase modulator," *IEEE Journal of Quantum Electronics*, vol.28, no.4, pp.908-20, 1992.

[114] L. Boivin, M. C. Nuss, S. T. Cundiff, W. H. Knox, J. B. Stark, "103-channel chirped-pulse WDM transmitter," Conference on Optical Fiber Communications. Technical Digest. Postconference Edition. 1997 OSA Technical Digest Series. Vol.6 (IEEE Cat. No.97CH36049). Opt. Soc. America. 1997, pp.276-7. Washington, DC, USA.

[115] M. C. Nuss, W. H. Knox, U. Koren, "Scalable 32 channel chirped-pulse WDM source," *Electronics Letters*, vol 32, no. 14, pg 1311-2, July 4, 1996.

[116] L. Boivin, M. Wegmuller, M. C. Nuss, W. H. Knox, Y. Sun, A. K. Srivastava, J. W. Sulhoff, C. Wolf, "Transmission over 362 km of 110 channels at 2.35 Gb/s from a spectrum-sliced femtosecond laser," *IEEE Photonics Technology Letters*, vol.11, no.10, October 1999, pp.1319-21.

[117] H. P. Sardesai, C.-C. Chang, A. M. Weiner, "A femtosecond code-division multiple-access communication system test bed," *IEEE Journal of Lightwave Technology*, vol. 16, p. 1953, 1998.

[118] Y. C. Tong, L. Y. Chan, H. K. Tsang, "Fibre dispersion or pulse spectrum measurement using a sampling oscilloscope," *Electronics Letters*, vol.33, no.11, 22 May 1997, pp.983-5.

[119] P. C. Chou, H. A. Haus, J. F. Brennan III, "Reconfigurable time-domain spectral shaping of an optical pulse stretched by a fiber Bragg grating," *Optics Letters*, vol. 25, no. 8, p. 524-6, 2000.

[120] M. D. Pelusi, Y. Matsui, A. Suzuki, K. Ogawa, "Suppression of third-order fibre dispersion by phase modulation of stretched optical pulses," 24th European Conference on Optical Communication. ECOC '98 (IEEE Cat. No.98TH8398). Telefonica. Part vol.1, 1998, pp.525-6 vol.1. Madrid, Spain.

[121] M. D. Pelusi, Y. Matsui, A. Suzuki, "Fourth-order dispersion suppression of ultrashort optical pulses by second-order dispersion and cosine phase modulation," *Optics Letters*, vol.25, no.5, 1 March 2000, pp.296-8.

[122] H. Sotobayashi, K. Kitayama, "325 nm bandwidth supercontinuum generation at 10 Gbit/s using dispersion-flattened and non-decreasing normal dispersion fibre with pulse compression technique," *Electronics Letters*, vol. 34, no. 13, p. 1336-7, 1998.

[123] T. Morioka, K. Mori, and M. Saruwatari, "More than 100-wavelength-channel picosecond optical pulse generation from single laser source using supercontinuum in optical fibres," *Electronics Letters*, vol. 29, no. 10, p. 862-4, 1993.

[124] S. V. Chernikov, Y. Zhu, J. R. Taylor, and V. P. Gapontsev, "Supercontinuum self-Q-switched ytterbium fiber laser," *Optics Letters*, vol. 22, no. 5, p. 298-300, 1997.

Mode-locked Fiber Lasers

[125] K. Tamura, E. P. Ippen, H. A. Haus, and L. E. Nelson, "77-fs pulse generation from a stretched-pulse mode-locked all-fiber ring laser," *Optics Letters*, vol. 18, no. 13, p. 1080-2 1993.

[126] E. Snitzer, *Physical Review Letters*, vol. 7, p. 444, 1961.

[127] C. J. Koester, E. Snitzer, *Applied Optics*, Vol. 3, p. 1182 (1964).

[128] L. E. Nelson, D. J. Jones, K. Tamura, H. A. Haus, E. P. Ippen, "Ultrashort-pulse fiber ring lasers," *Applied Physics B*, vol. 65, p. 277-97, 1997.

[129] K. Tamura, H. A. Haus, and E. P. Ippen, "Self-starting additive pulse mode-locked erbium fibre ring laser," *Electronics Letters*, vol. 28, no. 24, p. 2226-8, 1992.

[130] N. Pandit, D. U. Noske, S. M. J. Kelly, J. R. Taylor, "Characteristic instability of fibre loop soliton lasers," *Electronics Letters*, vol. 28, no. 5, pp. 455-7, 1992.

[131] C. X. Yu, S. Namiki, and H. A. Haus, "Noise of the Stretched Pulse Fiber Laser: Part II Experiments," *IEEE Journal of Quantum Electronics*, vol. 33, no. 5, p. 660-8, 1997.

[132] S. Namiki and H. A. Haus, "Noise of the Stretched Pulse Fiber Laser: Part I-Theory," *IEEE Journal of Quantum Electronics*, vol. 33, no. 5, p. 649-59, 1997.

[133] K. Tamura, C. R. Doerr, L. E. Nelson, H. A. Haus, E. P. Ippen, "Technique for obtaining high-energy ultrashort pulses from an additive-pulse mode-locked erbium-doped fiber ring laser," *Optics Letters*, vol. 19, no. 1, pp. 46-8, 1994.

[134] K. Tamura, E. P. Ippen, and H. A. Haus, "Pulse dynamics in stretched-pulse fiber lasers," *Applied Physics Letters*, vol. 67, no. 2, p. 158-60, 1995.

[135] L. E. Nelson, S. B. Fleischer, G. Lenz, and E. P. Ippen, "Efficient frequency doubling of a femtosecond fiber laser," *Optics Letters*, vol. 21, no. 21, p. 1759-61, 1996.

[136] E. P. Ippen, H. A. Haus, and L. Y. Liu, "Additive pulse mode locking," *Journal of the Optical Society of America B*, vol. 6, no. 9, p. 1736-45, 1989.

[137] H. A. Haus, J. G. Fujimoto, and E. P. Ippen, "Structures for additive pulse mode locking," *Journal of the Optical Society of America B*, vol. 8, no. 10, p. 2068-76, 1991.

[138] H. A. Haus, E. P. Ippen, and K. Tamura, "Additive-Pulse Modelocking in Fiber Lasers," *IEEE Journal of Quantum Electronics*, vol. 31, no. 1, p. 200-8 1994.

[139] H. A. Haus, J. G. Fujimoto, E. P. Ippen, "Analytic Theory of Additive PUlse and Kerr Lens Mode Locking," *IEEE Journal of Quantum Electronics*, vol. 28, no. 10, pp. 2086-96, 1992.

[140] H. A. Haus, K. Tamura, L. E. Nelson, and E. P. Ippen, "Stretched-Pulse Additive Pulse Mode-Locking in Fiber Ring Lasers: Theory and Experiment," *IEEE Journal of Quantum Electronics*, vol. 31, no. 3, p. 591-8, 1995.

[141] K. Tamura and M. Nakazawa, "Optimizating power extraction in stretched-pulse fiber ring lasers," *Applied Physics Letters*, vol. 67, no. 25, p. 3691-3, 1995.

[142] K. Tamura, T. Komukai, and M. Nakazawa, "Optimization of power extraction in a high-power soliton fiber ring laser containing a chirped fiber grating," *Applied Physics Letters*, vol. 69, no. 11, p. 1535-7, 1996.

[143] H. A. Haus, *Waves and Fields in Optoelectronics*, Prentice-Hall, Englewood Cliffs, NJ, 1984.

[144] K. Tamura, E. Yoshida, T. Sugawa, and M. Nakazawa, "Broadband light generation by femtosecond pulse amplification with stimulated Raman scattering in a high-power erbium-doped fiber amplifier," *Optics Letters*, vol. 20, no. 15, p. 1631-3, 1995.

[145] C. R. Doerr, H. A. Haus, E. P. Ippen, M. Shirasaki, and K. Tamura, "Additive-pulse limiting," *Optics Letters*, vol. 19, no. 1, p. 31-3, 1994.

[146] H. A. Haus, I. Sorokina, and E. Sorokin, "Raman-induced redshift of ultrashort mode-locked laser pulses," *Journal of the Optical Society of America B*, vol. 15, no. 1, p. 223-31, 1998.

[147] J. P. Gordon, "Theory of the soliton self-frequency shift," *Optics Letters*, vol. 11, no. 10, p. 662-4, 1986.

[148] D. J. Jones, L. E. Nelson, H. A. Haus, E. P. Ippen, "Diode-pumped environmentally stable stretched-pulse fiber laser," *IEEE Journal of Selected Topics in Quantum Electronics*, vol. 3, no. 4, p. 1076-9, 1997.

Optical Communications

[149] N. S. Bergano, V. J. Mazurczyk, C. R. Davidson, "Polarization scrambling improves SNR performance in a chain of EDFAs," OFC'94 Proceedings, February, 1994, San Jose, CA, pg. 255-6.

[150] N. S. Bergano, V. J. Mazurczyk, C. R. Davidson, "Polarization hole-burning in erbium-doped fiber-amplifier transmission systems," ECOC '94. 20th European Conference on Optical Communication. Ist. Int. Comun. Part vol.2, 1994, pp.621-8 vol.2. Genova, Italy.

[151] F. Heismann, R. W. Smith, "High-speed polarization scrambler with adjustable phase chirp," *IEEE Journal of Selected Topics in Quantum Electronics*, vol.2, no.2, June 1996, pp.311-18.

[152] F. Heismann, "Compact electro-optic polarization scramblers for optically amplified lightwave systems," *Journal of Lightwave Technology*, vol.14, no.8, Aug. 1996, pp.1801-14.

[153] F. Heismann, D. A. Gray, B. H. Lee, R. W. Smith, "Electrooptic polarization scramblers for optically amplified long-haul transmission systems," *IEEE Photonics Technology Letters*, vol.6, no.9, Sept. 1994, pp.1156-8.